2-9-2011

Studies of a cyanine-based biosensor and light-induced antibacterial activities of oligo(phenylene ethynylene)s

Zhijun Zhou

Zhijun Zhou
Candidate

Department of Chemistry and Chemical Biology
Department

This dissertation is approved, and it is acceptable in quality and form for publication:

Approved by the Dissertation Committee:

, Chairperson

STUDIES OF A CYANINE-BASED BIOSENSOR AND LIGHT-INDUCED ANTIBACTERIAL ACTIVITIES OF OLIGO (PHENYLENE ETHYNYLENE)S

by

ZHIJUN ZHOU

B.S., Chemistry, Lanzhou University, 2001

DISSERTATION

Submitted in Partial Fulfillment of the
Requirements for the Degree of

Doctor of Philosophy

Chemistry

The University of New Mexico
Albuquerque, New Mexico

December, 2010

DEDICATION

This dissertation is dedicated to my mother Liangying Li, father Longhao Zhou, my wife Li Jiang and my four-year son Hanhan.

ACKNOWLEDGEMENTS

I would like to thank my advisor and mentor Dr. David G. Whitten. His optimistic, friendly, and encouraging personalities have a great impact on my life. He is always available if I need any help about either my life or my research. Moreover, he took a lot of time to discuss issues and progress of my projects, and help to find ways to make these projects moving forward in the right direction. Dr. Whitten always understands the situation of a foreign student and explains scientific events in a very concise way. His enthusiasm for science has greatly influenced us.

I would like to give thanks to my committee: Dr. Keller, Dr. Guo, Dr. Canavan, and Dr. Schanze for reviewing this dissertation. Your invaluable suggestion, comments have made this dissertation and defense possible.

I appreciate the colleagues: Dr. Yanli Tang, Dr. Komandoor Achyuthan, Dr. Anand Parthasarathy, Dr. Thomas S. Corbitt, Dr. Eunkyung Ji, Mr. Ying Wang, and Ms. Linnea K. Ista. It is my honor to work with all of you and I enjoyed the time. Yanli helped me with absorbance and fluorescence spectrometry and synthesis of OPEs; Komandoor gave me detailed instruction for Caspase 3 assay. Anand carried out all the transient absorption spectroscopy and singlet oxygen measurements at University of Florida in Schanze group; Most of flow cytometry experiments were done by Tom. Eunkyung worked with me to obtain the Laser scanning Confocal Microscopy images; Ying measured the fluorescence quantum yields of EO-OPE-1s; Linnea trained me for all microbiological operation.

I want to show my thanks to others: Dr. Eva Chi, Dr. Steve Graves, Dr. Gabriel P. Lopez, Dr. Scott Sibbett, Ms. Jingshu Zhu, Mr. Phanindhar Shivapooja, Mr. Yongqian Gao, Ms. Nicolette B. Estrada, Ms. Kristin Wilde, Ms. Jennifer Rice, Mr. Taylor Canady, Mr. Eric Hill, Dr. John Grey, Ms. Karen M. McElveny, Ms. Isela Roeder, Ms. Stephanie G. Sanchez, Dr. Liping Ding, Ms. Jo W. Whitten, Dr. Bruce Armitage, etc.

I apologize that I omitted some people whom I want to say thanks to. Thank you all for your support and help.

Finally, many thanks are given to financial support from Defense Threat Reduction Agency, contract# W911NF-07-1-0079.

STUDIES OF A CYANINE-BASED BIOSENSOR AND LIGHT-INDUCED ANTIBACTERIAL ACTIVITIES OF OLIGO (PHENYLENE ETHYNYLENE)S

by

ZHIJUN ZHOU

ABSTRACT OF DISSERTATION

Submitted in Partial Fulfillment of the
Requirements for the Degree of

Doctor of Philosophy

Chemistry

The University of New Mexico
Albuquerque, New Mexico

December, 2010

STUDIES OF A CYANINE-BASED BIOSENSOR AND LIGHT-INDUCED ANTIBACTERIAL ACTIVITIES OF OLIGO (PHENYLENE ETHYNYLENE)S

By

Zhijun Zhou

Center for Biomedical Engineering
Department of Chemistry and Chemical Biology
University of New Mexico

2010

B.S. Chemistry, Lanzhou University, 2001
Ph.D., Chemistry, The University of New Mexico, 2010

ABSTRACT

This dissertation has been focusing on two subjects: biosensor development and light-activated antimicrobials. A cyanine-based fluorescent biosensor is developed with high sensitivity to detect the presence and activity of caspase-3/7. We demonstrated that supramolecular self-assembly can be useful for designing biosensors. A series of p-Phenylene Ethynylenes (OPEs) have been synthesized. Further photophysical studies show that these molecules have good singlet oxygen yields. The antimicrobial capability increases dramatically when exposed to UV-365 radiation, though dark biocidal activity can be obtained as well. This phenomenon is probably due to the high yields of singlet oxygen of these OPEs, which oxidizes unsaturated membrane and inner components of bacteria, such as protein, DNA, etc.

Coupled with our previous work about the interactions of EO-OPE-1s with DOPC/cholesterol vesicles, we believe the biocidal process involves (1) EO-OPE-1s penetrate the bacterial membrane, (2) EO-OPE-1s photosensitize the generation of singlet oxygen and other reactive oxygen species and (3) singlet oxygen and/or reactive oxygen species trigger the cytotoxicity.

TABLE OF CONTENTS

ACRONYMS & ABREVIATIONS

TFA	trifluoroacetic acid
DMF	dimethylformamide
DMSO	dimethyl sulfoxide
TMS	trimethylsilyl
DOPC	1,2-dioleoyl-*sn*-glycero-3-phosphocholine
ROS	reactive oxygen species
TA	Transient absorption
ISC	intersystem crossing
RNA	oxyribonucleic acid
DNA	deoxyribonucleic acid
HTS	High throughput screening
S/B	signal background ratio
TIPS	triisopropylsilane
mM	millimolar
μM	micromolar
HA	hyaluronic acid
CD	circular dichroism spectroscopy
UV	ultraviolet
STM	scanning tunneling microscope
τ_F	fluorescence lifetime
Φ_F	fluorescence quantum yield
EO-OPE	“end-only” oligo(phenylene ethynylene)
CPE	conjugated polyelectrolyte
OPE	oligo(phenylene ethynylene)
PPE	poly(phenylene ethynylene)
HPLC	high-performance liquid chromatography
CMA	carboxymethyl amylose
CMC	carboxymethyl cellulose
Val	valine
Glu	glutamic acid
Asp	aspartic acid
Fmoc	fluorenylmethyloxycarbonyl
EDC	1-ethyl-3-[3-dimethylaminopropyl]carbodiimide
RNA	oxyribonucleic acid
DNA	deoxyribonucleic acid
DEVD	Asp-Glu-Val-Asp
PMT	photomultiplier tube
CLSM	confocal laser scanning microscope

Chapter 1 Introduction

1.1 Biosensors

1.1.1 Review of biosensors

The detection of the trace presence of a substance with real-time sampling, ultra sensitivity and specificity has emerged as an important topic in environmental, biological, medical, and life sciences. Traditional methods, such as atomic absorption spectrometry, inductively coupled plasma mass spectrometry, anodic stripping voltammetry,[1] high pressure liquid chromatography,[2] gas chromatography, and capillary electrophoresis,[3] are often compromised by high cost, inconvenience and low sensitivity. Biosensor, as defined by IUPAC[4,5] is a type of chemical sensor comprising a biological or biologically derived recognition element either integrated within or intimately associated with a physical and chemical transducer. From this definition, a biosensor is a device that is composed of three components: a). A biological recognition element. Usually it is a biomolecule, such as a protein, DNA,[6,7] RNA,[7,8] carbohydrate,[9] Lipid,[10] ribosome,[9] whole cell[11] or microbe,[11] *etc.* which is able to interact with other molecules. There are two situations we should be aware that the biological element could be either an analyzer or an analyte. In order to avoid the conceptual confusion, I will restrict the biological element as analyzer or recognition element, instead of an analyte in this dissertation. b). A target substance or analyte such as metal ions, small molecules, contaminants, and gas. c). A transducer. A transducer can be understood as an energy converter. In other words, any

device that involves energy conversion can be considered as a transducer, and this conversion could be electrical, electromagnetic, photonic, electro-mechanic, thermal, and acoustic, *etc*. Additional devices, such as wires, amplifiers, screen, digital display, *etc*., can be found in an integrated biosensor.

The first report of a biosensor can probably date back to 1956,[12] when Clark described an "enzyme electrode" and 1962, when Clark and Lyons described an enzymatic glucose biosensor using glucose oxidase as a selective bio-recognition molecule for glucose (Scheme 1-1) that directly led to the commercial development of glucose analyser for whole blood.

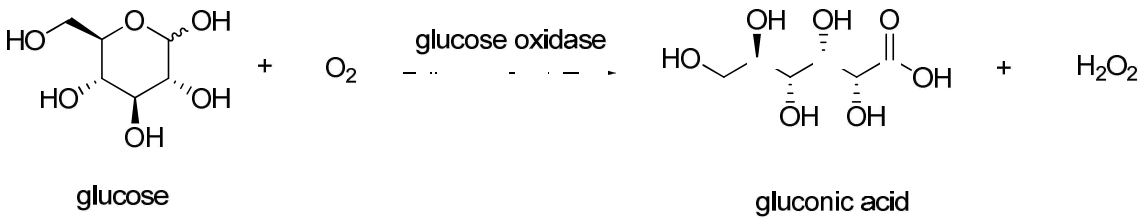

Scheme 1-1. Glucose reacts with oxygen to generate H_2O_2 under the catalyst-glucose oxidase.

To date, the blood glucose biosensor has been the most widespread, well developed, and commercial example of a biosensor, which uses the enzyme glucose oxidase to break down blood glucose. The process involves a number of steps. Firstly, it oxidizes glucose and uses two electrons to reduce the FAD (a component of the enzyme) to $FADH_2$. This in turn is oxidized by the electrode (accepting two electrons from the electrode) in a number of steps. The resulting current is a measure of the concentration of glucose, which is the indicator of diabetes (Fig. 1-4).

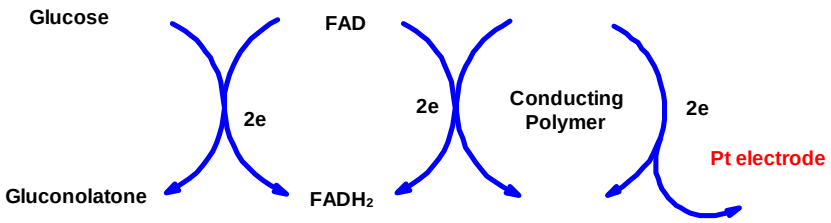

Fig. 1-1 The principle of glucose biosensor. The process involves a series of red-ox reactions.

Biosensor has long been recognized as an efficient, fast-readout and high selectivity device, thus obtained intense fundamental and applied studies. The first paper entitled "biosensor" was published in 1966. Since then, the design and applications of biosensors in various fields of analytical science have continued to grow tremendously as seen by the statistical data (Fig. 1-5). With the increase of amount, the biological elements have been expanded to DNA,[13] RNA,[14] Lipid bilayer,[12] whole cell,[13] and whole microbe.[12f] So far, numerous types of biosensors have been developed to recognize target molecules in recent years to monitor the presence and level of some molecules such as to detect glucose level of diabetic patients in medical sciences,[14,15] pathogens in public health,[16] organophosphate in pesticides,[17] and toxic metabolites such as mycotoxins in food industry,[18] *etc*.

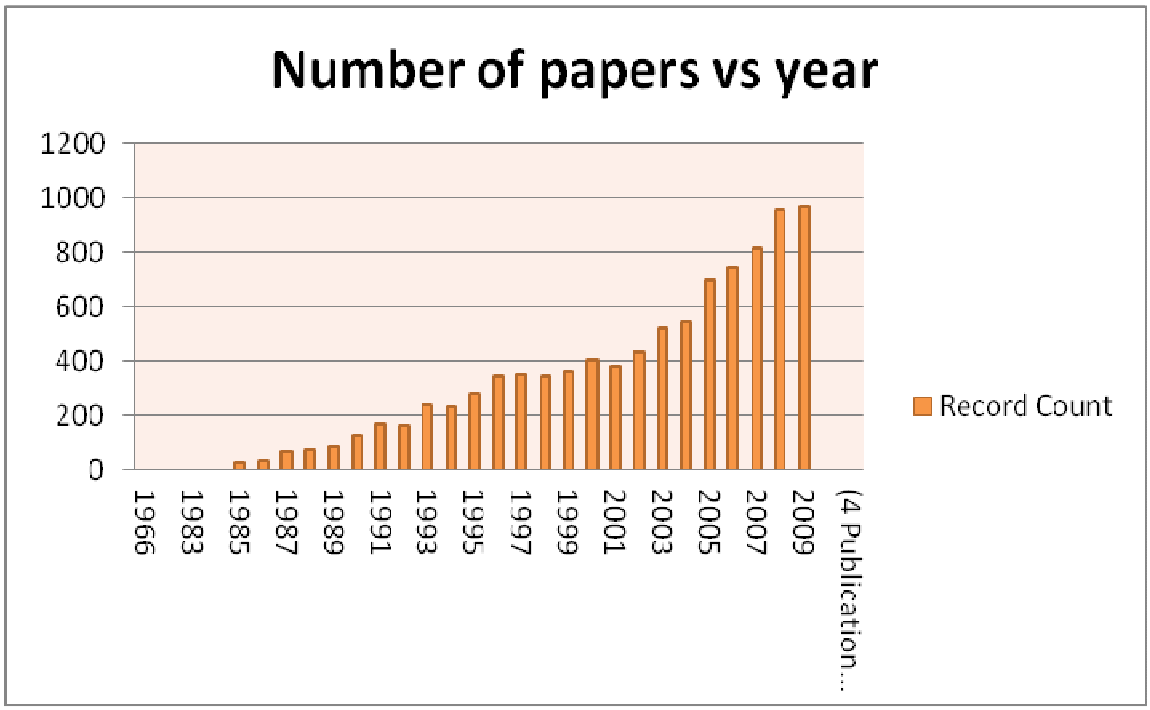

Fig. 1-2 Number of papers *vs* year 1960-2009. Data is from ISI web of Sciences (Biosensor* as the title in the search entry).

According to the biological recognition element, biosensors fall into the following categories:

DNA biosensors

The interest for DNA-based diagnostic tests has been growing in recent years. The development of systems allowing DNA detection and recognition is motivated by applications in such fields as gene analysis, fast detection of biological warfare agents, DNA diagnostics, and forensic applications. Furthermore, detection of mutant points opens up the feasibility of performing reliable diagnostics even before any symptom of a disease appears.

Basically, DNA detection systems are based on the principle of hybridization between a DNA probe which is present either in solution or on a solid support (Fig. 1-3) and its complementary DNA sequence.

Regarding the readout, most of DNA biosensors are based on either optical signal[19,20,21] or electrochemical signal.[22,23] Very few papers are based on piezoelectric transduction modes.[24]

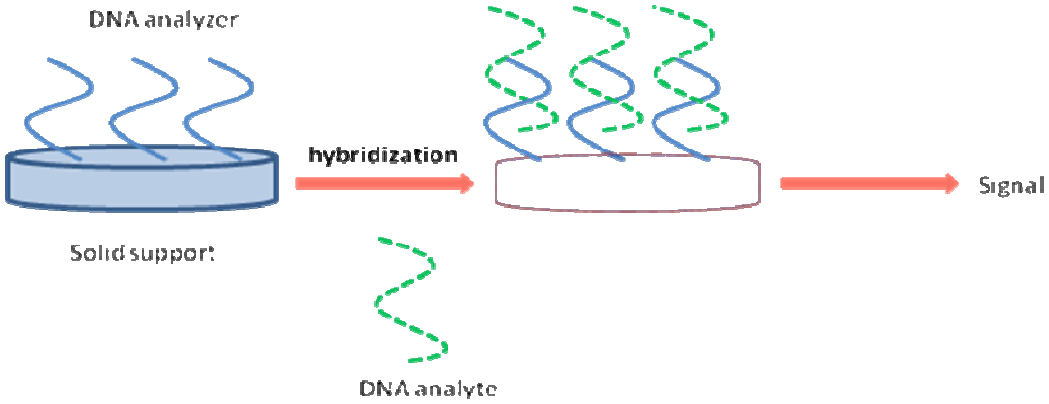

Fig. 1-3. Steps involved in the detection of a DNA sequence. DNA analyzer refers to immobilized sequences and DNA analyte refers to sequences in the sample being captured.

Enzyme biosensors

The most pronounced property of an enzyme-catalyzed reaction is its high efficiency and good selectivity. This unique property can be understood with the classic "Lock and Key" model, which was suggested by Emil Fisher in 1894,[25] and was further modified by Daniel Koshland in 1958.[26] Biosensors that use enzymes as recognition elements have attracted a great deal of attention and now been most extensively studied and

commercialized. As a result of high efficiency, good selectivity and relatively straightforward instrumentation of the enzymatic biosensors, it is potentially most promising in the applied area requiring ultra high sensitivity and selectivity. Another reason could be attributed to the fast development of enzymology which makes properties of numerous enzymes better understood.

Other biosensors

Besides the biosensors we have mentioned above, there are still numerous biosensors in use such as carbohydrate biosensors,[27] whole cell biosensors, and lipid biosensors. This dissertation is focusing on the enzyme-based biosensors, therefore, much attention is given to the important aspects of enzymatic biosensors.

1.1.2 Significant aspects of enzymatic biosensors

1.1.2.1 The trend of enzyme inactivation

Though the enzymatic biosensors are most extensively studied and even commercialized, it won't work well if it is not dealt with carefully and properly. An enzyme has a tertiary structure that comprises the active site of the enzyme. The tertiary structure is held by non-bonding forces, such as hydrophobic/hydrophilic forces, van der Waals forces, and/or hydrogen bonding, and all of these forces are weak interactions. Hence, the tertiary structure is sensitive to environmental changes, such as pH, ionic strength, and temperature.

1.1.2.2 Enzyme immobilization

In most cases, the steps involving immobilization on a solid support can be the major reasons leading to destabilization of an enzyme partially or completely and it is extremely important as the immobilization method can affect the working life-time and shelf-time (or storage time). There are four types of enzymatic immobilization methods: Physical adsorption, physical confinement, physical entrapment (Fig. 1-4)[28]and chemical bonding (Fig. 1-5). Physical adsorption mechanisms are governed by electrostatic attraction, hydrophobic interaction and van der Waal's forces. Adsorption offers several advantages: simplicity, mildness, little or no loss of enzymatic activity and higher sensitivity. However, because of weak adsorption forces, reproducibility is poor and adsorbed enzyme is easily washed off. Confinement and entrapment, which confine the enzyme with a semi-permeable membrane that allows the free passage of small molecules but entraps the enzyme utilizing the cross-linking of the polymer, are the improvement of physical adsorption. The approach of chemical bonding makes the most solid between the enzyme and the support, hence, it can not be washed off by conventional methods. Moreover, the enzyme can be used repeatedly, therefore, this method is widely used. The method of chemical bonding involves the modification of an enzyme and a solid support so that they are able to connect with each other. Recently, lots of bonding methods have been developed (Fig. 1-5).

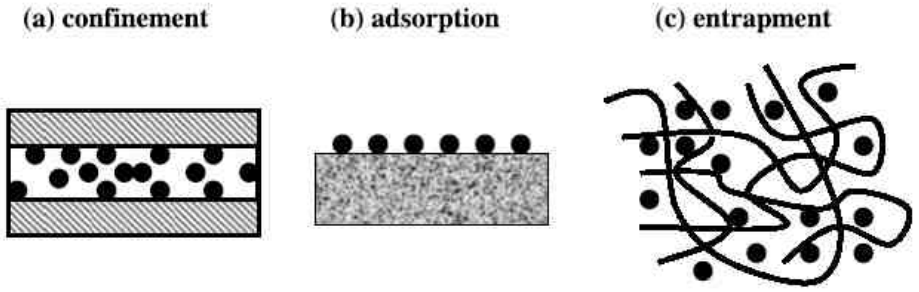

Fig. 1-4 Description of physical immobilization of enzyme: The black ball denotes enzyme.

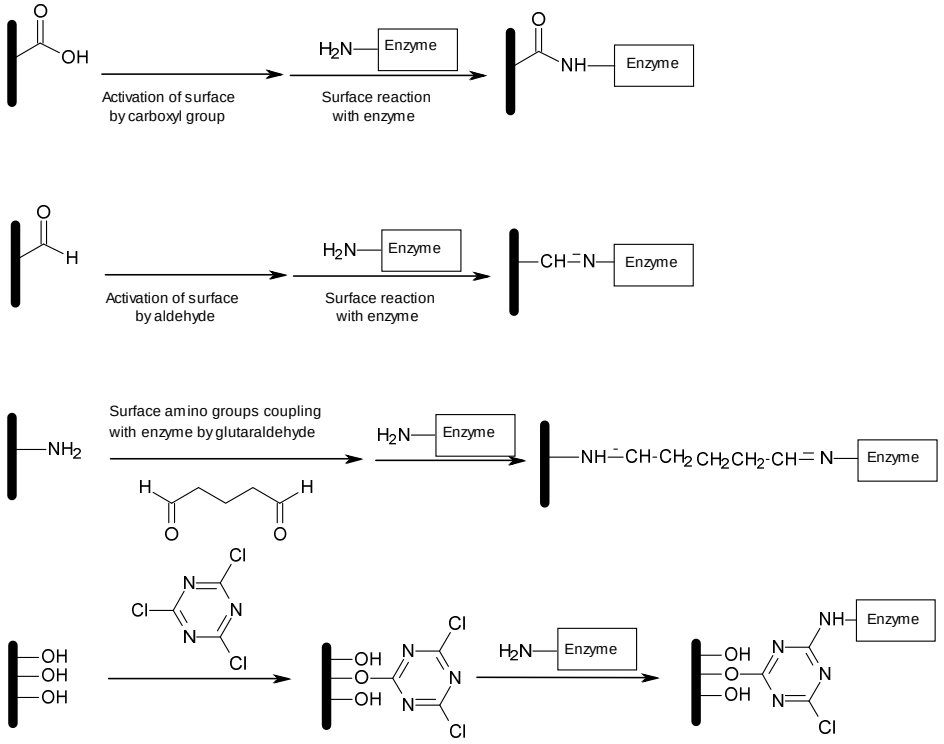

Fig. 1-5 Representative modification of substrate and enzyme.[32]

1.2 Cyanines

1.2.1 Definition, structure and classification of cyanine

Cyanine dye is a non-systematic naming of synthetic dye family, which belongs to the

polymethine group.[20] Based on different structures, cyanine dyes can be divided into the following three types:

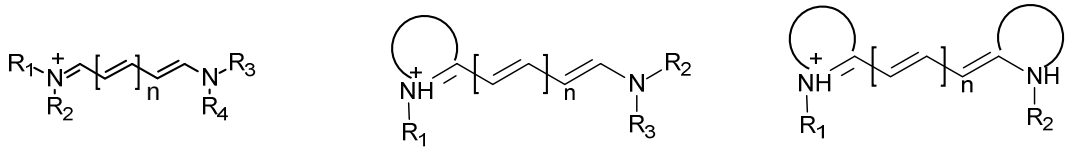

a.open chain cyanines b. hemicyanines c. closed chain cyanines

Fig. 1-6. General structures of cyanines.

1.2.2 Self-assembly of cyanine

1.2.2.1 Self-assembly

What is the self-assembly? Briefly speaking, in the absence of external forces, a disorderly multi-component system automatically processes from a disordered situation into an ordered system. By this definition, there are two distinctive features to be noticed. First, the process is spontaneous and there are no external forces to promote it and weak interactions (van de Waal's, π-π interaction, Coulombic attraction and/or repulsion, and hydrogen bonding) are involved in the process. The formation of micelle is a classic example of self-assembly, which is consequence of hydrophobic effect (driving force). From the energetic view, the self-assembly process is mostly entropic favorable. The self-aggregation of hydrocarbons frees water molecules and gives the water structure a higher entropy, which, according to the second law of thermodynamics, indicates the direction of a spontaneous process. Secondly, the product is more ordered aggregates.

The assembly is not only molecule-molecule, but also spans a wide range of nano- and mesoscopic structures.

1.2.2.2 J-aggregate and H-aggregate

The self-aggregation of dyes in solution or at solid-liquid interface is a very common phenomenon in dye chemistry due to strong intermolecular van der Waals-like attractive forces between the dye molecules. Among self-aggregations, J-aggregation[29] and H-aggregation[30] (Fig. 1-7) are particularly interesting, and have drawn intense research focusing on those aggregations. J-aggregates are understood as occurring owing to the end-to-end stacking of monomers, and the aggregate absorption is recognized typically as a sharp, narrow, and red-shifted band correspond to that of the monomer, while H-aggregates are due to a face-to-face stacking of monomers and appear most commonly as a broad blue-shifted band relative to the monomer band (Fig. 1-8).[54,55] Many cyanine dyes are capable of forming J-aggregates spontaneously in a relatively narrow concentration range in solution, but some are sensitive to solvent composition，pH value, viscosity, and ionic strength. More complex behavior occurs in interfacial systems such as surfactant, polymer, DNA, or soluble clays, where the aggregation is governed by the extent of surface charge, steric factors, or hydrophobic forces such that a variety of changes are expected to occur in J-aggregate structure. This may, in turn, induce changes in the morphology of the host template via cooperative interactions. However, these effects have been little explored.

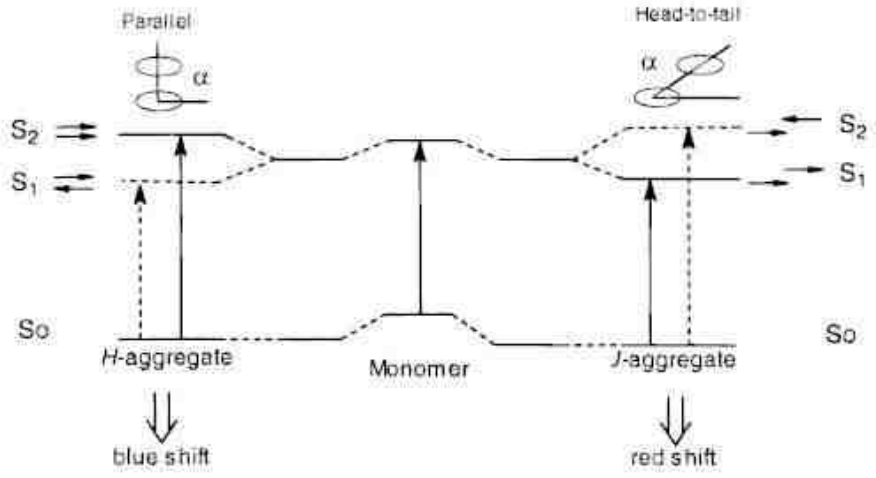

Fig. 1-7 Diagram demonstration of energy levels for J-aggregate and H-aggregate.[31]

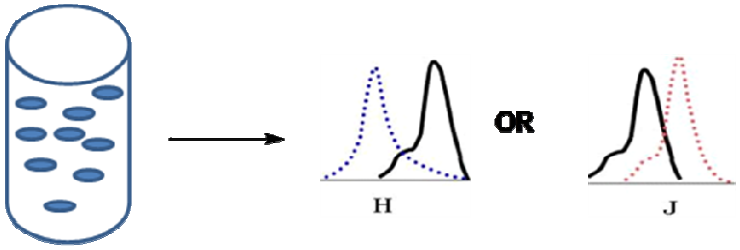

Fig. 1-8 Spectral changes of self-assembly. fluorescence spectrum has blue shift (blue line) and red shift (red line) in the case of H-aggregate and J-aggregate, respectively.[32]

The J-aggregation of cyanine dyes onto nanoparticles or ordered polymer templates such as carboxymethyl amylose (CMA),[33,34] carboxymethyl cellulose (CMC),[34,35] DNA[36,37] has attracted great interest because of the unique photophysical properties arising from the non-covalent binding. The properties have been used in biosensing.[38] J-aggregates with the characteristic sharp low energy absorption are derived from the exciton delocalization energy and a high optical polarization in the J-aggregates, thereby creating distinctive photophysical and nonlinear optical (NLO) properties, which provide a great

opportunity for technical applications in such fields as optical communications.

1.3 Poly(phenylene ethynylene) (PPE) and oligo(phenylene ethynylene) (OPE)

1.3.1 Photophysical and photochemical properties of PPE

PPE has been recognized to be a new class of π-conjugated materials that contain a delocalized π electron system. PPE can absorb sunlight like an antenna, and subsequently create photogenerated charge carriers, and transport these charge carriers. PPE polyelectrolytes are functionalized PPE derivatives. This usually involves adding functioning side chains, such as a charged side chain. The physical and photophysical properties of PPE and PPE polyelectrolytes have been the subject of many recent investigations.[39,40,41,42,43]

One of the most pronounced properties of PPEs are amplified fluorescence quenching, or referred to superquenching in some literatures. This unique character has been applied to the development of chemical sensors, because they easily transform chemical signals into measurable optical or electrical signals. In comparison to microelectronic devices, the enhanced sensitivity (signal amplification) is derived from the ability of a conjugated polymer to serve as a highly efficient transport medium. However, unlike a silicon circuit, which transports electrons or holes, PPEs transport electronic excited states. Swager's group at MIT built up a model in 1995[44] and conducted extensive research in this field. Whitten's group[45,46,47,48,49,50,51] and Schanze's group[52,53,54,55,56,57,58] have applied this

important property into biosensor development. So far, a lot of theoretical and experimental work has been done in the last decade.

1.3.2 Biocidal activity of PPE

Interestingly, it has been found that PPEs can serve as biocides.[59,50] Especially interesting and attractive are antimicrobial coatings that can function catalytically and that can be used in a variety of environments. Whitten's group reported the use of cationic conjugated polyelectrolytes (CPEs) supported on colloids as antimicrobials that could entrap Gram-negative bacteria such as *Pseudomonas aeruginosa* and *Cobetia marina* in a dark process at the colloid-suspension interface and subsequently kill the bacteria on irradiation with visible light.[60] Schanze's group and Whitten's group have collaborated to investigate the light-induced antimicrobial properties of PPEs. They reported a remarkably enhanced light-activated biocidal activity of micron-sized polyelectrolyte hollow capsules consisting of alternating layers of a pair of anionic and cationic phenylene ethynylene-type CPEs.[49] These novel photoactive polyelectrolyte capsules function in a manner reminiscent of the insect entrapping “Roach Motels” with respect to their ability to attract, concentrate, and kill bacteria trapped within and on the surface of the capsules. Furthermore, a mechanism has been proposed to explain the light-induced biocidal activity (Fig. 1-9).

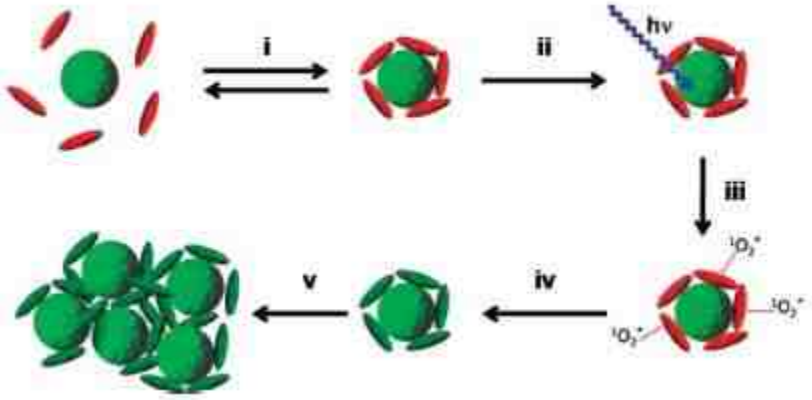

Fig. 1-9 Ⅰ. Reversible bacteria adhesion to the particle; Ⅱ. Photoexcitation of CPE; Ⅲ. Singlet oxygen generation; Ⅳ. Killing bacteria by singlet oxygen; Ⅴ. Aggregation of particles.[6]

1.3.3 Synthesis of OPE

To understand the relationship of structure and reactivity, OPEs, which are rigid rod-like conjugated oligomers have been studied in a variety of aspects. The synthesis of OPEs is generally straightforward and the key step is Pd/ Cu-catalyzed cross-coupling. Tour's group has made significant contributions to the synthesis. They have studied the solid synthesis of OPE monomers, dimers, tetramers, and octamers with ethyl substituents, and it turned out that a fast and simple method could be developed by using two sets of reaction conditions for the entire iterative synthetic sequence: (1) Pd-catalyzed cross-coupling of trimethylsilylacetylene with an aryl halide and (2) in situ desilylation/Pd-catalyzed coupling with an aryl iodide. This method provides a fast synthetic route to short length oligo (1,4-phenylene ethynylene)s by oligomer growth at both ends.[61,62,63,64,65] Bo's group reported a facile synthetic route to monodisperse

asymmetric OPEs by combining the selective deprotection and the Sonogashira coupling. In this case, the acetylenic trimethyl siliyl protecting group could be removed selectively by the treatment with tetrabutylammonium floride in methylene chloride, whereas both 2-(trimethylsilyl) ethyl and trimethyl siliyl protecting groups were cleaved in tetrahydrofuran.[66] Based on the backbone-rigidification, Gong's group has developed helical foldamers by incorporating intramolecular H-bond along the backbone of aromatic oligoamides in non-polar solvent or polar media.[67,68,69]

1.3.4 Photophysical properties of OPEs

OPEs have opened up a broad range of research: Molecular wires, supramolecular self-assembly, chemical sensors, coatings, *etc*. In 2003, Meyyappan's group reported the possibility of OPEs as molecular wires by studying the topography and transport properties of self-assembled monolayer of two types of oligo(phenylene ethynylene)s using scanning tunneling microscopy.[70] Moore's group was the first to explore supramolecular organization of oligo (m-phenylene ethynylene)s in the solid-state using a series of oligo(m-phenylene ethylene)s having triethylene glycol ester-linked side chains (i.e., 2-[2-(2- methoxyethoxy)ethoxy]ethyl esters).[71] Martin's group found oligo(m-phenylene ethynylene)s in the solid state could pack into helical nanotubles.[72] Linderoth's group explored the adsorption structures formed from OPEs on the Au (III) surface under ultrahigh vacuum conditions characterized by using scanning tunneling microscopy (STM), and they found that the molecules had different geometries, linear, bent, or three-spoke, but all consisted of a conjugated aromatic backbone formed from

three or four benzene rings connected by ethynylene spokes and functionalized at all ends with an aldehyde, a hydroxyl, and a bulky tert-butyl group. Sánchez's group studied the solvent effect for the self-assembly behavior of triangle-shape OPEs, decorated in their periphery with variable number of hydrophilic and hydrophobic substitutes.[73] Moore's research group has studied the role of helicogenicity of solvents in the conformational equilibrium of oligo(m-phenylene ethynylene)s which has implications for foldamer research. They demonstrated that through UV and CD spectroscopic experiments, the helical conformation was increasingly stabilized with increasing solvent polarity in the absence of specific solvent-chain interactions. Surprisingly, very few solvents are capable of fully denaturing the helix, indicating the strength of the solvophobic driving forces in this cooperative system. Whitten's group studied the self-assembling behavior of OPEs which have quaternary ammonium salts as pendent groups in water, and they found OPEs strongly formed J-aggregates or planarized with CMA and CMC in water which led to significant enhancement of fluorescence.[74] Now, our group has applied these properties into biosensor developments and biocidal studies.

1.4 Biocides

1.4.1 Structural properties of bacteria

Bacteria are tiny single-celled organisms. They can be found almost everywhere, from the deepest sea trenches to the highest mountains, from the glaciers to hot springs, even in the radioactive waste. They are so small that we are not even aware of all the bacteria living in our body. Bacteria play very important roles in the environment. Most bacteria are

beneficial, or at least harmless, but a small number of bacteria are harmful to us, causing infectious diseases, skin infections, intestinal infections, and other unpleasant reactions.

Based on the outcome of Gram stain, bacteria fall into two categories: Gram-positive bacteria and Gram-negative bacteria. Gram-positive bacteria are those that are stained dark blue or violet by Gram staining, while Gram-negative bacteria are those that take up a counterstain and appear red or pink by Gram staining.[75] More detailed structure studies have shown that the different results derive from differences in the outer structure of bacteria. Gram-positive bacteria have a thick mesh-like cell wall composed of peptidoglycan (50-90% of cell wall), while Gram-negative bacteria have a thinner layer (10% of cell wall). Gram-negative bacteria also have an additional outer membrane which contains lipids, membrane proteins, *etc*. and the outer membrane is separated from the cell wall by the periplasmic space (Fig. 1-10a and Fig. 1-10b).

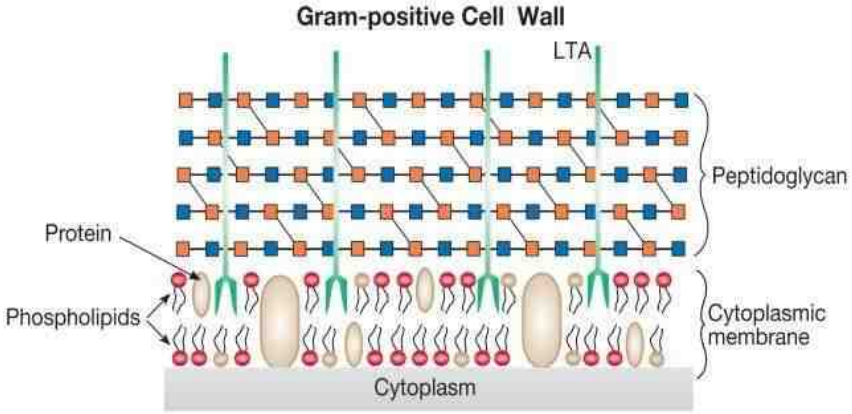

Fig. 1-10a. Structure of Gram-positive Cell Wall and Cytoplasmic membrane.

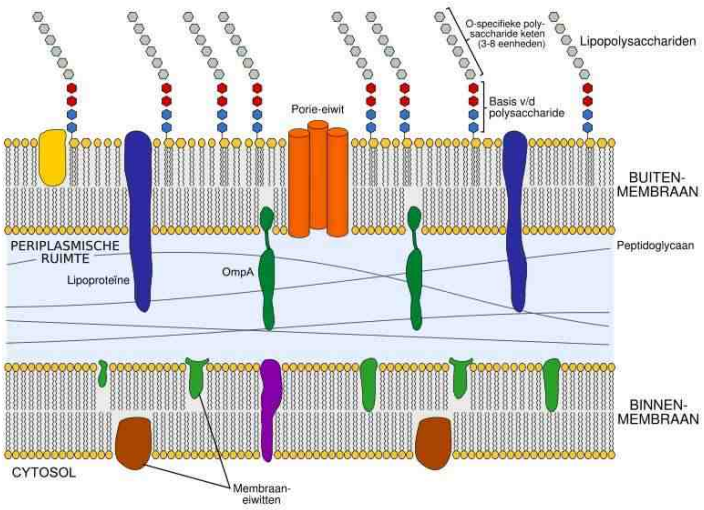

Fig. 1-10b. Structure of Gram-negative cell wall and membrane.

The membrane is mainly composed of phospholipids (hydrophilic head groups and hydrophobic chains) and membrane proteins, which are mobile and function as selectively semi-permeable membrane for the passage of nutrients and waste. Hence, the membrane is ubiquitous as a target for many drugs or biocides. With the distortion or destruction of the cell membrane, there is a loss of nutrients within the cell, ultimately leading to cell dysfunction and/or death.

1.4.2 Strategies for fighting bacteria

Before we discuss the strategies for fighting bacteria, it is important to understand the mechanisms leading to cell death. From the view of biocides (apoptosis and some physical methods have not been included in this dissertation, such as heating and membrane lysis), basically, there are two mechanisms involved in cell death. First, leakage mechanism- damage of membrane results in the loss of nutrients, proteins, DNA,

and other important components of cell, therefore, the cell fails to perform the normal physiological function; secondly, damage mechanism- damage of inner components of cell, such as proteins, RNA, or DNA. In this case, proteins, RNA or DNA will be damaged through chemical reaction with intruding molecules, thus the bacteria can not reproduce or perform normal functions, ultimately leading to death.

Based on the mechanisms mentioned above, two strategies have been developed. One is to damage the membrane by chemical or physical methods targeting at membrane phospholipids or proteins, so as to achieve the purpose of killing bacteria; another is to deactivate the normal function of macromolecules, such as proteins, RNA or DNA through chemical reactions. This dissertation involves both mechanisms.

1.4.3 Classification of biocides

There are many ways for the classification of biocides. Based on whether light involves in the inactivation process, biocides have been divided into two categories: general biocides[76] that do not need light to deactivate bacteria and light-activated biocides [65,80] that need light in the deactivation process.[77] We have developed biocides that can perform via both processes.

1.5 Scope

(1) This dissertation focuses on the synthesis, self-assembly and biosensor development of cyanines for caspase 3/7 activity.

(2) This dissertation also focuses on the synthesis, photophysics, self-assembly, and light-induced biocidal activities of OPEs.

Chapter 2 Synthesis, properties and biosensing of DEVD-cyanine

2.1 Introduction

Caspases are a family of cysteine proteases, which play important roles in cell apoptosis, inflammation, and necrosis in most stages of adult life, and have been known as the "executioner" proteins for their roles within the cell. Failure of apoptosis often leads to tumour development and autoimmune system diseases. The groups are so important that they have attracted much interest as potential therapeutic targets since they were discovered in the mid 1990s.[78,79,80]

Caspase-3 has been identified to be a key member of the caspase family,[84] which is characterized as an effector or executioner caspase. During apoptosis, caspase-3 cleaves protein substrates inside the cell, and this results in the development of characteristic morphology as an indication of apoptosis. In most substrates of the caspase-3, the peptide recognition sequence is Asp-Glu-Val-Asp (DEVD, the single-letter code for amino acids, Fig. 2-1) is most common used, and cleavage occurs after the second D.

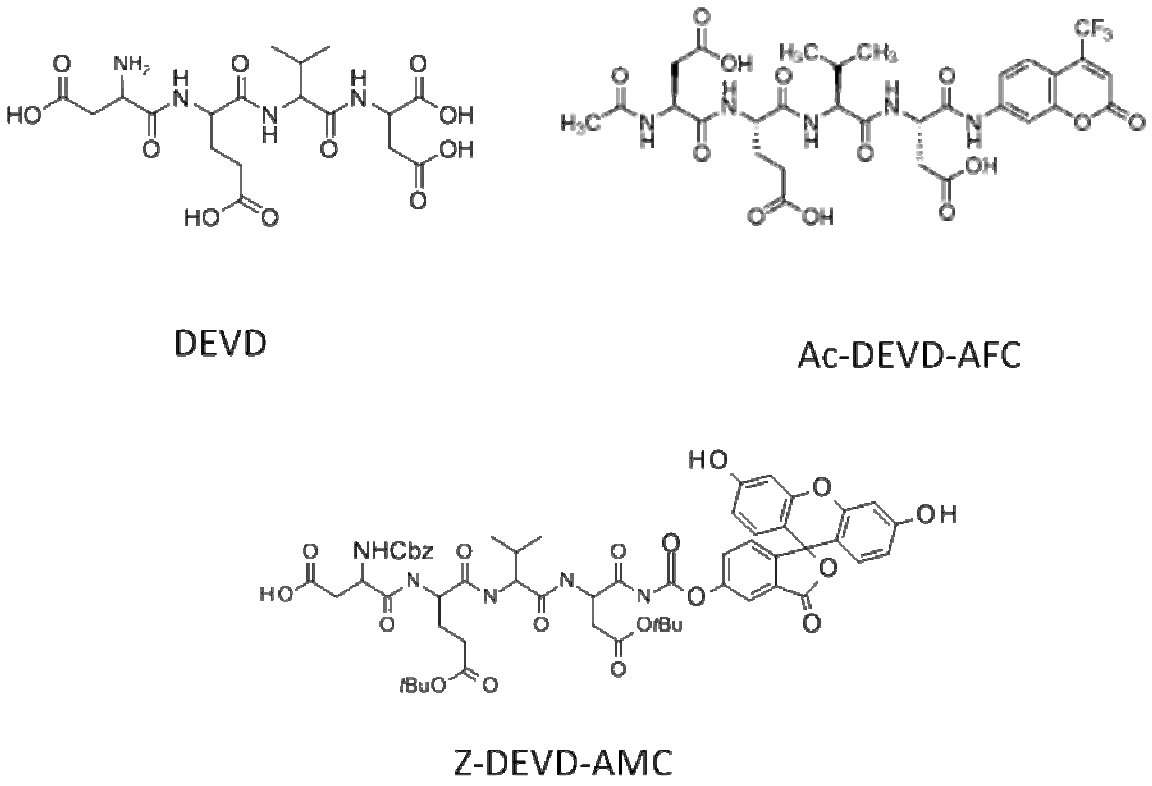

Fig. 2-1 The structure of DEVD, Ac-DEVD-AFC and Z-DEVD-AMC.

Giving that DEVD peptide sequence can be cleaved by caspase-3 specifically, a series of assays based on DEVD peptide have been developed to detect the presence and activity of caspase-3. Fluorometric methods based on peptide substrates labeled with cleavable fluorophores have been widely used for assaying various proteases, including caspase.[81] Early fluorogenic substrates such as Ac-DEVD-AFC and Z-DEVD-AMC (Fig. 2-1) based on coumarin dye are commonly used for determining the activity of caspase-3 from cellular lysates.[82] However, their short wavelength, low extinction coefficient and high fluorescent background result in low assay sensitivity and limit their biological applications. Wang, *et al*. reported novel caspase-3 fluorogenic substrates for cell based

apoptosis assay (Scheme 2-1),[83] which can detect caspase-3 with significantly higher enzyme turnover rate and more sensitivities both in solution and living cells than other fluorogenic substates.

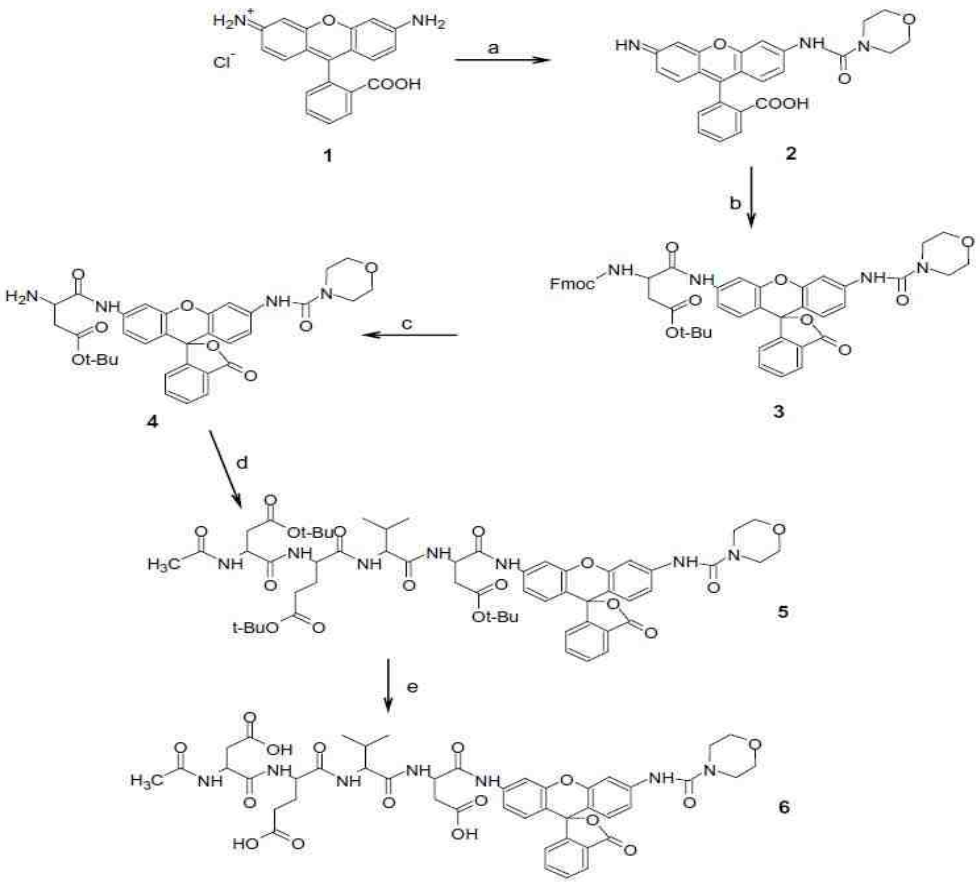

Scheme 2-1. Synthesis of N-Ac-DEVD-N0-MC-R110. Reagents: (a) morpholinecarbonyl chloride/DMF/NEt(i-Pr)2, yield 82%; (b) N-Fmoc-Asp(OtBu)/EDC /pyridine/DMF, yield 84%; (c) piperdine/chloroform, yield 88%; (d) Ac-Asp(OtBu)-Glu(OtBu)-Val/EDC/pyridine e/DMF, yield 82%; (e) TFA/anisole/chloroform, yield 52%.

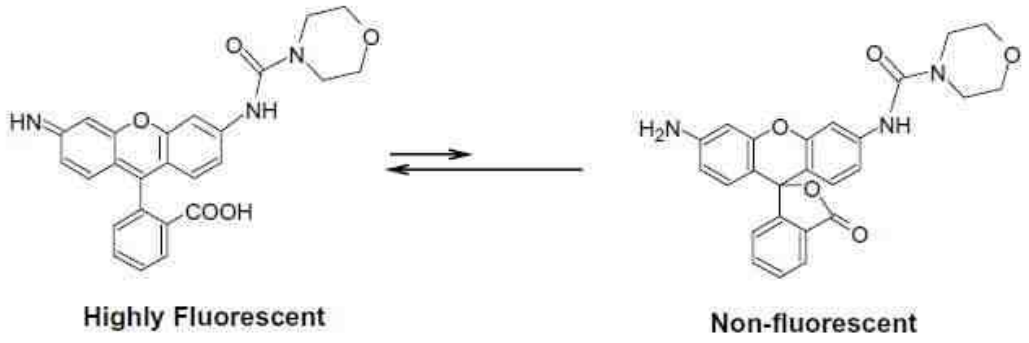

Fig. 2-2 The equilibrium of highly fluorescent species and non-fluorescent species. After cleavage by Caspase-3, the fluorescence will be released because of the highly fluorescent molecule.

We previously showed that a class of chromosphores known as cyanines was capable of spontaneously self-assembling upon a variety of biopolymers including carbohydrates, DNA, RNA, *etc*. [84, 85] Cyanines are photosensitive dyes composed of two quaternary nitrogen-containing and heterocyclic ring structures, which are linked by a polymethine bridge. Cyanines are characterized by high molar absorptivity, low intrinsic fluorescence and large fluorescence enhancement following self-assembly upon various templates. Supramolecular self-assembly involves reversible, non-covalent, and electrostatic interactions including hydrogen and/or charge bonding, van der Waals and hydrophobic forces. Cyanine self-assembly is sometimes accompanied by strong, sharp and bathochromic fluorescence, characteristic of J-aggregates.[86] Cyanines are also capable of forming hypsochromic, nonfluorescent or very weakly fluorescent H-aggregates.[85] Controlling and tuning the supramolecular self-assembly processes will offer insights to enable programmability to achieve desired functional nanomaterials. We therefore further

investigated the self-assembling of cyanines from our molecular "library" in order to identify a chromosphore that was capable of forming intensely fluorescent J-aggregates.

We previously reported that the nonfluorescent cyanine dye **1** (Fig. 2-3) formed fluorescent "J-aggregates" when the anionic biopolymer CMA was added to solutions of **1**. While the glucose polymer amylose exists in non-aqueous media as a helical structure, the chemical addition of carboxyl groups renders the resultant CMA water-soluble. However, repulsions between nearby carboxyl groups destabilize the helical structure such that the CMA exists as an "interrupted helix" in water. The association of **1** with CMA is thus a cooperative self-assembly process, and the resulting

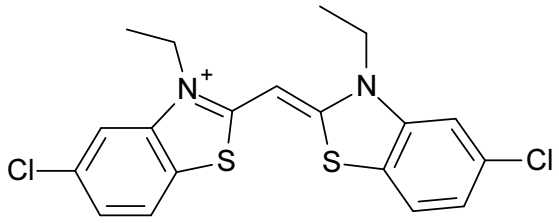

Fig. 2-3. Structure of compound **1** with a molecular mass of 408.[39] Cyanine **1** was modified to introduce a terminal amino group as shown in Scheme 2-3. This amino group was used to tether the cyanine 2a covalently to the DEVD tetrapeptide.

host-guest complex is helical, involving strong association of **1** with itself and with CMA[87]. The relatively broad absorption of **1** becomes red-shifted and sharpened upon association with CMA, and a sharp, strong fluorescence is observed. These spectral features along with strong, biphasic-induced circular dichroism are characteristic features

of the “J-aggregate” of achiral **1**, in which molecules of **1** were associated with each other in an end-on-end association.[86,88] Subsequent to our discovery of highly fluorescent J-aggregate formation between **1** and CMA, we developed bioassays based on cooperative self-assembly. We showed that the addition of CMA to non-fluorescent solutions of **1** resulted in a strongly fluorescent **1**-CMA complex, thus detecting the presence of the biopolymer. We also found that the salivary amylase enzyme unraveled the complex by hydrolyzing CMA and leading to a decrease in the fluorescence, producing a dose-response tracing that was an index of amylase activity.[34,89] Similar results were obtained with complexes that were formed between **1** and other anionic biopolymers such as CMC or hyaluronic acid (HA), [89, 90] and thus assays were developed for the hyaluronidase enzyme in order to detect HA hydrolysis.[90] Finally, we found that the fluorescent complex between **1** and CMA was quenched by a cationic cyanine absorbing at longer wavelengths than the **1**-CMA J-aggregate complex and that the fluorescence quenching resulted in the sensitization of the quencher fluorescence.[88]

We took these concepts to a higher level by focusing upon the development of novel biosensing approaches based upon the release of the cyanine chromosphore from a covalent adduct due to protease activity and thus demonstrating a new approach to sensing that extended the scope of the biopolymer-dye J-aggregate formation. This dissertation involves studies with an unsymmetrical cyanine 2a that was synthesized according to a multistep procedure (Scheme. 2-3). The synthetic sequence affords a

general method for preparing unsymmetrical cyanine dyes that can be coupled to biopolymers or oligomeric short peptide (as shown in Fig. 2-4). Such covalent conjugates can be useful in the design of enzyme assays, such as, for example, the proteases like Caspases that are involved in apoptosis (or programmed cell death) [91, 92, 93, 94] and therefore targets for drug discovery.[95]

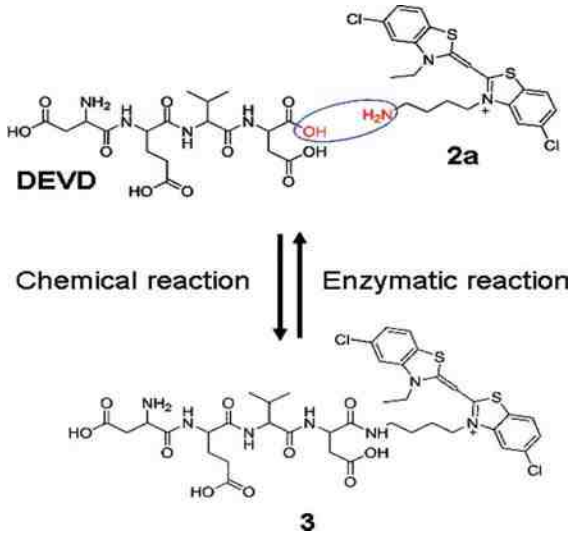

Fig. 2-4 Schematics of DEVD-cyanine 3 and hydrolysis by Caspase-3 and -7. This cartoon depicts the chemical coupling strategy of the deprotected DEVD tetrapeptide to aminocyanine 2a resulting in 3 (downward-pointing arrow). The enzymatic reaction (upward-pointing arrow) shows the hydrolysis of 3 through Caspase-3 and -7 proteolysis.

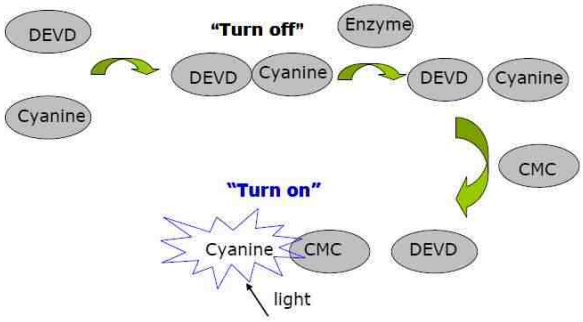

Fig. 2-5 The basic idea about the biosensing principle. The adduct of DEVD-Cyanine is non-fluorescent, but the strong fluorescence will be induced by the formation of J-aggregates of CMC and released cyanine through enzymatic reaction.

2.2 Materials, methods and instrumentation

2.2.1 Materials

2a, Cy2, DEVD-Cyanine, and synthetic intermediates were synthesized through multi-step reactions. The reagents involved in synthesis, caspase 3, and caspase 7 were purchased from Sigma-Aldrich (St. Louis, MO) and used as received. The protected DEVD synthetic peptide (except for the carboxy-terminal carboxyl group being free) was purchased from Bachem BioScience (King of Prussia, PA). All solvent were purchased from J&R solvent. Compound **1** is a gift from Eastman Kodak Co.

2.2.2 Methods

Stock solution for 2a and Cy2 were prepared with a concentration of 1 mM in 10% v/v DMSO in H_2O solution. The samples were prepared by diluting the stock solution into DI H_2O. These samples were ready for photophysical and self-aggregation studies. Caspase-3 and -7 ("combo kit"): one unit will cleave 1 nmol of the caspase substrate

DEVD-pNA (Nacetyl-DEVD-p-nitroanilide) per 1 h at pH 7.2 at 37 °C. Caspase-3 and -7 (individual reagent): one unit will hydrolyze 1.0 nmol of Ac-DEVD-AFC [N-acetyl-DEVD-7-amino-4-(trifluoromethyl) coumarin] per 1 min at pH 7.5 and 25 °C. The enzymes were stored in small aliquots at -80 °C until use. Enzyme aliquots were discarded after a single use and not subjected to more than a single freeze-thaw cycle. CMA and CMC were dissolved in water as 1 and 2 mM solutions, respectively, and stored under refrigeration. The substrate was dissolved in methanol as a 4 mM stock solution and stored refrigerated. The assay buffer consisted of 20 mM sodium phosphate, pH 7.5, supplemented with 100 mM sodium chloride, 0.1% 3-[(3-cholamidopropyl)-dimethylammonio]-1-propanesulfonate detergent, 10% glycerol, and 2 mM ethylenediaminetetraacetic acid. Just prior to use, freshly made dithiothreitol was added to the buffer at a concentration of 5 mM. Enzymatic reactions were carried out using 96- or 384-well white microplates (Optiplate, Perkin- Elmer, Waltham, MA). Both the enzyme and the substrate were diluted in the above buffer just prior to use. Typically, 5 µL of the enzyme solution was mixed with 5 µL of the DEVD-cyanine substrate. The enzymatic hydrolysis of the substrate was carried out at 37°C after tightly sealing the plate using commercial sealing tape (ImmunoWare Sealing Tape, Pierce, Rockford, IL) in order to minimize evaporative losses arising due to assay miniaturization. Reactions were terminated by dilution to a total volume of 280 µL (96-well plate reactions) or 95 µL (384-well plate reactions) using a mixture of methanol/water (20:80). Unless indicated otherwise, J aggregation of the liberated cyanine was initiated by the addition of 20 µL

(96-well plate reactions) or 5 µL (384-well plate reactions) of a mixture of CMA and CMC scaffolds, such that the final concentrations of the twin scaffolds were approximately 65 µM CMA and 35 µM CMC. The final volume in each well was thus 300 µL (96-well plate reactions) or 100 µL (384- well plate reactions). The plates were then incubated at room temperature (25 °C for 30 min) before taking fluorescence measurements. Control reactions to determine background fluorescence included reaction wells containing enzyme only, substrate only, or the reaction buffer without enzyme and substrate.

2.2.3 Instrumentation

Absorption were performed with a Shimadzu UV-Vis spectrometer, model UV-Vis 2501. Fluorescence was carried out at a Varian Cary Eclipse spectrophotometer. Protease reaction data was collected by the Molecular Device (SpectroMax M-5 microplate reader, Molecular Devices).

2.3 Synthesis and characterization

The synthesis of unsymmetric 2a: The synthesis of the unsymmetrical cyanine 2a was accomplished through a multi-step scheme outlined in Scheme 2-3 and is generally useful for preparing cyanines of similar structure for covalent attachment. The details for the synthesis are described below.

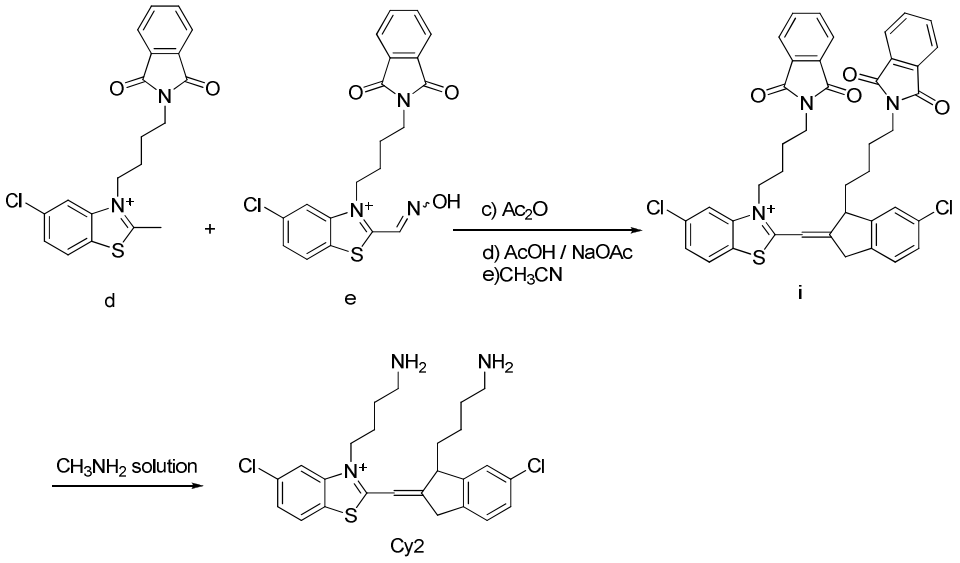

Scheme 2-2. Synthesis of Cy2

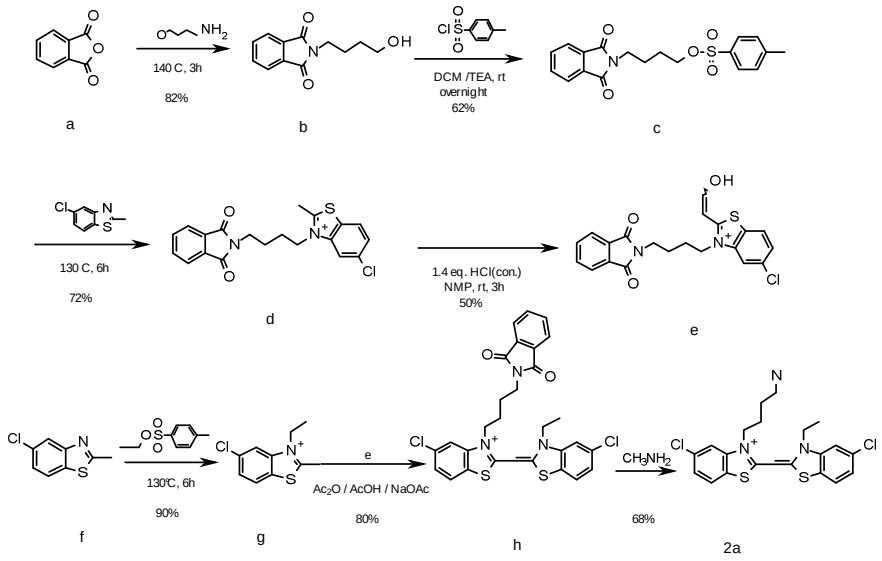

Scheme 2-3. Synthesis of 2a through multi-step reactions.

Synthesis of b: b was prepared by following the procedure described in the literature.[96]

Synthesis of c: To a solution of b (200 mg, 0.91 mmol) in 2 mL of dichloromethane, cooled to 0 °C, was added 4-toluenesulfonyl chloride (208 mg, 1.09 mmol) and triethylamine (184 mg, 0.25 mL, 1.82 mmol) under nitrogen atmosphere. The solution was allowed to warm up to room temperature and kept stirring overnight. The product was extracted by ethyl acetate, washed with 5 mL of H_2O, then washed with 2×5 mL of saturated sodium chloride solution, and dried by anhydrous $MgSO_4$. The product was purified by silica gel column chromatography with a ratio of 2:1 hexane/ethyl acetate to provide 211 mg of white solid. Yield: 62%. ^{1}H NMR (500 MHz, $CDCl_3$): δ7.835 (dd, J1 = 3 Hz, J2 = 5.5 Hz, 2H), 7.792 (d, J = 8 Hz, 2H), 7.724 (dd, J1 = 3 Hz, J2 = 5.5 Hz, 2H), 7.342 (d, J = 8 Hz, 2H), 4.069 (t, J = 6 Hz, 2H), 3.661 (t, J = 6.5 Hz, 2H), 2.436 (s, 3H), 1.707 (m, 2H), 1.317 (m, 2H).

Synthesis of d: Compound c (1.662 g, 4.45 mmol) was added into a 25 mL ground-glass flask, followed by 5-chloro-2-methylbenzo[d]thiazole (0.82 g, 4.45 mmol). The reaction mixture was heated to 130 °C slowly under a N_2 atmosphere and allowed to stir for 6 h. It was then cooled to room temperature, and a solid was formed. Ethyl ether (5 mL) was added into the resulting mixture, which was stirred for 10 min and then filtered to provide a slightly green powder. The product was purified by inverse silica gel chromatography to give 1.78 g of white solid product. Yield: 72%. ^{1}H NMR (500 MHz, $CDCl_3$): δ8.263 (d, J = 8.5 Hz, 1H), 7.851 (s, 1H), 7.842 (dd, J1 = 3 Hz, J2 = 5 Hz, 2H), 7.748 (dd, J1 = 3 Hz, J2 = 5 Hz, 2H), 7.635 (d, J = 8.5 Hz, 1H), 7.594 (d, J = 7.5 Hz, 2H), 7.058 (d, J = 7.5 Hz,

2H), 4.927 (t, J) 7.5 Hz, 2H), 3.407 (s, 3H), 2.298 (s, 3H), 1.977 (m, 2H), 1.417 (t, J = 8 Hz, 2H), 1.111 (m, 2H).

Synthesis of e: A solution of d (200 mg, 0.371 mmol) in 3 mL of 1-methyl-2-pyrrolidinone was cooled to 0 °C, and to this solution was then added a 37% hydrochloride solution (43 μL, 0.519 mmol) and $C_4H_9NO_2$ (0.05 mL, 0.445 mmol). The mixture was stirred for 3 h at room temperature, and then 3 mL of dichloromethane was added into the mixture to give a precipitate. The white solid was provided after filtration, washed with dichloromethane and ethyl ether, and then air-dried to give 84 mg of product. Yield: 50%. The product was directly used for the next step without further purification. ^{1}H NMR(500 MHz, DMSO-d6): δ 8.411 (s, 1H), 7.825 (s, 1H), 7.634 (d, J = 9 Hz, 0.75H), 7.583 (d, J = 8.5 Hz, 0.25H), 7.063 (d, J = 8.5 Hz, 1H), 7.030 (m, 4H), 4.082 (t, J = 7.5 Hz, 1.5H), 4.003 (t, J = 8 Hz, 0.5H), 2.806 (t, J = 6.5 Hz, 2H), 1.044 (m, 4H).

Synthesis of g: This was prepared by following the procedure described in the synthesis of d. Yield: 90%. ^{1}H NMR (500 MHz, $CDCl_3$): δ8.093 (d, J = 8.5 Hz, 1H), 7.848 (s, 1H), 7.633 (d, J = 8.5 Hz, 1H), 7.591 (d, J = 8 Hz, 2H), 7.042 (d, J = 8 Hz, 2H), 4.900 (q, J = 7.5 Hz, 2H), 3.377 (s, 3H), 2.290 (s, 3H), 1.575 (t, J = 7 Hz, 3H).

Synthesis of h: A solution of e (100 mg, 0.222 mmol) in 1.5 mL of acetonitrile was cooled to 0 °C, and then g (85.2 mg, 0.222 mmol), acetic anhydride (34 mg, 0.333 mmol), acetic acid (20 mg, 0.333 mmol), and sodium acetate (27 mg, 0.333 mmol) were added into the mixture. The reaction was stirred at 0 °C for 2 h. The resulting suspension was filtered

and washed with dichloromethane and a small amount of ice water to give yellow powder. The product was purified by inverse silica gel column chromatography to give 110 mg of a yellow solid. ^{1}H NMR (500 MHz, DMSO-d6): δ8.240 (d, J = 8.5 Hz, 1H), 8.115 (s, 1H), 8.067 (s, 1H), 7.801 (d, J = 8.5 Hz, 1H), 7.779 (d, J = 7.5 Hz, 1H), 7.570 (d, J = 7.5 Hz, 1H), 7.741 (d, J = 8.0 Hz, 2H), 7.103 (d, J = 8.0 Hz, 2H), 6.653 (s, 1H), 4,650 (q, J = 8 Hz, 2H), 2.825 (t, J = 7.5 Hz, 2H), 1.911 (m, 2H), 1.742 (m, 2H), 1.378 (t, J = 8.4 Hz, 2H), 1,265 (t, J = 8 Hz, 3H).

Synthesis of 2a: Solid h (540 mg, 0.875 mmol) was added into 30 mL of a 40% CH_3NH_2 aqueous solution, which was then allowed to stir overnight at room temperature. The solvent and CH_3NH_2 were removed by rotary evaporator to give yellow solid. The product was purified by inverse-phase silica gel column chromatography to give 290 mg of yellow solid. ^{1}H NMR (500 MHz, DMSO-d6): δ8.271 (d, J = 8.5 Hz, 1H), 8.124 (s, 1H), 7.594 (d, J = 8.5 Hz, 1H), 7.465 (d, J = 7.5 Hz, 1H), 7.101 (d, J = 7.5 Hz, 1H), 6.72 (s, 1H), 5.74 (s, 1H), 4.701 (q, J = 8 Hz, 2H), 2.788 (t, J = 7.5 Hz, 2H), 2.273 (s, 2H), 1.822 (m, 2H), 1.645 (m, 2H), 1.371 (t, J = 8.4 Hz, 2H), 1.225 (t, J = 8 Hz, 3H). MS (ESI). Calcd: m/z 450.06. Obsd: m/z 450.0627.

The synthesis of the DEVD-cyanine covalent conjugate was carried out as described below.

Synthesis of protected DEVD-cyanine: A solution of protected DEVD (100 mg, 0.134 mmol) in 2 mL of N,N-dimethylformamide was cooled to 0 °C, and then

hydroxybenzotriazole (27.2 mg, 0.201 mmol) and diisopropylcarbodiimide (20.3 mg, 0.161 mmol) were added into the mixture. The resulting mixture was allowed to stir for 10 min, followed by the addition of 2a (65 mg, 0.134 mmol). This mixture was stirred overnight, and then the solvent was removed under reduced pressure with an oil pump to give yellow solid. The product was purified by inverse-phase silica gel column chromatography to provide 139 mg of product. Yield: 85%. ^{1}H NMR (500 MHz, DMSO-d6): δ8.258 (d, J = 7.5 Hz, 1H), 8.116 (s, 1H), 7.885 (m, 3H), 7.732 (m, 2H), 7.577 (d, J = 8.5 Hz, 1H), 7.468 (d, J = 7.5 Hz, 1H), 7.183 (d, J = 7.5 Hz, 1H), 7.101 (s, 1H), 6.713 (s, 1H), 5.293 (m, 2H), 4.698 (m, 2H), 4.344 (m, 4H), 2.622 (m, 6H), 2.154 (m, 4H), 1.585 (m, 2H), 1.408 (s, 36H), 1.208 (m, 4H), 1.058 (t, J = 7 Hz, 3H), 0.725 (d, J = 6.5 Hz, 6H). MS (ESI). Calcd: m/z 1176.47. Obsd: m/z 1176.4669.

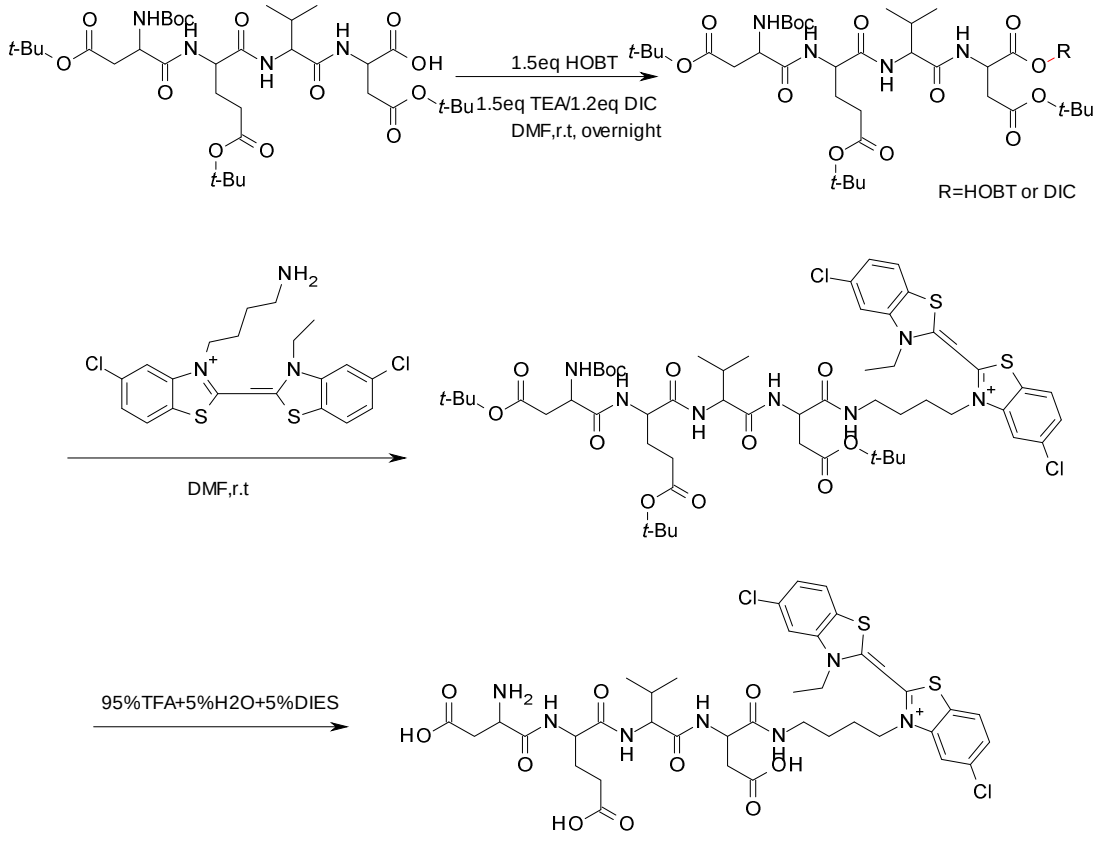

Scheme 2-4. Synthesis of DEVD-Cyanine through multi-step reactions.

Synthesis of DEVD-cyanine: A solution of protected DEVD-cyanine (100 mg, 0.085 mmol) in 1.8 mL of a CF_3COOH solution was cooled to 0 °C. To this solution was then added 0.1 mL of H_2O and 0.1 mL of triisopropylsilane (TIPS), and the resulting mixture was stirred overnight. The solvent was removed by vacuum evaporation to give yellow oil. The product was further purified by inverse-phase silica gel column chromatography to provide 77 mg of a yellow solid. Yield: 92%. ^{1}H NMR (500 MHz, DMSO-d6): δ8.558 (d, J = 7.5 Hz,1H), 8.250 (s, 1H), 8.120 (m, 3H), 7.860 (d, J = 8.5 Hz, 2H), 7.573 (d, J = 7.5 Hz, 1H), 7.453 (d, J = 7.5 Hz, 1H), 7.077 (s, 1H), 6.700 (s, 1H), 4.677 (m, 3H), 4.380

(m, 1H), 3.645 (m, 4H), 3.116 (m, 5H), 2.351 (m, 2H), 2.275 (m, 2H), 1.878 (m, 2H), 1.445 (m, 4H), 1.222 (m, 3H), 0.969 (m, 6H). MS (ESI). Calcd: m/z 908.23. Obsd: m/z 908.0247.

Synthesis of i: e (180 mg, 0.333 mmol) was added into a 25 mL round bottom flask, followed by f (2 mL) combined. Stir at 0 °C for 10 min, then a (180 mg, 0.333 mmol), c (51 mg, 0.499 mmol) and d (30 mg, 0.499 mmol) were added. Keep stirring for another 30 min, filtrate to remove solvent to give green solid. The solid was washed with ice water for 3 times and acetone, vacuum dry for two days to give 110 mg of i.

Synthesis of Cy2: i (100 mg, 0.127 mmol) was added into 5 mL round bottom flask with 2 mL of 40% CH_3NH_2 solution. Keep stirring for 2 days for form yellow suspension. Filtrate to give yellow powder after washing with ice water and acetone.

It should be noticed here that the reaction from h to 2a is a tricky one. We tried quite a few methods to deprotect compound h, such as NH_2-NH_2 in methanol / ethanol under reflux, m-Cresol/Methylamine in acetonitrile under reflux, Na_2S in aqueous THF, and methylamine in H_2O. Finally we found that methylamine solution is a good way for the deprotection of compound h. In addition, we got a mixture of cis- and trans- isomers with a ratio being 3: 1, but we didn't isolate the isomers and performed the next step directly, instead.

2.4 Results and discussion

2.4.1 Absorbance and fluorescence measurements

All the absorption and fluorescence were measured upon self-assembling of 2a with biopolymers and synthetic clay, but for Cy2, just the substrates CMC and CMA were measured. In this dissertation, most studies are centered on 2a and its adduct DEVD-Cyanine. Basically, the absorption of 2a in water is very similar to that of compound **1** (Fig. 2-7), where the monomeric peak occurs at 427 nm. It is not surprising to get this result giving that both molecules share the same chromosphere. There is a shoulder peak appears at around 408 nm (Fig. 2-6), which should be attributed to dimers or aggregates of 2a. Like other cyanines, 2a has a large molar extinction coefficient that makes it easy trap visible light. It has been reported that cyanines are prone to aggregation in water even at low concentration, in consistent with those observations, this phenomenon occurs for 2a when its concentration is 1~15 μM, but the monomeric peak is still very pronounced.

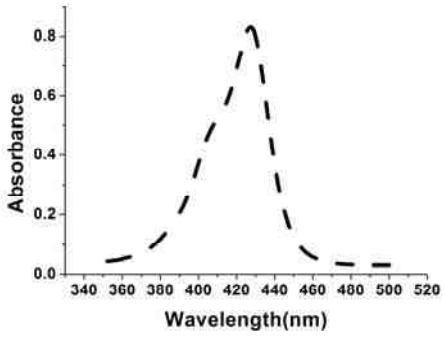

Fig. 2-6 Absorption spectrum of 2a in pure H_2O with concentration of 10 μM.

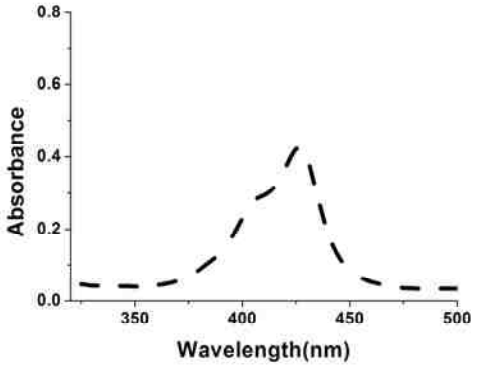

Fig. 2-7 Absorption spectrum of **1** in pure H_2O with concentration of 10 μM.

Among all substrates (CMA, CMC, HA, and synthetic clay), CMA (Fig. 2-8) and CMC (Fig. 2-9) are were found easily to form J-aggregates with 2a. The J-aggregates were formed gradually with the addition of aliquots of CMA or CMC aqueous solution, which could be seen through spectral changes, where the monomeric peak was decreasing, while the J-aggregates with the red-shifted bands were formed increasingly. The red-shifted bands show the highest intensity at 466 nm.

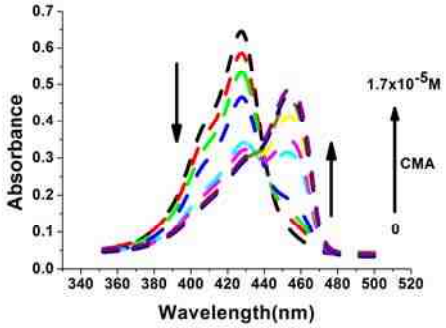

Fig. 2-8 J-aggregate formation of 2a on the substrate CMA, [2a]= 10 μM.

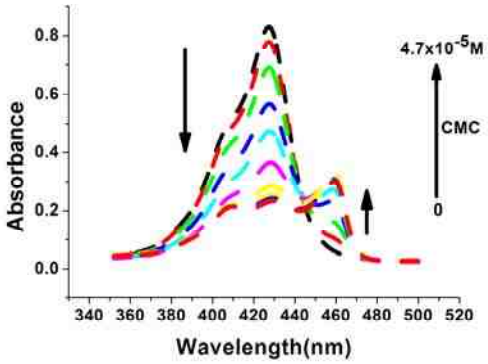

Fig. 2-9 J-aggregate formation of 2a on the substrate CMC, [2a]= 10 μM.

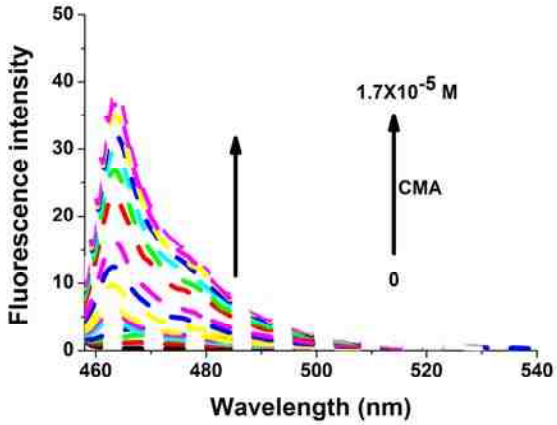

Fig. 2-10 Fluorescence spectra for the system of 2a/CMA with concentration at 10 Mm.

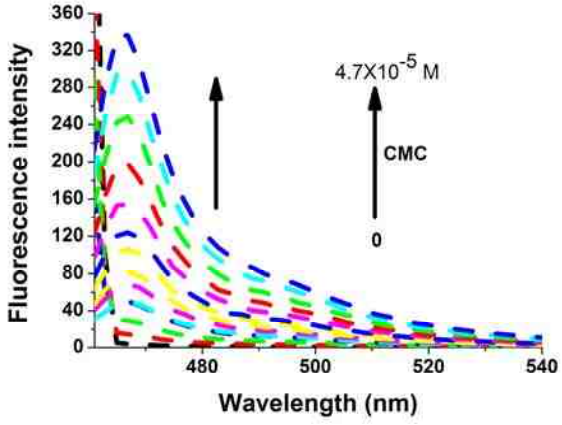

Fig. 2-11 Fluorescence spectra for the system 2a/CMC with concentration at 10 μM.

To verify the formation of J-aggregates, fluorescence spectrometry was performed with

excitation at 460 nm. The results show in Fig. 2-10, 2-11, 2-18, and 2-19. Like other cyanines, 2a shows very weak fluorescence when excited at 460 nm, which in turn increases the signal background ratio (S/B) when self-assembling onto substrates. However, dramatic enhancement of fluorescence intensity was observed when CMC or CMA solution was added into 2a aqueous solution and the highest bands appeared at 466 nm with the concentration of 17 μM and 47 μM, respectively. The calculated Stokes shift is 6 nm. To be noticeable, the fluorescence intensity for the system of 2a/CMC (Fig. 2-11) is much stronger than that of 2a/CMA (Fig. 2-10). Meanwhile, the absorption band of 2a/CMC is very sharp, yet, relatively broad in the system of 2a/CMA. The narrow band indicates that structured J-aggregates have been formed. Therefore one can expect that strong emission could occur. In addition, the system of 2a/CMA is more easily saturated. The saturated concentration for CMA and CMC are 17 μM and 47μM, respectively. The structure of CMA and CMC show below:

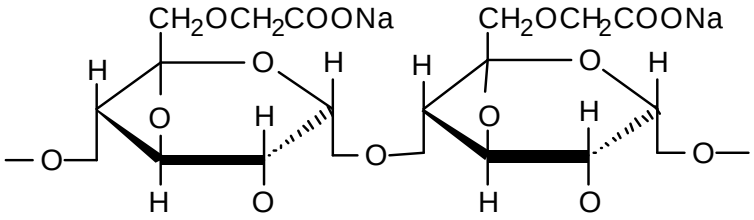

Fig. 2-12 Structure of CMA.

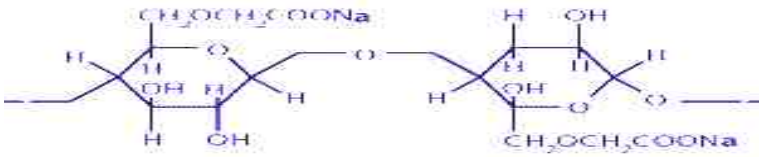

Fig. 2-13 Structure of CMC.

To understand in depth whether the topology of CMA and CMC had any changes induced by 2a, circular dichroism spectroscopy (CD) was performed (Fig. 2-14, 2-15). The results show that no detectable CD signal is produced in these systems of 2a/CMC and **1**/CMC, and no CD signal is observed for individual compound either, but strong signal can be induced in the systems of 2a/CMA and **1**/CMA. Giving that 2a, **1** are achiral, there must be a chiral product generated by the self-assembly. On the other hand, the absorption of the product is around 460 nm which only can be attributed to the self-assembly of **1** or 2a with CMA. So we can conclude that the **1** and 2a are able to induce the formation of helices of CMA while they are associating with it. To understand that CMC is not able to be induced to form the helices, computer modeling (Chem3D, Chemoffice suite) was applied for the structural study. We noticed that linear distances between anionic groups in CMA and CMC are 0.7154 nm and 1.2264 nm, respectively. We propose that the structural characteristics of CMC are favorable to form random assemblies instead of helices.

The kinetics of J-aggregation was investigated. Generally, J-aggregation is a very fast process because of the electro-static attraction. Time course experiments have been done in our system. Aliquots of CMC or CMA were added into 2a aqueous solution with stirring by pipette, followed by the immediate measurement of fluorescence to give intensity , after 30 min, fluorescence intensity was recorded. We found that no significant difference was observed. The fast formation of J-aggregation makes our assay time economic and good for real time analysis in the kinetic studies.

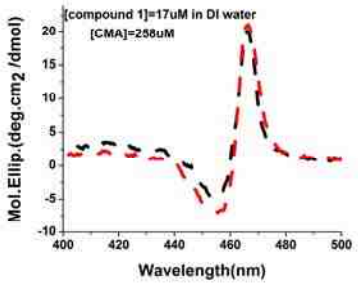

Fig. 2-14 CD spectrum for the system **1**/CMA.

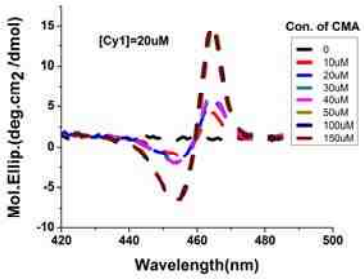

Fig. 2-15 CD spectrum for the system 2a/CMA

We have also tried other substrates, such as HA. But no significant J-aggregation occurs in these systems (Fig. 2-16, Fig. 2-17, Fig. 2-18, and Fig. 2-19). Instead, some decreased absorption was observed. Regarding the emission, the resulting product is nearly non-fluorescent. We believe the interactions between 2a and HA/clay are too weak to form J-aggregates. Most likely, there are some 2a precipitates produced during the addition of HA or clay because of Coulombic attraction between 2a and HA, which is consistent with the decrease of absorption.

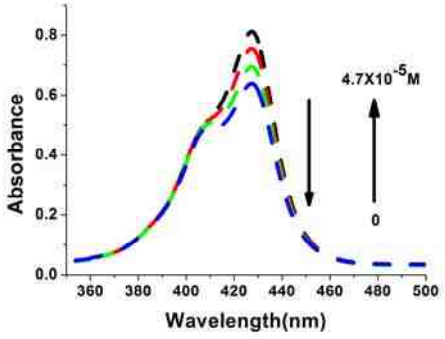

Fig. 2-16 Absorption spectra of 2a/HA with concentration at 10 μM.

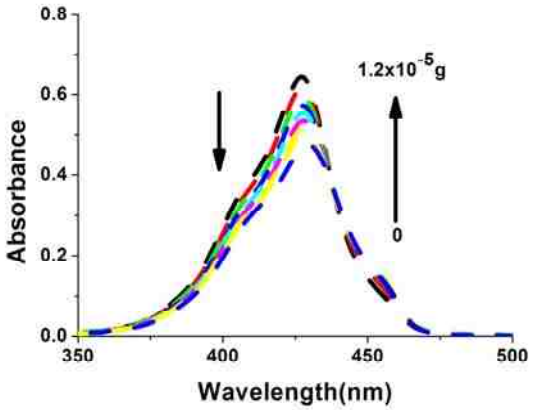

Fig. 2-17 Absorption spectra of 2a/clay with concentration at 10 μM.

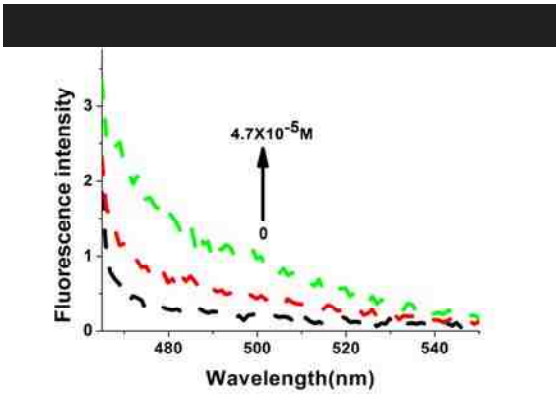

Fig. 2-18 Fluorescence spectra for the system of 2a/HA with concentration at at 10 μM.

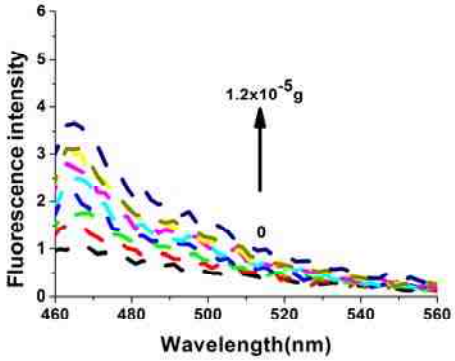

Fig. 2-19 Fluorescence spectra for the system of 2a/HA with concentration at at 10 μM.

2.4.2 Protease assay

2.4.2.1 Fluorescence Measurements

Fluorescence measurements were taken using a Molecular Devices (Sunnyvale, CA) microplate reader. Samples were excited over the wavelength range of 415-440 nm, and the emission intensity was measured at 470 nm. In some experiments, both the excitation and emission wavelengths were varied in order to achieve optimal conditions for fluorescence detection of DEVD-cyanine cleavage by protease. Fluorescence emission was corrected for the small extent (typically <10% of maximal fluorescence from the J-aggregate) of intrinsic light emission from the DEVD-cyanine intact substrate molecule. Microplate-based assays were designed, keeping the design principles described by us recently.[97]

2.4.2.2 Data Analysis

All reactions were carried out in triplicate, and the values were calculated as average (standard deviation for each determined parameter. Kaleidagraph software (version 4.03, Synergy software, Reading, PA) was used to generate the tracings shown for the various experiments. The control reaction giving the maximal background fluorescence was used to correct the signal arising from the complete enzymatic reaction. In these experiments, the low intrinsic fluorescence arising from DEVD-cyanine (minus the Caspase) was used for correction, and the resultant tracing was represented as relative fluorescence units (RFUs). Values are the average of triplicate measurements for each determined parameter.

Where not visible, error bars are masked within the symbol. The limits of detection and quantitation were calculated as described previously.[98] Data obtained from a study of the effects of the substrate concentration on the reaction velocity were transformed using the Eadie-Hofstee equation [V/(V/S)] using the software program EnzymeKinetics Pro! (version 2.36, SynexChem LLC, Fairfield, CA). This transformation allowed us to calculate the enzyme kinetic parameter Km. Km, sometimes called the Michaelis constant, involves the equilibrium between the formation of the enzyme-substrate (ES) complex as well as its breakdown into enzyme and products (E + P). While Km does not refer to the binding constant or binding strength of the substrate to the enzyme, it does encompass the affinity of the substrate for the enzyme as well as the rate at which the substrate bound to the enzyme is converted into product(s). A basic definition of Km is that it represents that concentration of a given substrate at which the enzyme-catalyzed reaction reaches half of the maximal velocity. Thus, Km = Vmax/2. In other words, a high Km value denotes a substrate that is not efficiently converted into product because it requires a larger concentration of substrate to achieve half of the maximal velocity. Conversely, a low Km indicates a greater affinity of the substrate for the enzyme and a higher rate of substrate conversion into product. In certain experiments, the S/B ratio was used to evaluate the data.

2.4.2.3 Results and discussion

In the present study, a protected tetrapeptide containing the canonical sequence Asp-Glu-Val-Glu (DEVD) for specific recognition by Caspase-3 and -7 was covalently

linked to a modified unsymmetrical cyanine (2a; Scheme 2-3). Compound 2a was synthesized in good overall yield by the scheme outlined in Scheme 2-3. The reactions used in this synthetic scheme can be generally useful for the synthesis of unsymmetrical cyanines for covalent attachment. Herein, 2a was coupled using N-hydroxysuccinimide activation with a synthetic protected peptide (DEVD) at the unprotected carboxyl terminus to afford a protected tetrapeptide. The protected peptide was then deprotected in a one-step reaction with trifluoroacetic acid in dichloromethane to yield the DEVD-cyanine peptide 3. The DEVD-cyanine peptide 3 was designed as a substrate for the proteases Caspase-3 and -7. As we expected, 2a is nonfluorescent (very low fluorescence quantum yield either in H_2O or in methanol), soluble in H_2O and polar organic solvents, such as DMSO, DMF, and methanol. But the fluorescence strength was dramatically enhanced when CMA or CMC solution was added into cyanine solution, the absorbance band approximately has 35 nm of red shift, and Stokes shift is about 6 nm for the complex of 2a and substrate. The phenomenon is responsible for J-aggregate formation between 2a and CMA or CMC. The J-aggregation behaves more structured with CMA than CMC at excited states of absorption, but the aggregation has stronger fluorescence with CMC than CMA. It is hard to form J-aggregate with the substrate Clay due to disk-like in shape of clay which is consistent with absorbance and fluorescence (Fig. 2-16, 2-17, 2-18, and 2-19). DEVD-cyanine can not form J or H type aggregate, which has been demonstrated by the titration experiment. The system did not show any new band in absorbance and fluorescence. We assume that the DEVD-cyanine is much

more favorable to form random complex with oppositely charged substrate like CMA or CMC since DEVD is a bulky group. Compound **1** is more favorable to form J-aggregate with CMA in comparison with 2a, however, 2a prefers to form J-aggregate with CMC.

The synthetic tetrapeptide 3 (DEVD-cyanine, shown as a deprotected peptide in Scheme 2-4) was selected as a prototype for a wide array of biomolecules incorporating a sequence that is recognized by a specific enzyme and can subsequently be reacted to release a reporter molecule, in this case 2a. The sequence recognized by Caspase-3 and -7 is a short tetrapeptide, DEVD.[91, 94, 99,] DEVD when linked to cyanine 2a and then deprotected is a dianion at neutral pH. As anticipated, DEVD-Cyanine in an aqueous solution did not associate with CMA or CMC, and the appended cyanine was non-fluorescent both in aqueous media and in aqueous solutions in the presence of anionic biopolymers such as CMA or CMC. However, the dicationic cyanine 2a (in neutral aqueous solutions) is released by the enzymatic cleavage of DEVD-Cyanine. For hydrolysis of the DEVD-cyanine substrate, we purchased Caspase-3 and -7 from Sigma-Aldrich. The enzymatic reaction was carried out essentially as described by us previously.[102] The “free” 2a that was liberated by enzymatic hydrolysis readily self-assembles upon CMC or CMA scaffolds to form a fluorescent J-aggregate and provides a sensitive assay of Caspase-3 and/or -7 to hydrolyze DEVD-Cyanine.

There was an increase in fluorescence between 450 and 550 nm emission wavelengths as a function of the enzyme concentration when Caspase-3 was incubated with 3 and then

either CMC or CMA was added post-catalysis (Fig. 2-20A). The excitation wavelength was varied from 415 to 440 nm in 5 nm intervals. For each excitation wavelength, fluorescence from the J-aggregates of the released cyanine 2a self-assembling upon the scaffold was measured over an emission wavelength range of 410-550 nm (Fig. 2-20A). It is important to note that in these experiments the intact DEVD-cyanine substrate did not self-assemble upon the carbohydrate scaffolds. Consequently, there were only very low levels of light emission from the substrate in the absence of the Caspase-3 enzyme. We considered this as background and either corrected for it (ΔRFU) or used the background emission values to calculate the ratio of signal to background (S/B). It was only the cleaved product, the "free" cyanine, which was capable of efficient self-assembly upon the twin carbohydrate scaffolds (Fig. 2-20 and 2-21). A clear increase in the fluorescence emission was particularly noticeable between wavelengths of 460 and 470 nm (Fig. 2-20B). The maximum fluorescence was detected at a peak emission wavelength of 470 nm (Fig. 2-20B). A chart of the S/B values showed that the excitation wavelengths between 420 and 440 nm gave optimum fluorescence emission without serious signal degradation due to the rising blank fluorescence (Fig. 2-21). At excitation wavelength values above or below this threshold, S/B declined, even though the fluorescence signal strength continued to increase up to 450 nm excitation wavelength and decline thereafter (Fig. 2-21). However, we considered the deterioration in the S/B values at excitation wavelengths of 450 nm or higher as unacceptable in the delivery of a robust protease assay. Therefore, in all further experiments, the emission wavelength was

fixed at 470 nm and the fluorescence from the reaction samples was measured by excitation of the samples between the wavelengths of 420 and 445 nm at 5 nm intervals. It is also important to note that the results shown in Fig. 2-20 and 2-21 were conducted under assay conditions that had not yet been sufficiently optimized. There were also some differences in the magnitude of the separation between the tracings of the various concentrations of Caspase-3 enzyme depending upon the excitation wavelengths (Fig. 2-20). These experiments were done for the sole purpose of establishing the optimal excitation and emission wavelengths. This might also explain the differences in the tracings of Fig. 2-20 compared to Fig. 2-22 that are discussed elsewhere in this dissertation.

The J-aggregation may be perturbed by enzymatic reaction components such as buffer salts, sodium chloride, detergent, or thiol reagent. We therefore investigated the effects of well volume upon the fluorescence emission intensity and S/B. We found that diluting the well volume 30-fold (96-well reactions) or 10-fold (384-well reactions) using a methanol/water mixture before adding CMA and CMC facilitated a more optimal self-assembly of the liberated cyanine upon the carbohydrate scaffolds. Preliminary experiments showed that for 96-well plate reactions a final well volume of 150-300 μL yielded maximum fluorescence emission and higher S/B values. The decline in the fluorescence intensity and S/B values observed with well volumes flanking these limits (50 and 100 μL and 350 and 400 μL, respectively) could be due to interference from

assay buffer components at lower volumes and suboptimal scaffold concentrations due to increased dilution at higher volumes. At the lower well volumes of 50 and 100 μL, there might also be an “inner filter effect” arising from the higher scaffold concentrations and resulting in a fluorescence quench.

Two different batches and lots of Caspase-3 were tested in order to confirm the hydrolysis of the DEVD-cyanine 3 substrate in our new high-throughput screening (HTS) assay system for proteases. The results were overall similar to those of proteolytic digestion of the substrate taking place linearly between Caspase-3 concentrations of 0.5 and 15 U/mL (or 0.1 and 1.0 μg/mL) and reaching a plateau in the reaction rate, thereafter indicating saturation of the reaction velocity (Fig. 2-22). Because the canonical sequence DEVD is recognized by both Caspase-3 and -7, our novel synthetic peptide substrate was hydrolyzed by both enzymes (see below for the data on Caspase-7). These reactions were demonstrated by two different investigators working in two separate laboratories located several miles apart. This showed the reproducibility, repeatability, and robustness of the assay.

We next investigated the reaction kinetics by conducting a time course of Caspase-3 hydrolysis of the DEVD-cyanine 3. The results are presented in Fig. 2-23 and show that the novel substrate was utilized rapidly and efficiently by Caspase-3. Hydrolysis of the DEVD-cyanine substrate was evident within 2 min of mixing of the enzyme at a concentration of 0.2 μg/mL with 250 μM substrate and incubating at 37 °C (Fig. 2-23).

These results are reminiscent of our earlier study with Caspase-3 enzyme. Saturation of the reaction was progressively reached between 20 and 90 min of reaction. The purpose of the experimental results described in Fig. s6 and 7 was to establish the initial reaction rate conditions wherein substrate depletion does not take place. Such conditions will enable us to determine the affinity constant for the DEVD-cyanine 3 substrate for the Caspase-3 enzyme (described below).

A rectangular hyperbola type of tracing was obtained when increasing concentrations of the DEVD-cyanine 3 substrate were titrated into reaction wells containing a constant amount of enzyme (10 U/mL) (Fig. 2-24A, B). This type of chart indicated that the classical Michaelis-Menten type of enzyme kinetics was operating during hydrolysis of the substrate by Caspase-3. There was a progressive increase in both blank-corrected fluorescence (Fig. 2-24A) and S/B (Fig. 2-24B) between DEVD-cyanine 3 concentrations of 10 and 250 μM. The Caspase-3 catalysis was saturated at concentrations greater than 250 μM. We utilized the Eadie- Hofstee transformation of these data to obtain an affinity constant of the substrate for the enzyme, a Km value of 22.7 (2.6 μM DEVD-cyanine 3. This value is similar to the micromolar Km values reported in the literature using substrates that contained the same canonical DEVD tetrapeptide sequence but different reporter molecules such as coumarin derivatives (fluorescent assays) or p-nitro derivatives (colorimetric assays).[100] This observation suggested that the catalytic behavior of the Caspase-3 enzyme was not significantly altered due to the cyanine

reporter group in our substrate relative to the chromogenic or fluorogenic reporter molecules tethered to the DEVD sequence in these earlier reports. We therefore used the 250 μM DEVD-cyanine 3 concentration routinely in our experiments, this value being 10-fold greater than Km and assured of substrate excess in order to maintain first-order reaction rate conditions.

We next focused our attention upon further assay optimization by determining the concentration of the carbohydrate scaffolds CMA and CMC necessary to generate maximal fluorescence following supramolecular self-assembly of the cyanine released from the DEVD-cyanine 3 covalent adduct through Caspase-3 catalysis. The results showed that a minimum concentration of approximately 20 μM CMA was necessary to detect fluorescence (Fig. 2-25). The fluorescence intensity increased linearly between 25 and 70 μM CMA followed by a decline between 150 and 300 μM CMA (Fig. 2-25). The reasons for the decline in fluorescence emission at high concentrations of the scaffold were documented by us previously and included perturbations to the J-aggregate and "inner filter" effects. We next fixed the CMA scaffold concentration at 65 μM and executed a titration experiment with increasing concentrations of CMC. The data showed that approximately 40 μM CMC resulted in a 3-fold increase in fluorescence over 65 μM CMA alone. On the basis of these results, we used a combination of 65 μM CMA and 35 μM CMC to effect scaffolding. We thus formulated a 1:1 mixture of 2 mM CMA and 1 mM CMC for addition to the reaction wells as described under the Materials and

Methods section of the chapter. By combining the twin scaffolds into a single solution, we also eliminated one operational step in the reaction protocol and simplified the assay conditions.

Fluorescence was detected immediately (less than 1 min) after the addition of the CMA + CMC scaffolds to the reaction wells. A 2-fold or greater increase in fluorescence resulted when the entire reaction mixture (post addition of the scaffolds) was allowed to incubate at room temperature (25 °C) for 30 min before taking fluorescence measurements (Fig. 2-25). This suggested a time dependence to the self-assembly process of cyanine upon the carbohydrate scaffolds, hinting at the self-assembly kinetics as well as the stability of the self-assembled ensemble. Thus, the self-assembly kinetics of the cyanine upon the carbohydrate scaffolds of CMC and CMA are also reminiscent of the self-assembly of the same cyanine upon various nucleic acid scaffolds of DNA and RNA as reported by us recently. Depending upon the end-user requirements, the overall assay may be configured for either speed (2 min Caspase-3 catalysis as seen in Fig. 2-22 and measurement of the fluorescence emission intensity “immediately”) or for greater sensitivity (by waiting 30 min post-addition of the scaffolds mixture before taking fluorescence measurements).

Finally, we executed the Caspase-7 assay using the DEVD-cyanine substrate in 384-well plates for documenting the activity of this enzyme toward our novel peptide cyanine substrate and for qualifying our assay to the HTS format appellation. The results are presented in Fig. 2-11. Caspase-7 also utilized DEVD-cyanine as a substrate because it

too recognized the canonical DEVD tetrapeptide sequence. Similar to Caspase-3 reaction kinetics (Fig. 2-23), the Caspase-7 reaction proceeded linearly up to 20 min and began to plateau thereafter. The data scatter observed in Fig. 2-27 required a polynomial (second-order) curve fit using Kaleidagraph, unlike the interpolative tracings of Fig. 2-23. We attribute the data scatter to manual pipetting operations with the tiny wells of a 384-well microplate. Such scatter might be eliminated through robotic liquid handling, enabling more precise reagent dispensing and mixing that is a routine practice in high-throughput industrial laboratories.[97] It must be noted that we have not yet optimized the protease assay completely in the 384-well plate format with either Caspase-3 or -7. Such optimization will also involve a thorough characterization of Caspase-7 kinetic parameters with the DEVD-cyanine substrate (for example, Km).

In conclusion, we demonstrated the utility of supramolecular self-assembly processes to generate a new class of enzyme substrates. Potentially, our substrate may be used to detect intracellular Caspase-3 and -7 activities because the cyanine also self-assembled upon nucleic acid scaffolds of DNA and RNA in addition to the carbohydrate scaffolds. In this respect, our substrate is at the same time similar and different from the thiazole orange derivative of a DNA intercalating dye that was coupled to DEVD as a substrate for caspases[101]. We are aware that the cyanine J-aggregate fluorescence is sensitive to environmental milieu[102] and that the toxicity (cytotoxicity and anti-proliferative activities) or the lack thereof of the cyanines[103,104] will influence any utilities involving intracellular

events tracking.

The cyanine dye offers the prospect of self-assembly upon a broad range of scaffolds including CMA, CMC, HA, and single- and double-stranded, linear, or circular DNA and RNA. Future studies will also involve the coupling of other signaling molecules in addition to cyanine as well as the exploration of other types of organic and inorganic scaffolds (such as proteins and clay nanoparticles) for the sensitive detection of a wide range of biochemical analytes. We plan to use our novel scaffold formation, disruption, destruction, or dye release enzymatic assays in a HTS format for the multiplexed, in vitro detection of a broad range of chemical biological analytes.

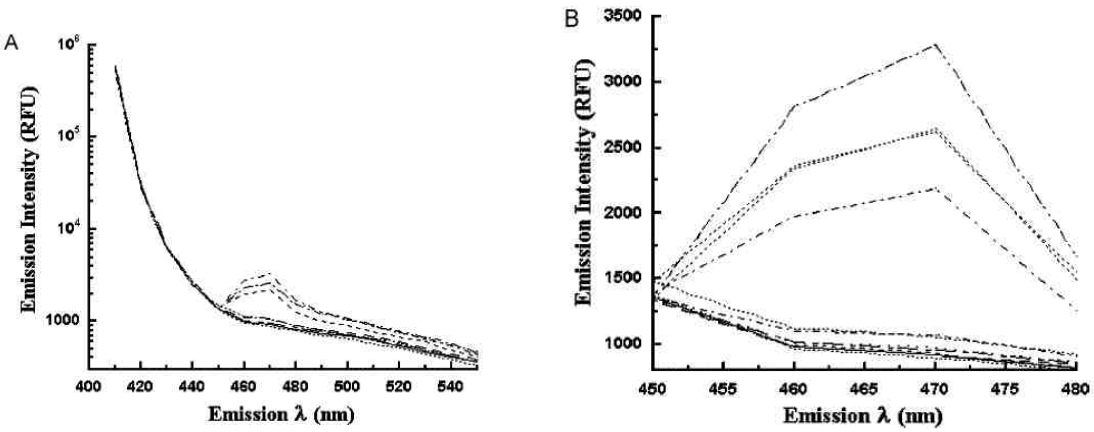

Fig. 2-20 (A) Emission wavelength scan of the reactions of DEVD-cyanine with increasing concentrations of Caspase-3. Only a representative example of the scan for λex) 400 nm is shown in this Fig. . The various tracings represent progressively increasing concentrations of Caspase-3 (0, 1, 2.5, 5, 10, 15, 30, and 60 U/mL) utilized to catalyze the hydrolysis of the DEVD-cyanine substrate. Fluorescence emission was

scanned over the indicated wavelength range in 2 nm intervals. (B) Exploded view of the desired range of fluorescence emission wavelengths between 450 and 480 nm. This Fig. 2-20 is intended to show clearly the Caspase-3 concentration dependent increase in the peak fluorescence at 470 nm.

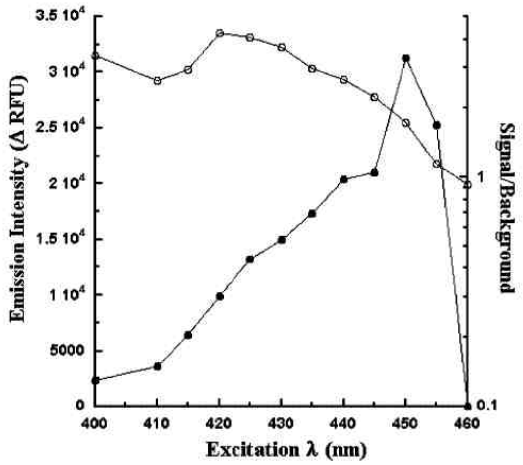

Fig. 2-21 Effect of the excitation wavelength on the fluorescence emission intensity at 470 nm and the S/B of Caspase-3 catalysis. Caspase-3 (30 U/mL) was used to catalyze the hydrolytic reactions of DEVD-cyanine. The open circles represent the S/B values, and the closed circles represent the fluorescence emission intensity corrected for background fluorescence (ΔRFU) from DEVD-cyanine in the absence of enzyme. The reaction samples were scanned over excitation wavelengths of 400-460 nm in 5 nm intervals.

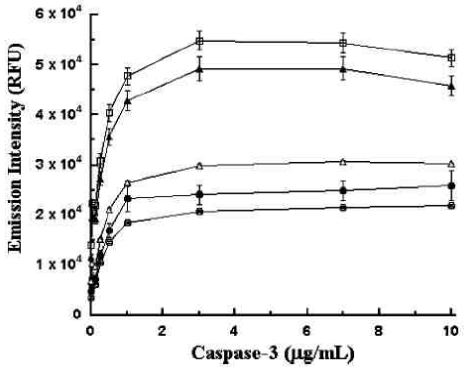

Fig. 2-22 Caspase-3 dose-response chart. Increasing and indicated concentrations of Caspase-3 enzyme were reacted with 250 μM DEVD-cyanine substrate at 37 °C for 90 min. The various tracings represent increasing fluorescence emission intensities observed at 470 nm emission wavelength and several different excitation wavelengths as follows: open circles, 420 nm; closed circles, 425 nm; open triangles, 430 nm; closed triangles, 435 nm; open squares, 440 nm. All other conditions are as described in the Materials and Methods.

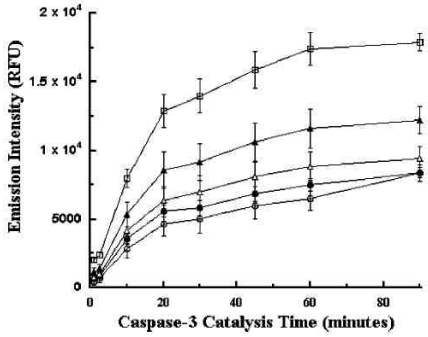

Fig. 2-23 Caspase-3 reaction kinetics. This chart shows the reaction progress curves for Caspase-3-catalyzed hydrolysis of the DEVD-cyanine substrate. Caspase-3 (0.2 μg/mL) was reacted with 250 μM substrate at 37 °C for the indicated reaction time periods. All other conditions were as described in the legend of Fig. 2-22.

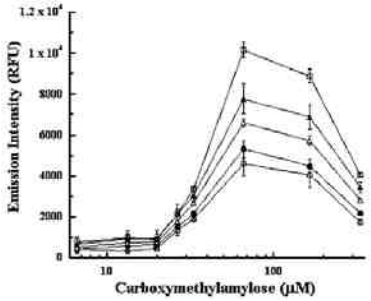

Fig. 2-25 Optimization of the CMA scaffold. Increasing and indicated concentrations of the CMA scaffold were added to 0.2 μg/mL Caspase-3-catalyzed reactions carried out at 37 °C for 30 min. The fluorescence emission was monitored at 470 nm following excitation of the samples at 420 nm (open circles), 425 nm (closed circles), 430 nm (open triangles), 435 nm (closed triangles), and 440 nm (open squares).

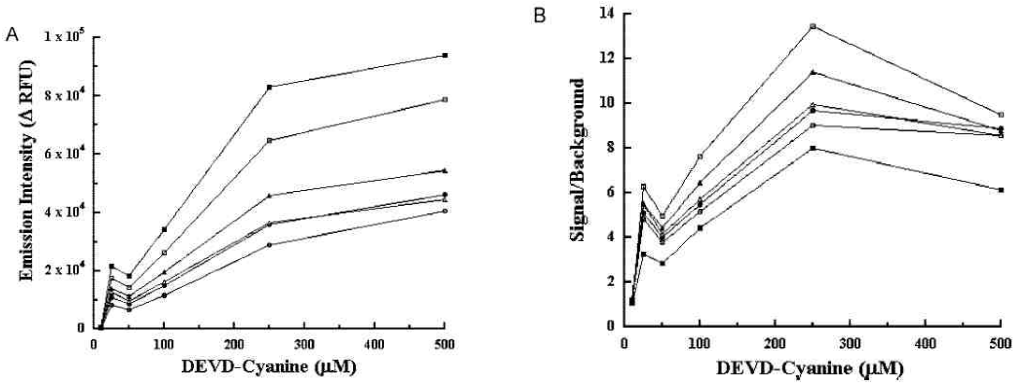

Fig. 24 (A) DEVD-cyanine substrate dose-response curves. Increasing and indicated concentrations of the DEVD-cyanine substrate was reacted in the presence and absence of Caspase-3 under conditions described in the legends of Fig. 22 and 2-23.

A substrate concentration-dependent increase in the fluorescence emission intensity was observed up to 250 μM DEVD-cyanine, followed by a plateau at 500 μM substrate. The reaction samples were monitored for emission at 470 nm following excitation at the several different wavelengths of 420 nm (open circles), 425 nm

(closed circles), 430 nm (open triangles), 435 nm (closed triangles), 440 nm (open squares), and 445 nm (closed squares).

It is seen that the fluorescence emission intensity increases as the excitation wavelength increased from 420 to 445 nm. (B) Effect of the DEVD-cyanine concentration upon S/B. All reaction conditions were as described in the legend of part A. Unlike the fluorescence emission intensity (Fig. 24A), the S/B increased with increasing excitation wavelength only up to 440 nm. The S/B at 445 nm was sharply lower relative to the S/B values observed at the other excitation wavelengths.

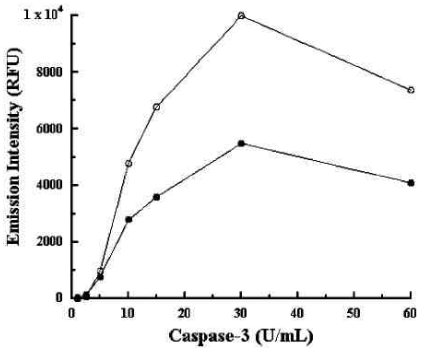

Fig. 26 Self-assembly kinetics. Increasing and indicated concentrations of the Caspase-3 enzyme was reacted with a 50 μM DEVD-cyanine substrate at 37 °C for 2 h. Fluorescence emission was detected immediately after the addition of the CMA + CMC scaffolds mixture (closed circles) or 30 min postaddition of the scaffolds (open circles). All other conditions were as described in the Materials and Methods section of the dissertation.

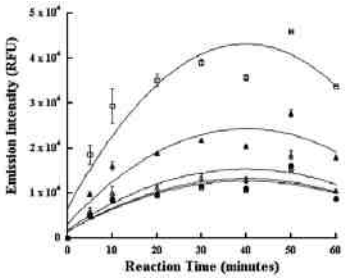

Fig. 27 Caspase-7 HTS assay format. In this experiment, 2 μg/ mL of Caspase-7 was reacted with 500 μM DEVD-cyanine in an assay buffer at 37 °C for the indicated reaction periods. Caspase-7 catalysis was stopped at the various time intervals by diluting the reaction well volume to 95 μL using a methanol/water mixture. At the end of 60 min, the CMA and CMC scaffolds mixture was added to the wells, followed by fluorescence measurements. The reaction samples were monitored for fluorescence emission at 470 nm following excitation at 420 nm (open circles), 425 nm (closed circles), 430 nm (open triangles), 435 nm (closed triangles), and 440 nm (open squares).

2.5 Summary of this chapter

(1) Two cyanines were synthesized: 2a and Cy2. A synthetic method has been developed for the synthesis of unsymmetric cyanines with high overall yield which possibly can be applied for other unsymmetric cyanine synthesis.

(2) Study of self-assembly: Both cyanines are very weak or non-fluorescent dyes, but strong fluorescence will be induced upon addition of some biomolelcules such as CMA and CMC, and the red-shifted peak is characterized by J-aggregate. We also found 2a could induce the formation of helices by determination with Circular

Dichroism.

(3) Development of a biosensor based on DEVD-Cyanine. The DEVD-Cyanine is non-fluorescent, but strong fluorescence can be induced once DEVD-Cyanine is cleaved by Caspase-3/7 following by the addition of CMC/CMA solution. The dramatic fluorescence enhancement could be used for assaying Caspase-3/7, which has been demonstrated in this dissertation.

Chapter 3 Synthesis and photophysics of S-OPE-1s and EO-OPE-1s

3.1 Introduction

In chapter 1, we have reviewed synthesis and photophysics of OPEs. We have been interested in the studies of photophysics such as photobleaching, quenching, triplet state, sensitization of OPEs to generate singlet oxygen, and host-guest chemistry. We hope these studies could give us an insight into the relationship of structure and reactivity. Meanwhile, these oligomers can serve as light-induced biocides for biocidal studies.

We previously reported four cationic OPEs and one zwitterionic OPE with remarkable photophysical properties.[80,105] (Fig. 3-1) All of these molecules are solid and readily soluble in water and organic solvents such as methanol, DMF, and DMSO. The synthesis for these molecules is straightforward but low yields were obtained for steps involving the conversion of diiodo compounds to mono-substituted iodo compounds (for asymmetric OPEs). Interestingly, these molecules have two absorption bands at 300/325 nm for OPE-1 and 320/375 nm for OPE-2 (Fig. 3-2). Further studies by computer modeling in another group indicate that these molecules have two HOMOs and one LUMO, therefore two transitions from HOMO-1 to LUMO and HOMO-2 to LUMO may occur when OPEs are excited, which are responsible for two absorption bands (Fig. 3-3).[106] These molecules are moderately fluorescent and fluorescence quantum yields are recorded in the Table 3-1 and 3-2. Except for S-OPE-1(H), all other OPEs have poor fluorescence quantum yields in H_2O, but good in CH_3OH

(Table 3-1, 3-2). However, a very high Φ_F was obtained for S-OPE-1(H) in H_2O. Another notable feature of S-OPE-1(H) is its relatively high triplet state yield. Kinetic quenching might contribute to the low Φ_F of OPE-1, OPE-2, S-OPE-1(COOEt), and S-OPE-1(COO^-) in H_2O. In contrast, these compounds have much higher Φ_F in CH_3OH than in H_2O due to less solvent quenching and self-quenching occurring in these systems.

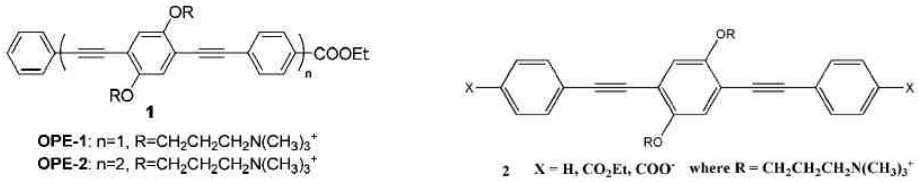

Fig. 3-1 The structure of OPE-1, OPE-2 (the structure on the left) and S-OPE-1s (the structure on the right) with X=H, CO_2Et, COO^- and R=$CH_2CH_2CH_2N(CH_3)_3^+$.

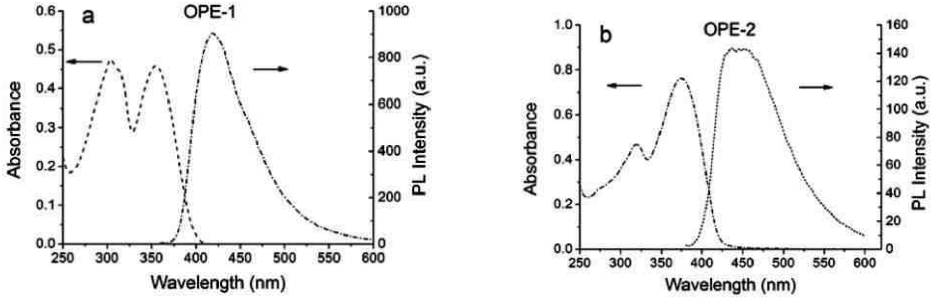

Fig. 3-2 Absorbance and fluorescence spectra of OPE-1 and OPE-2 in water. [OPE-1] = [OPE-2] = 15 μM. OPE-1 and OPE-2 are excited at 355 and 375nm, respectively. [80]

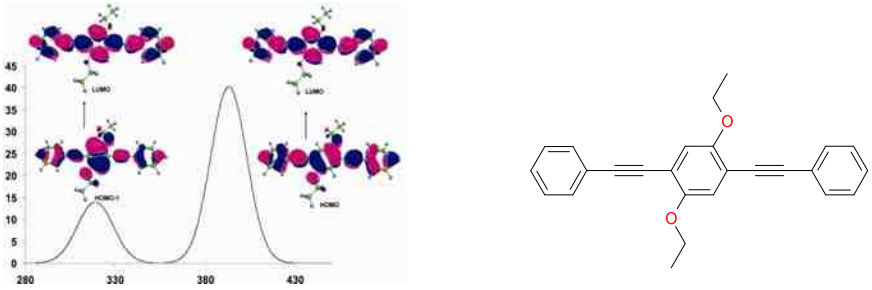

Fig. 3-3 A simplified model for substituted OPE. The absorption bands are due to two transitions of HOME-1 to LUMO and HOMO-2 to LUMO, respectively. [106]

compound	solvent	Φ_f	τ_f (ns)
OPE-1	H_2O	0.15	0.78
	methanol	0.68	1.57
OPE-2	H_2O	0.01	0.37
	Methanol	0.68	0.92

Table 3-1. Fluorescence quantum yields and fluorescence lifetimes for OPE-1 and OPE-2. [80]

	Abs. (nm)	Em. (nm)	ϕ_f in H_2O	τ (ns)	τ_{TA} (μs)	ϕ_f in CH_3OH	τ (ns)
OPE-1	303, 355	420	0.15 ± 0.018	1.5	107	0.68 ± 0.028	1.6
S-OPE-1 (H)	303, 348	397	0.80 ± 0.011	1.6	216	0.82 ± 0.030	1.4
S-OPE-1 (COO^-)	310, 355	422	0.70 ± 0.010	1.5	136	0.74 ± 0.042	1.3
S-OPE-1 (COOEt)	314, 362	465	0.023 ± 0.001	1.0	77	0.75 ± 0.019	1.4
OPE-1/CMC[b]	325, 381	472	0.34 ± 0.004				
S-OPE-1 (H)/CMC[c]	308, 318, 367	423	0.81 ± 0.017				
S-OPE-1 (COOEt)/CMC	333, 412	458	0.39 ± 0.023				

[a] The standard is quinine sulfate.
[b] The quantum efficiency is obtained where the concentration of OPE-1 or S-OPE-1 (H) is 1×10^{-5} M.

Table-3-2. Absorption, emission, fluorescence quantum yields in H_2O and CH_3OH, fluorescence lifetimes, and triplet state lifetimes for S-OPE-1s. [105]

Whitten's group has also studied the self-assembly behavior of OPEs in H_2O. Basically, OPE-2 and S-OPE-1(COOEt) are capable of self-assembling onto CMA and CMC scaffolds to form J-aggregates or planarization (Fig. 3-4, 3-5), however no characteristic J-aggregates were observed for S-OPE-1(H) and zwitterionic

S-OPE-1(COO^-) in a neutral condition. Upon the addition of CMC solution, the resulting spectral pattern shows red shifts both for absorption and fluorescence with Stoke shifts being 83 nm and 75 nm for OPE-1 and OPE-2, respectively. There are 5-fold and 13-fold enhancement in fluorescence intensity for OPE-1 and OPE-2, respectively. These oligomers are expected to have little barrier to rotation of the phenyl groups in the ground state (which is consistent with computational results), so the changes in absorption spectra can be attributable to planarization.[134] However, a recent study of OPEs structurally related to OPE-1 suggests that whereas rotation should be restricted very little a planar ground state is the lowest energy form.[106, 133] Interestingly, the authors obtain similar absorption and fluorescence spectra to those shown in Fig. 3-2 and calculate absorption spectra having similar transition wavelengths for conversion of the planar ground state to the excited state. The study also suggests that fluorescence should occur from a planar excited state, and thus we infer that planarization should involve some shifts in absorption and small shift in emission considering the great enhancement in emission intensity. Coupled with π-π stack effect, spectral changes can be attributed to monomeric planarization or J-aggregation. This phenomenon could occur with assistance of CMA, CMC as well as vesicles.[133]

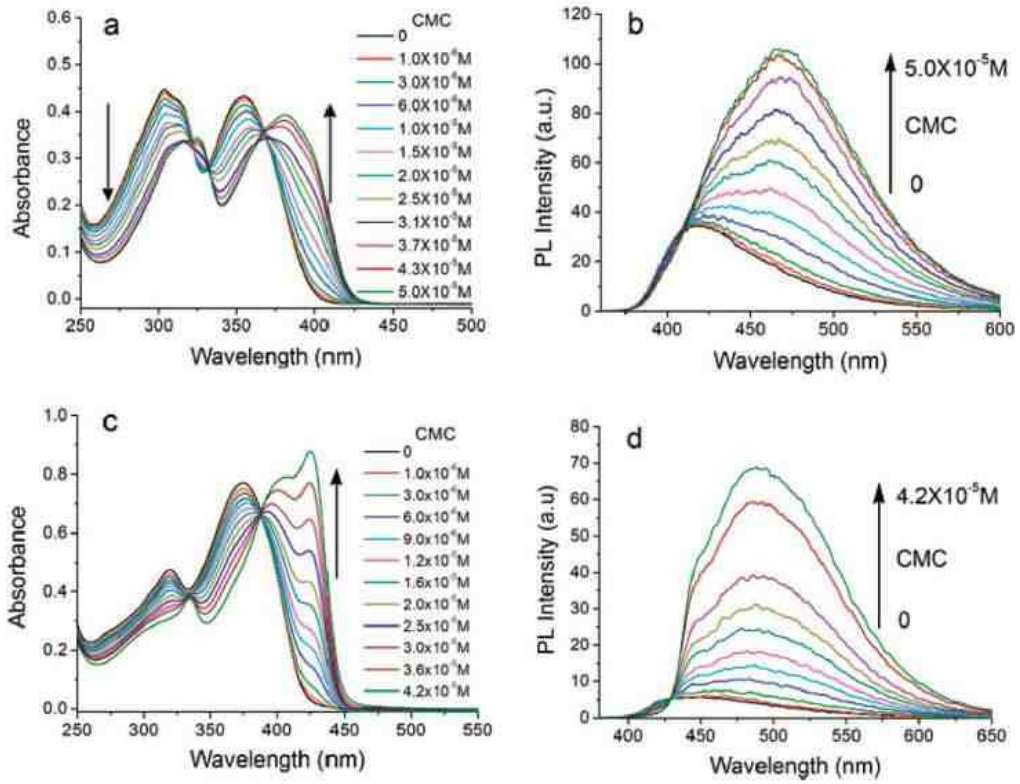

Fig. 3-4 (a) Absorption spectra of OPE-1 upon addition of CMC. [OPE-1] = 1.5 × 10^{-5} M. (b) Fluorescence spectra of OPE-1 upon addition of CMC. [OPE-1] = 1.5 × 10^{-5} M and [CMC] = 0 ~ 5.0 × 10^{-5} M. (c) Absorption spectra of OPE-2 upon addition of CMC. [OPE-2] = 1.5 × 10^{-5} M. (d) Fluorescence spectra of OPE-2 upon addition of CMC. [OPE-2] = 1.5 × 10^{-5}M and [CMC] = 0 ~ 4.2 × 10^{-5} M. Both excitation and emission slits are 2.5 nm. Excitation wavelength for OPE-1 and OPE-2 is 355 nm and 375 nm, respectively.

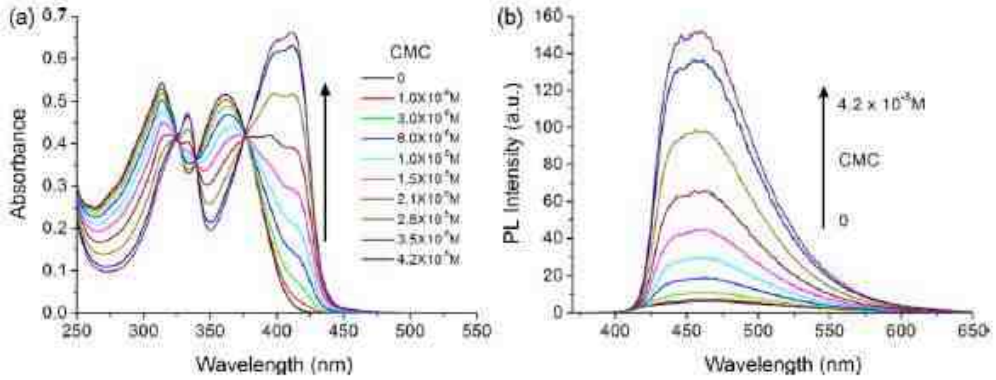

Fig. 3-5 Absorption spectral changes (a) and fluorescent spectral changes (b) upon addition of aliquots of CMC to an aqueous solution of S-OPE-1 (COOEt).

[S-OPE-1(COOEt)] = 15 μM, [CMC] = 0~42 μM, ex. 362 nm.

Based on these results, we decided to synthesize a new class of OPEs with quaternary ammonium salts on both ends (EO-OPE-1s), and to study in depth the relationship between structure and reactivity. We also synthesized more S-OPE-1s by functionizing both ends with different functional groups.

3.2 Materials and methods

EO-OPE-1s, S-OPE-1s, and all synthetic intermediates were synthesized through multi-step reactions; 2,5-diiodothiophene, ethynyl(trimethyl)silane, 2,2-dioxide,3-chloro-N, CuI, diisopropylamine, N-dimethyl-propan-1-amine, K_2CO_3, potassium biocarbonate, pd catalyst, Oxathiolane, Calf-thymus DNA, 2-chloro-N,N-dimethyl-ethanamine, CMA (D.S.=0.7), CMC, 4-iodoaniline, AQS, 1,4-diiodo-2,5-dimethoxy-benzene, ethyl 4-benzoate, 4-iodophenol, 1-(4-iodophenyl)ethanone, Sodium hydroxide, hydrogen chloride acid, 1,4-dimethoxy benzene, boron tribromide, sodium iodate, potassium iodide, acetic acid, and 1,4-diiodobenzene were purchased from Sigma-Aldrich (St. Louis, MO) and used as

received. Solvents were HPLC grade and purchased from Honeywell (Morristown, NJ) and no further purification was applied.

For the absorption and fluorescence spectroscopy, a stock solution was prepared with concentration of 1 mM and 10% v/v solution of DMSO in H_2O. 30 μL of the suspension of each EO-OPE-1 or S-OPE-1 was diluted into 3 mL aqueous solution in a quartz cuvette to give the concentration of 10 μM. Absorption and fluorescence were recorded on a Molecular Device (SpectroMax M-5 microplate reader, Molecular Devices) at 24^{o}C. Transient absorption spectra were recorded for EO-OPE-1 samples both in methanol and water (Anand Parthasarathy, University of Florida) using laser systems that are described elsewhere.[107,108] The optical density was adjusted to ~0.7 at the excitation wavelength 355 nm with the laser energy being 6~7 mJ. Solutions were purged with argon for 45 min before making transient absorption spectroscopy measurements.

3.3 Synthesis and characterization

The general methods for the synthesis of S-OPE-1s (Fig. 3-6) are straightforward, and Sonogashia coupling is the key steps. 1,4-diiodo-2,5-dimethoxy benzene was generated through iodization of 1,4-dimethoxy benzene in the presence of iodide, sodium iodate, sulfuric acid, H_2O, and acetic acid. Compound f was the key intermediate for the following steps and obtained by subsequent reduction of b, electrophilic substitution with 3-chloro-N,N-dimethyl-propan-1-amine hydrogen chloride, Sonogashia coupling with ethynyl(trimethyl)silane and deprotection of TMS. The final products were obtained by the Sonogashia coupling of f with 4-iodoanisole,

methyl l,4-iodobenzoate, 4-iodobenzene, 4-iodoaniline, or 3-(4-iodophenoxy)-N,N-dimethyl-propan-1-amine followed by the conversion into salts. Basically, the purification for intermediates was performed through column chromatography, but target molecules were purified by washing with organic solvents, such as dichloromethane and acetone. Further purification could be accomplished through recrystallization in ethanol. ^{1}H NMR, ^{13}C NMR, and Mass Spectroscopy were used for the structural determination.

The general methods for the synthesis of EO-OPE-1s (Fig. 3-7) are straightforward, and key steps are Sonogashia coupling too. 2 was obtained by Sonogashia reaction of 1,4-diodobenzene with ethynyl(trimethyl)silane and deprotection of 1. A and B were obtained by the Sonogashia coupling of 2 with 6 and 5, respectively, followed by reacting with iodomethane. 4 was obtained by the reaction of 2,5-dibromothiophene with ethynyl(trimethyl)silane and deprotection of 3. C was obtained by Sonogashia coupling of 3 and 5 subsequent reacting with iodomethane. D was obtained by Sonogashia coupling of 2 and 7. Basically, the purification for intermediates was performed through column chromatography, but target molecules were purified by washing with organic solvent, such as dichloromethane and acetone. Further purification was carried out through recrystallization in ethanol. ^{1}H NMR, ^{13}C NMR, and Mass spectroscopy were used for the structural determination.

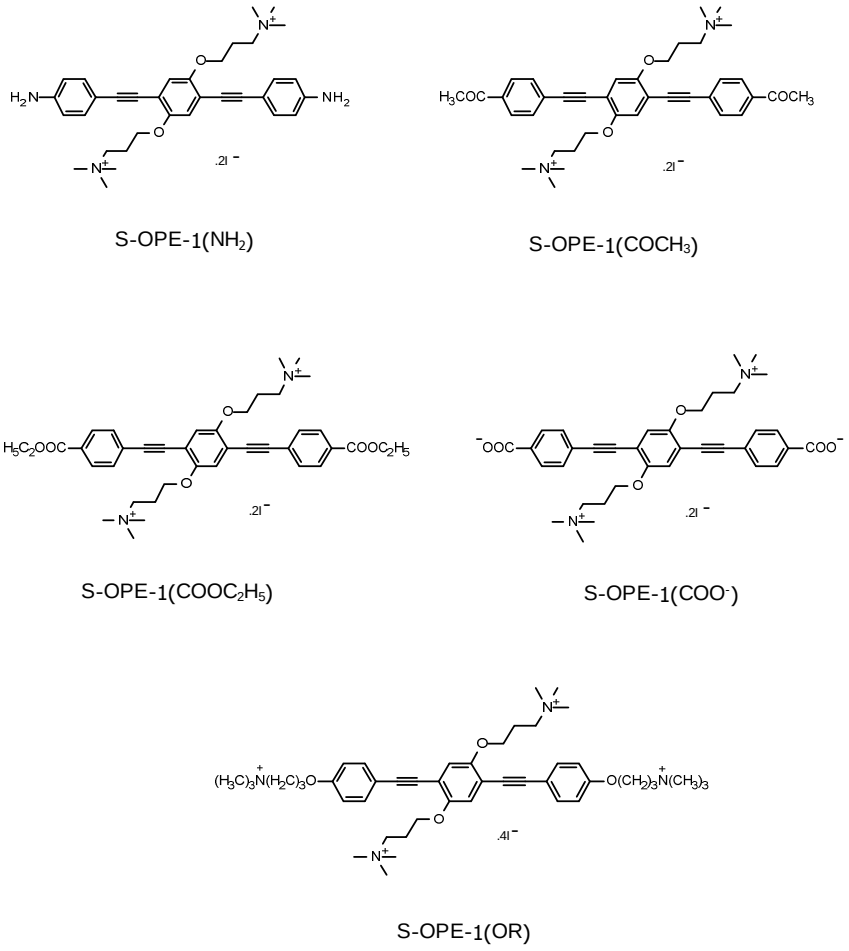

Fig. 3-6 Structures of S-OPE-1s. S-OPE-1(H), S-OPE-1(COOEt), S-OPE-1(COO^-), S-OPE-1(NH_2), S-OPE-1($COCH_3$), S-OPE-1(OR).

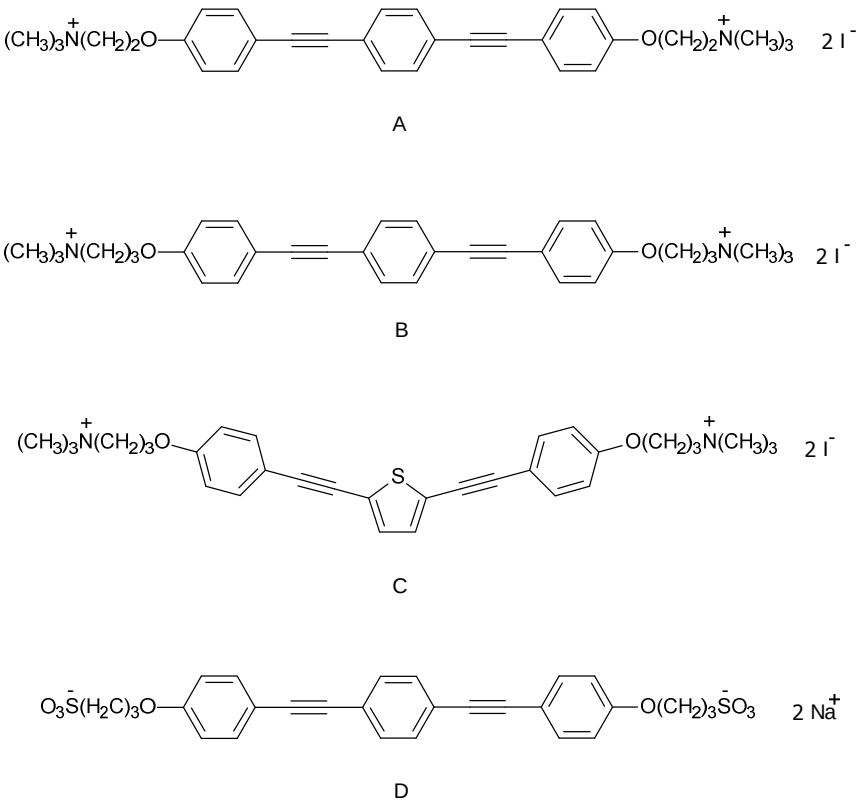

Fig. 3-7 Structures of EO-OPE-1s. A: EO-OPE-1(C2), B: EO-OPE-1(C3), C: EO-OPE-1(TH), D: EO-OPE-1(SO3). Note that A, B and D contain the same conjugated backbone, and C contains a thiophene ring in the middle.

3.3.1 Synthesis of S-OPE-1s

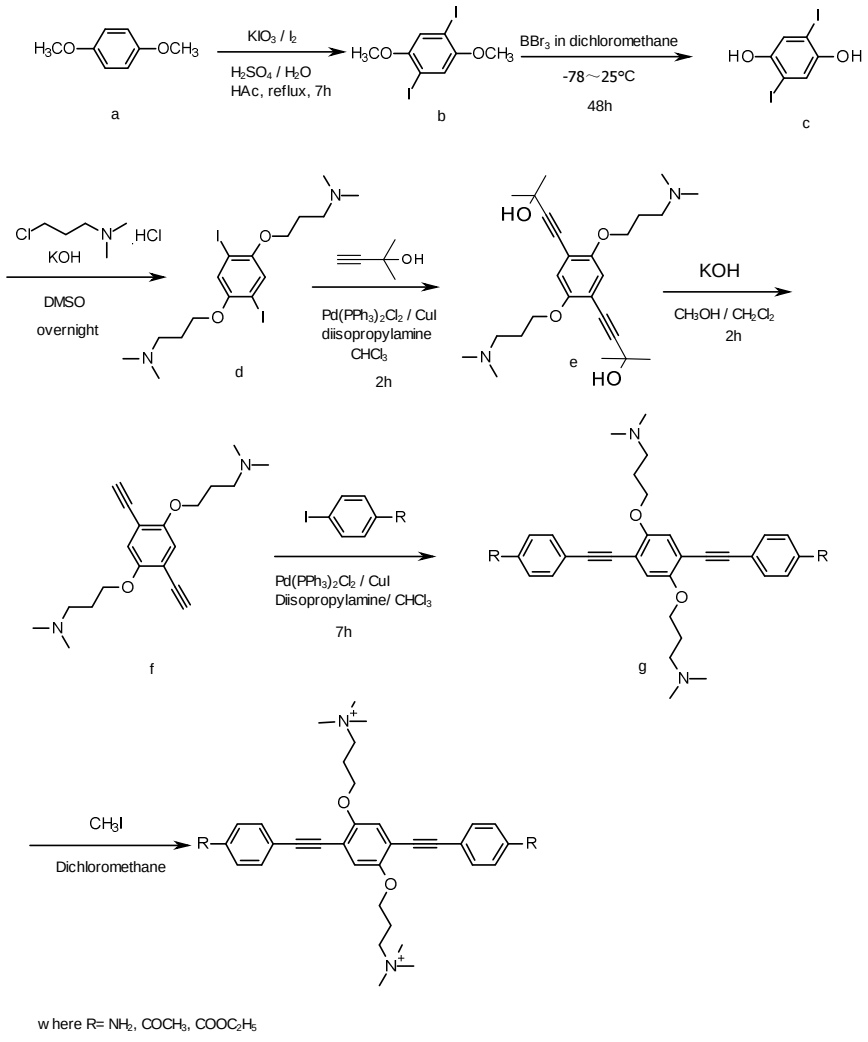

Scheme 3-1 Synthesis of S-OPE-1(NH_2), S-OPE-1(OR), S-OPE-1($COCH_3$)

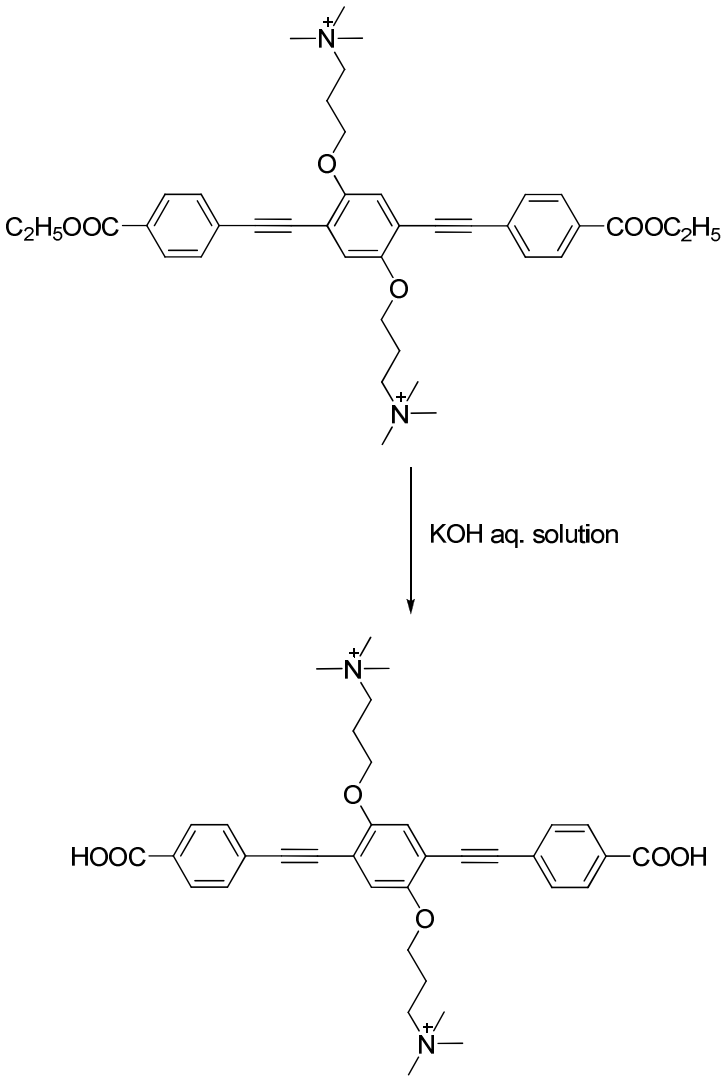

Scheme 3-2 Synthesis of S-OPE-1(COO^-)

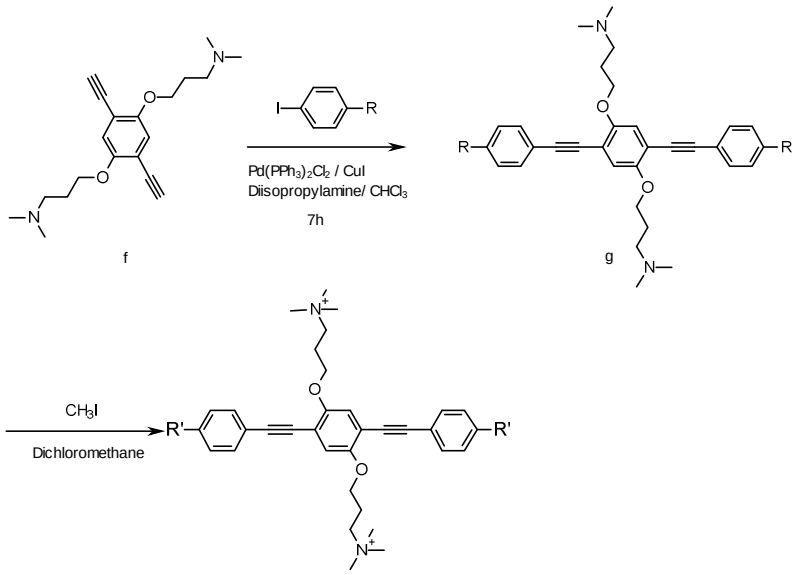

Scheme 3-3 The synthesis of S-OPE-1(OR)

Synthesis of b,c,d,e,f: see reference 105

Synthesis of g

General procedure for the synthesis of S-OPE-1(NH_2), S-OPE-1($COCH_3$), S-OPE-1($COOC_2H_5$): f was dissolved in a mixture of $CHCl_3$ and diisopropylamine, and degassed by purging with argon for 30 min. Then 4- iodo compound, $Pd(PPh_3)_2Cl_2$ (4 mol %), and CuI (8 mol %) were added. The mixture was allowed to react overnight, and the resulting reaction product was diluted with dichloromethane and washed with NH_4Cl, H_2O, and saturated NaCl. The organic layers were combined and dried over anhydrous $MgSO_4$ for 30 min, and filtration was conducted to remove $MgSO_4$. The solvent was removed by vacuum rotary evaporation, and residue was purified by column chromatography to give a yellow solid, followed by washing with

acetone and drying in a vacuum desiccator.

Synthesis of S-OPE-1(NH_2), S-OPE-1($COCH_3$), S-OPE-1($COOC_2H_5$), S-OPE-1(OR)

General synthetic procedure for the synthesis of target molecules: iodomethane was added into the solution of g and dichloromethane. The mixture was stirred for one hour followed by filtration to collect the solid.

^{1}H NMR (500 MHz, DMSO-d^6) for S-OPE-1($COCH_3$) δ 8.027 (d, *J=8*, 4H), δ 7.702 (d, *J=8*, 4H), δ 7.312 (s, 2H), δ 4.178 (t, 4H), δ 3.256 (t, 4H), δ 2.805 (s, 18H), δ 2.606 (s, 6H), δ 2.189 (m, 4H).

^{1}H NMR (500 MHz, DMSO-d^6) for S-OPE-1(OR) δ 7.519 (d, *J=8.5*, 4H), δ 7.221 (s, 2H), δ 7.028 (d, *J=8.5*, 4H), δ 4.136 (m, 8H), δ 3.518 (m, 8H), δ 3.107 (m, 36H), δ 2.223 (m, 8H).

Synthesis of S-OPE-1(COO^-): See reference 105

3.3.2 Synthesis of EO-OPE-1s

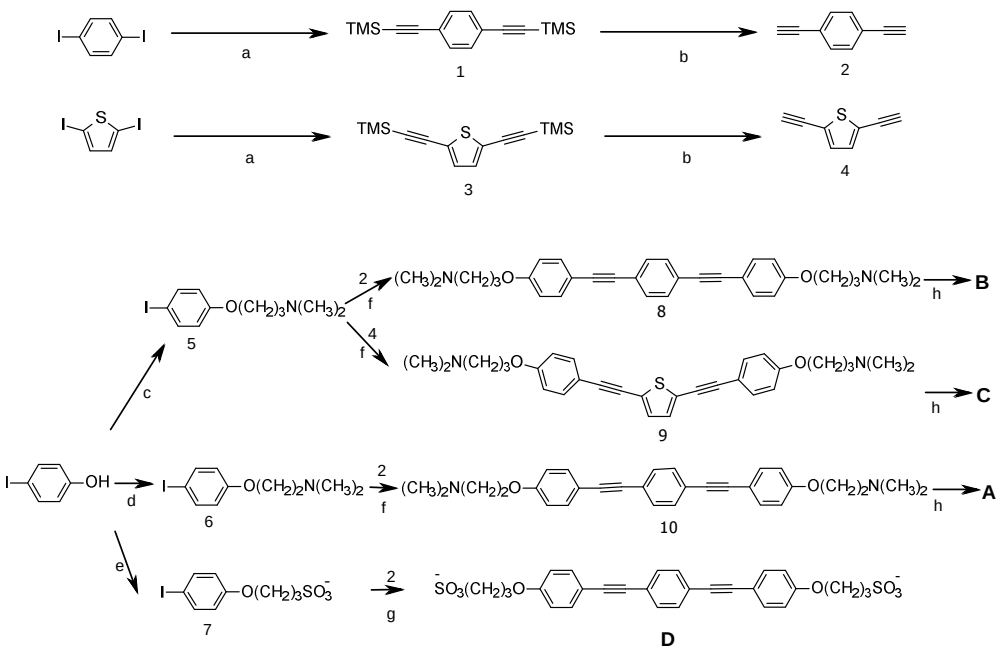

Scheme 3-4 the synthesis of EO-OPE-1(C2), EO-OPE-1(C3), EO-OPE-1(TH), and EO-OPE-1(SO3). (a) trimethyl silyl acetylene, $Pd(PPh_3)_2Cl_2$, CuI, diisopropylamine, $CHCl_3$, (b) K_2CO_3, CH_3OH, CH_2Cl_2, (c) KOH, DMSO, 3-chloro-N,N-dimethyl-propan-1-amine, (d) 2-chloro-N,N-dimethyl-ethanamine, (e) NaOH, dioxane, H_2O, oxathiolane, (f) $Pd(PPh_3)_2Cl_2$, CuI, diisopropylamine, $CHCl_3$, (g) $Pd(PPh_3)_2Cl_2$, CuI, H_2O, diisopropylamine, (h) CH_3I, CH_2Cl_2.

Compound 1, 2, 3, and 4 were synthesized according to literature procedures[109,110].

Synthesis of 5

A solution of 4-iodophenol (1 g, 4.54 mmol) in DMSO (5 mL) was prepared, then 3-chloro-N, N-dimethylpropylamine hydrochloride (2.73 g, 17.16 mmol) and crushed potassium hydroxide (2.5 g, 44.54 mmol) were added. The suspension was stirred at room temperature overnight. The resulting mixture was poured into 100 mL of H_2O to give a precipitate. The solid was collected by filtration, and the solid was washed with

H_2O 3 times and dried in a vacuum desicator to give 1.24 g of white solid. Yield: 89%. ^{1}H NMR ($CDCl_3$, 500 MHz), δ 7.544 (d, *J=9*, 2H), δ 6.687 (d, *J=9*, 2H), δ 3.986 (t, *J=6.5*, 2H), δ 2.455 (t, *J=6.5*, 2H), δ 2.251 (s, 6H), δ 1.969 (m, 2H).

Synthesis of 8

5 (1.53 g, 5.01 mmol), $CHCl_3$ (21 mL), and diisopropylamine (2 mL) were mixed and degassed by purging with argon for 30 min. 2 (383 mg, 3.0 mmol), $Pd(PPh_3)_2Cl_2$ (92 mg, 0.131 mmol) and CuI (46 mg, 0.24 mmol) were added to the mixture which was stirred overnight. The salt formed in the process was removed by filtration, and the solution was extracted with dichloromethane and washed with NH_4Cl solution, H_2O, and saturated NaCl. The organic layer was dried over anhydrous $MgSO_4$ for 30 min, and filtered to remove the $MgSO_4$. The solvent was removed by vacuum rotary evaporation, and the residual solid was purified by column chromatography using a mixture of CH_2Cl_2 and CH_3OH to give 520 mg of a white solid. Yield: 22%. ^{1}H NMR ($CDCl_3$, 500 MHz), δ 7.444 (m, 8H), 6.865 (d, *J=7.5*, 4H), ^{1}H NMR (DMSO-d^6, 500MHz), δ 4.054 (t, 4H), δ 2.461 (t, 4H), δ 2.264 (s, 12H), δ 1.970 (m, 4H).

Synthesis of B

Compound 8 (25 mg, 0.052 mmol) and dichloromethane were mixed, followed the addition of iodomethane (80 mg, 1.28 mmol). The mixture was stirred at room temperature for 1 h, then the solid was collected by filtration, and washed with dichloromethane for 3 times. 39 mg of yellow solid was obtained after vacuum drying. Yield: 99%. ^{1}H NMR (DMSO-d^6, 500 MHz), δ 7.53 (m, 8H), δ 7.017 (d, 4H), δ 4.099

(t, 4H), δ 3.473 (t, 4H), δ 3.09 (s, 18H), δ 2.193 (m, 4H). ^{13}C NMR (DMSO-d^{6}, 125 MHz) δ 156.6, δ 131.1, δ 129.4, δ 120.5, δ 113.0, δ 112.5, δ 89.4, δ 85.8, δ 62.9, δ 60.9, δ 50.3, δ 20.5. MS(ESI). Calcd: *m/z* 510.3246. Obsd: *m/z* 510.3226.

Synthesis of 6

4-iodo phenol (686 mg, 3.12 mmol), 2-chloro-N,N-dimethylethylamine hydrochloride (1.35 g, 9.35 mmol), potassium carbonate (2.34 mg, 17.16 mmol), and acetone (50 ml) were mixed together. The mixture was refluxing overnight. Acetone was removed under reduced pressure and the solid was dissolved in dichloromethane and washed with H_2O twice, dried over $MgSO_4$ for 30 min. $MgSO_4$ was removed by filtration and the solvent was removed under reduced pressure to give 863 mg of oil. Yield: 93%.^{1}H NMR ($CDCl_3$, 500 MHz), δ 7.537 (d, *J=9*, 2H), δ 6.697 (d, *J=9*, 2H), 4.016 (t, *J=6*, 2H), δ 2.709 (t, *J=6*, 2H), δ 2.313 (s, 6H).

Synthesis of 10

Compound 6 (319 mg, 1.10 mmol), $CHCl_3$ (16 mL) and diisopropylamine (0.6 mL) were mixed and degassed by purging with argon for 30 min. Followed by the addition of 2 (46 mg, 0.37 mmol), $Pd(PPh_3)_2Cl_2$(10 mg) and CuI (6 mg) with stirring overnight. The salt formed in the process was removed by filtration, and the solution was extracted over dichloromethane and washed with NH_4Cl solution, H_2O and saturated NaCl. Organic layer was dried over anhydrous $MgSO_4$ for 30 min followed by removal of $MgSO_4$ by filtration. The solvent was removed by vacuum rotary evaporation, and the resulting solid was purified by column chromatography to give

94 mg of white solid. Yield: 57%. ^{1}H NMR ($CDCl_3$, 500 MHz), δ 7.484 (d, *J=9*, 8H), δ 6.912 (d, *J=9*, 4H), δ 4.096 (t, *J=6*, 4H), δ 2.754 (t, *J=6*, 4H), δ 2.347 (s, 18H).

Synthesis of A

Compound 10 (84.5 mg, 0.187 mmol) and dichloromethane were mixed, then iodomethane (265 mg, 1.87 mmol) was added. The mixture was stirred at room temperature for 1 h, then the resulting was collected by filtration. The solid was washed with dichloromethane for 3 times to give 126 mg of light yellow solid. Yield: 92%. ^{1}H NMR (DMSO-d^6, 500 MHz), δ 7.578 (d, *J=8.5*, 8H), δ 7.073 (d, *J=8.5*, 4H), δ 4.502 (t, *J=6*, 4H), δ 3.786 (t, *J=6*, 4H), δ 3.166 (s, 18H). ^{13}C NMR (DMSO-d^6, 125 MHz)δ 157.8, δ 133.2, δ 131.6, δ 122.4, δ 115.2, δ 91.3, δ 88.0, δ 64.0, δ 61.8, δ 53.1, δ 28.0. MS (ESI). Calcd: *m/z* 482.2933. Obsd: *m/z* 482.2908.

Synthesis of 9

Compound 5 (325 mg, 2.46 mmol) was dissolved in $CHCl_3$ (15 mL) and diisopropylamine (1 mL) and degassed by purging with argon for 30 min. Compound 4 (1.36 g, 4.46 mmol), $Pd(PPh_3)_2Cl_2$ (56 mg, 0.08 mmol) and CuI (30 mg, 0.157 mmol) were added into the solution. The mixture was stirred at room temperature for 24 h followed by the removal of solvent under reduced pressure. Further purification was achieved by column chromatography to give 25 mg of brown solid. Yield: 16%. ^{1}H NMR ($CDCl_3$, 500 MHz), δ 7.448 (d, *J=9*, 4H), δ 7.098 (d, *J=8*, 2H), δ 6.882 (d, *J=9*, 4H), δ 4.056 (t, *J=6.5*, 4H), δ 2.511 (t, *J=6.5*, 4H), δ 2.303 (s, 12H), δ 2.014 (m, 4H).

Synthesis of C

Compound 9 (54 mg, 0.11 mmol) was dissolved in dichloromethane (2 mL) followed by the addition of iodomethane (70 mg, 0.47 mmol). The mixture was stirred at room temperature for 1 h and the solid was collected by filtration to give 85 mg of grey-brown powder. ^{1}H NMR (DMSO-d^{6}, 500 MHz), δ 7.532 (d, *J=8*, 4H), δ 7.339 (d, 2H), δ 7.017 (d, *J=8*, 4H), δ 4.112 (t, *J=5*, 4H), δ 3.488 (t, *J=5*, 4H), δ 3.091 (s, 18H), δ 2.184 (m, 4H). ^{13}C NMR (DMSO-d^{6}, 125 MHz)δ 159.1, δ 136.4, δ 133.2, δ 132.6, δ 123.5, δ 115.1, δ 94.2, δ 65.0, δ 62.9, δ 52.3, δ 22.5. Yield: 99%. MS (ESI). Calcd: *m/z* 516.2811. Obsd: *m/z* 516.2766.

Synthesis of 7

Under argon atmosphere, 4-iodophenol (0.5 g, 2.27 mmol) was rapidly dissolved in 2 mL of NaOH solution (10%) in an Erlenmeyer flask. A solution that contained oxathiolane (0.35 g, 2.84 mmol) and 2 mL of dioxane was added to the above-mentioned solution at once. The resulting mixture was then stirred at room temperature for 4 h, and a quantitative precipitate formed. After cooling in an ice-water bath, the reaction mixture was filtered under reduced pressure. The obtained solid was washed with cold acetone and collected as white powder of 0.88 g. Yield: 99.9%.

Synthesis of D

At room temperature, compound 7 (518 mg, 1.42 mmol) and compound 2 (100 mg, 0.79 mmol) were dissolved in a mixture of H_2O (5 mL) and diisopropylamine (5 mL) under argon atmosphere. This reaction was kept under argon atmosphere at room

temperature for 8 h. The reaction mixture was filtered under reduced pressure. ^{1}H NMR (DMSO-d^{6}, 500 MHz), δ 1.99 (t, 4H), 2.54 (m, 4H), 4.10 (t, 4H), 6.97 (d, 4H), 7.49-7.53 (m, 8H). ^{13}C NMR (DMSO-d^{6}, 125 MHz) δ 133.0, δ 131.4, δ 114.9, δ 79.3, δ 73.5, δ 66.9, δ 35.8, δ 30.8. MS (ESI). Calcd: *m/z* 553.0991. Obsd: *m/z* 553.0995.

3.4 Photophysics of S-OPE-1s and EO-OPE-1s

3.4.1 General methods

A stock solution was prepared with a concentration of 1 mM and stored in a 0°C refrigerator (10% v/v DMSO in water). For absorption and fluorescence experiments, 30 μL of the stock solution was added into a cuvette combining 2970 μL DI H_2O or methanol to give a final concentration of 10 μM. Both absorption and emission were measured on a plate reader (SpectroMax M-5 microplate reader, Molecular Devices). 2 nm of scan speed was applied for every sample with a cutoff at 325 nm for emission. The fluorescence quantum yields (Φ_F) have been calculated according to the formula in Eq. 3-1. Quinine sulfate (in 0.1 M H_2SO_4) was used as a standard compound (Φ_F = 0.54) and the optical density was controlled below 0.1 (generally ~0.06). The quantum yields and standard deviations were recorded as a result of an averaged value of 3 parallel tests.

Eq. 3-1 The formula for calculation of relative fluorescence quantum yields. R, Int, A, Φ, and n denote reference, integration of emission, optical density, fluorescence

quantum yield, and refractive index, respectively. Integration area was calculated by Origin 8.1, student edition (OriginLab corporation, Northampton, MA, USA)

The Circular Dichroism (CD) is a powerful tool to determine if a chiral compound or complex exists in a system. For CD experiments, the concentration of OPEs is the same as that in absorption and fluorescence experiments. Transient absorption spectra were recorded for EO-OPE-1 samples both in methanol and water (Anand Parthasarathy, University of Florida). Transient absorption spectra were collected using laser systems that are described elsewhere[111,112]. The optical density was adjusted to ~0.7 at the excitation wavelength (355 nm) with the laser energy being 6~7 mJ. Solutions were purged with argon for 45 min before making transient absorption spectroscopy measurements. Calf thymus DNA (Sigma-Aldrich, MO) powder was dissolved in DI H_2O and stored refrigerated.

3.4.2 Results and discussion

3.4.2.1 Absorption and fluorescence

Given that there are only two hydrophilic groups attached on both ends of EO-OPE-1s through a large hydrophobic aromatic segment, these compounds are poorly soluble in water, moderately soluble in CH_3OH, but quite soluble in DMF and DMSO. Further photophysical studies indicate that absorbance intensity at 1 min for A and C under the concentration at 10 μM in H_2O is the same as that measured at 30 min later, in contrast, the intensity of B is enhanced around 2 times over 30 min and D is enhanced 1.5 times than that measured at 1 min (Fig. 3-8~22). This indicates that B and D

dissolve in water more slowly than the other EO-OPE-1s. Basically, this series of biocides have been demonstrated to be very efficient light harvesters with large molar extinction coefficients in water (Table 3-1, Fig. 3-23~26), which are very similar to PPE. A, B, C, and D also have very good to moderate fluorescent quantum yields (Φ_F) in water being 0.34, 0.35, 0.11, and 0.14 respectively.

Table 3-1. Photophysical data for compounds A - D in methanol solution

parameter	solvent	A	B	C	D
λ_{max} (absorption / nm)	MeOH	326	328	355	327
λ_{max} (fluorescence / nm)	MeOH	355	358	390	360
Φ_F [a]	MeOH	0.73 ± 0.03	0.69 ± 0.03	0.12 ± 0.01	0.53 ± 0.02
Φ_Δ [b]	CD_3OD	0.20± 0.02	0.17± 0.03	0.45± 0.03	0.09± 0.02
τ_F / ns	MeOH	0.4	0.45	0.23	0.52 (97%) 2 (3%)
TT_{Abs} (λ / nm)	MeOH	598	603	506	547
TT_{Abs} (ΔA, t=0)	MeOH	0.28	0.26	0.37	0.07
$\tau_{triplet}$ (μs)	MeOH	2.8	2.3	1.6	3.7

[a] Measured using quinine sulfate in 0.1 M sulfuric acid (Φ_F = 0.54) as actinometer.
[b] Measured in CD_3OD using 2′-acetonaphthone ($\Phi\Delta$ = 0.79) as actinometer.

3.4.2.2 Singlet oxygen generation

Excited triplet states (ETS) play an essential role in the generation of ROS and $^1O_2$. For study of triplet states, in general, a lower intensity of transient absorption (TA) was observed in water than in methanol (Fig.3-28~35). Another important point to note is that all members of EO-OPE-1 series underwent fast photobleaching in water during TA experiments (approximately 40-50% reduction in signal intensity). To minimize the error due to photobleaching, fresh samples were prepared and used in each run. The results show that C gives the highest TA intensity (Fig. 3-32), however, A, B, and D are comparable (Fig. 3-28, 3-30, 3-34 and Table 3-1). On the other hand, the triplet lifetimes for A, B, C, and D are 18.7 μs, 17.9 μs, 7.2 μs, and 5.2 μs,

respectively (Tabel 3-1). Based on the above discussions, we would expect C will give a higher yield of $^1O_2$, with lower yields for A, B, and D.

In comparison to EO-OPE-1s, which show single absorption band, two absorption bands in absorption spectra both in water and methanol were observed for S-OPE-1 ($COCH_3$), S-OPE-1 (COOEt), S-OPE-1 (COO^-), S-OPE-1(NH_2), and S-OPE-1(OR). From computer modeling, OPEs with substitutes on the middle aromatic ring(s) show two-banded absorption, but single band for OPEs without pendant groups on the middle benzene ring(s), instead (Fig. 3-3).[117] Each compound also exhibits a relatively broad single absorption band with maxima in the range 397- 472 nm in methanol and DI H_2O. The fluorescence of S-OPE-1s is stronger in methanol than in water. S-OPE-1(OR) and S-OPE-1 (COO^-) show very strong fluorescence in aqueous solution near neutral pH. The lower fluorescence intensity for S-OPE-1(NH_2), S-OPE-1(COOEt), S-OPE-1($COCH_3$) may be attributable to excited singlet quenching, however S-OPE-1(COO^-) and S-OPE-1(OR) exhibit very good solubility in aqueous solution so that the quenching has been much decreased.

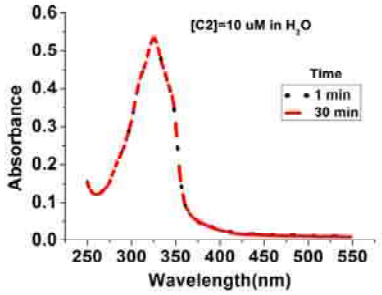

Fig. 3-8 Absorption spectra of A in H_2O were recorded over 30 min with a concentration of 10 μM.

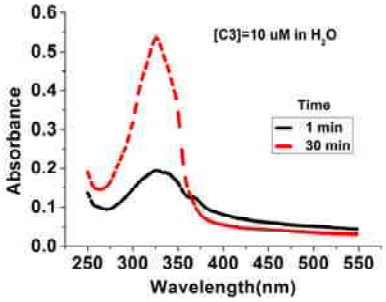

.

Fig. 3-9 Absorption spectra of B in H_2O were recorded over 30 min with a concentration of 10 μM.

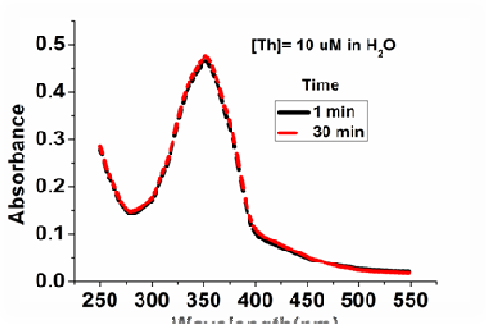

Fig. 3-10 Absorption spectra of C in H_2O were recorded over 30 min with a concentration of 10 μM.

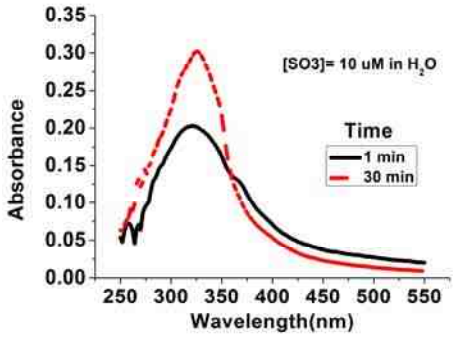

Fig. 3-11 Absorption spectra of D in H_2O were recorded over 30 min with a concentration of 10 μM.

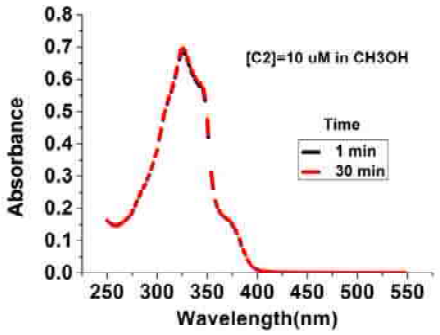

Fig. 3-12 Absorption spectra of A in CH_3OH were recorded over 30 min with a concentration of 10 μM.

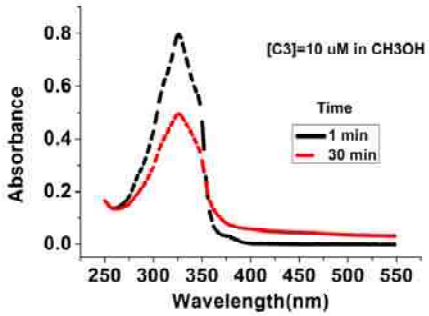

Fig. 3-13 Absorption spectra of B in CH_3OH were recorded over 30 min with a concentration of 10 μM.

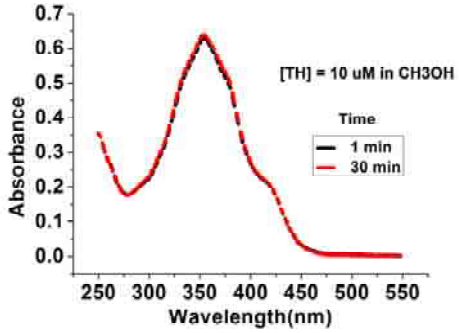

Fig. 3-14 Absorption spectra of C in CH_3OH were recorded over 30 min with a concentration of 10 μM.

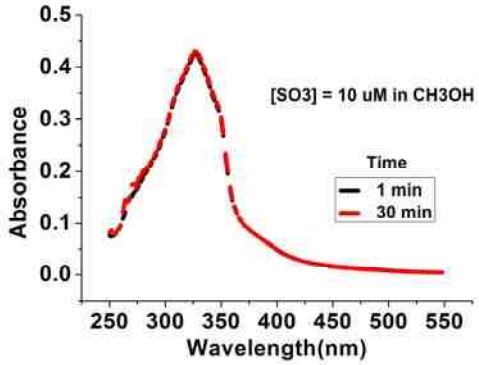

Fig. 3-15 Absorption spectra of D in CH_3OH were recorded over 30 min with a concentration of 10 μM.

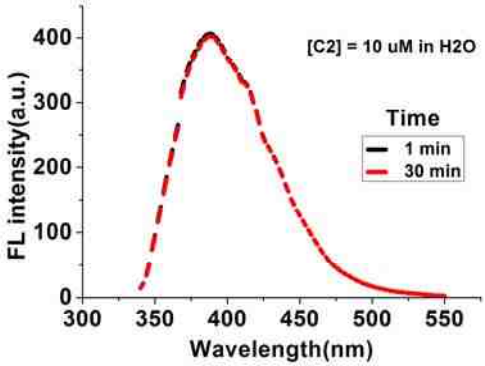

Fig. 3-16 Absorption spectra of A in H_2O were recorded over 30 min with a concentration of 10 μM.

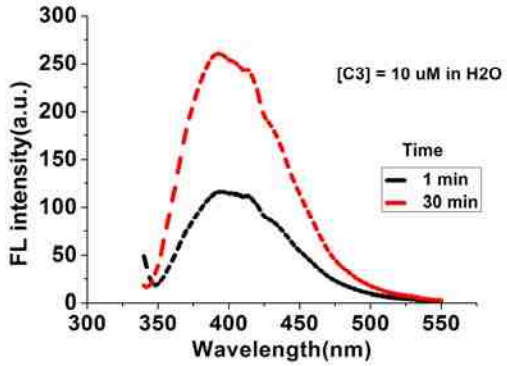

Fig. 3-17 Absorption spectra of B in H_2O were recorded over 30 min with a concentration of 10 μM.

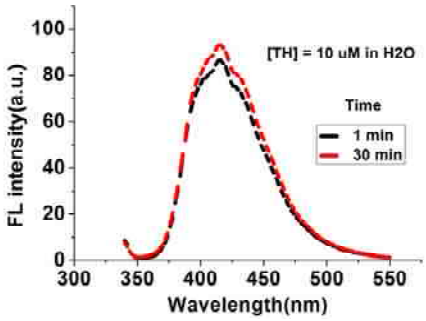

Fig. 3-18 Absorption spectra of C in H_2O were recorded over 30 min with a concentration of 10 μM.

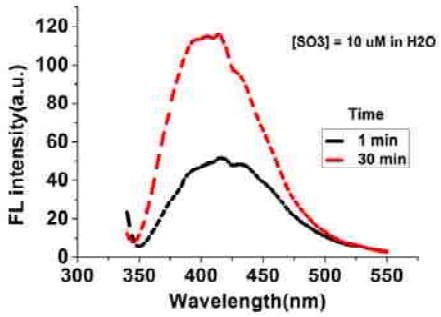

Fig. 3-19 Absorption spectra of D in H_2O were recorded over 30 min with a concentration of 10 μM.

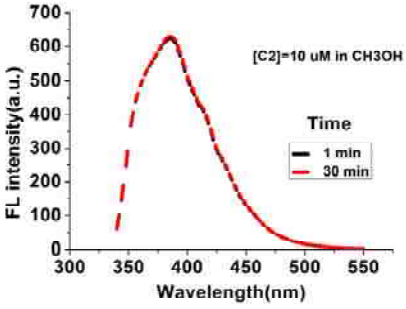

Fig. 3-20 Absorption spectra of A in CH_3OH were recorded over 30 min with a concentration of 10 μM.

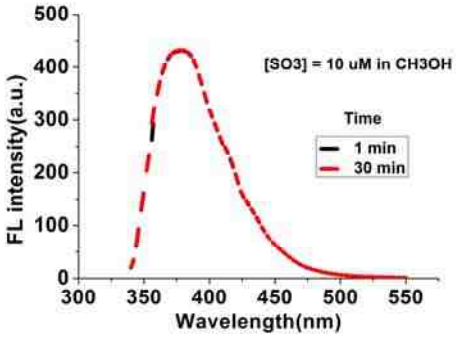

Fig. 3-21 Absorption spectra of D in CH_3OH were recorded over 30 min with a concentration of 10 μM.

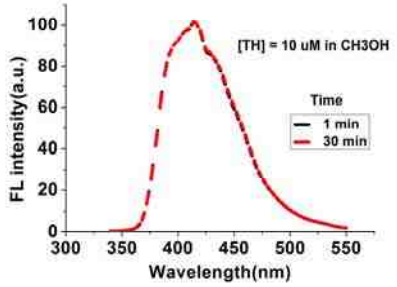

Fig. 3-22 Absorption spectra of C in CH_3OH were recorded over 30 min with a concentration of 10 μM.

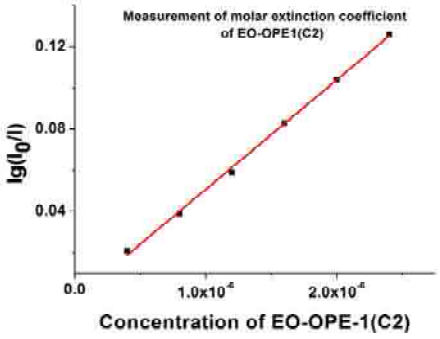

Fig. 3-23 Measurement of molar extinction coefficient of A. The black square denotes absorbance intensity at a specific concentration.

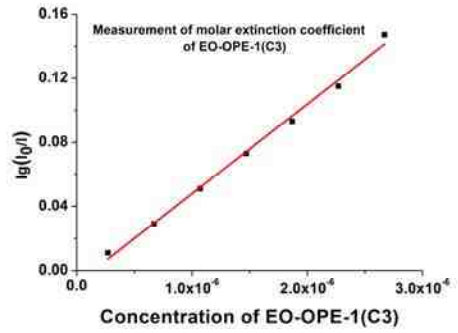

Fig. 3-24 Measurement of molar extinction coefficient of B. The black square denotes absorbance intensity at a specific concentration.

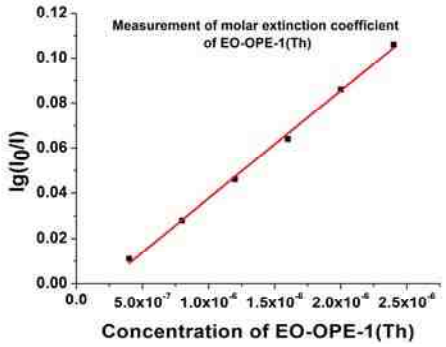

Fig. 3-25 Measurement of molar extinction coefficient of C. The black square denotes absorbance intensity at a specific concentration.

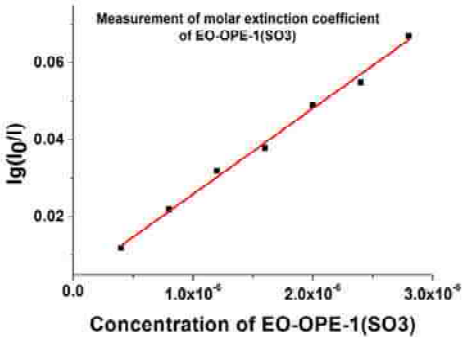

Fig. 3-26 Measurement of molar extinction coefficient of D. The black square denotes absorbance intensity at a specific concentration.

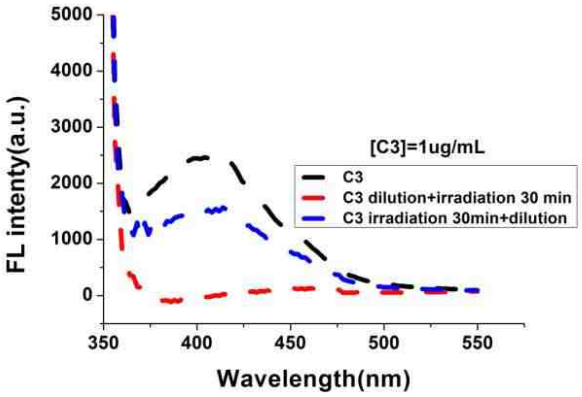

Fig. 3-27 Concentration-dependence experiments for B. Red dash line denotes the fluorescence pattern after irradiation for 30 min with UV-365 nm of diluted EO-OPE-1(C3) in 0.85% NaCl solution. [EO-OPE-1(C3)] = 1 μg/mL. The blue dash line was obtained by firstly irradiation of concentrated EO-OPE-1(C3) solution followed by diluted the EO-OPE-1(C3) solution into the same concentration with red dash line, and the black dash line refers to the diluted EO-OPE-1(C3) solution without irradiation. All these samples were excited at 330 nm and fluorescence experiment was performed at a Molecuar device.

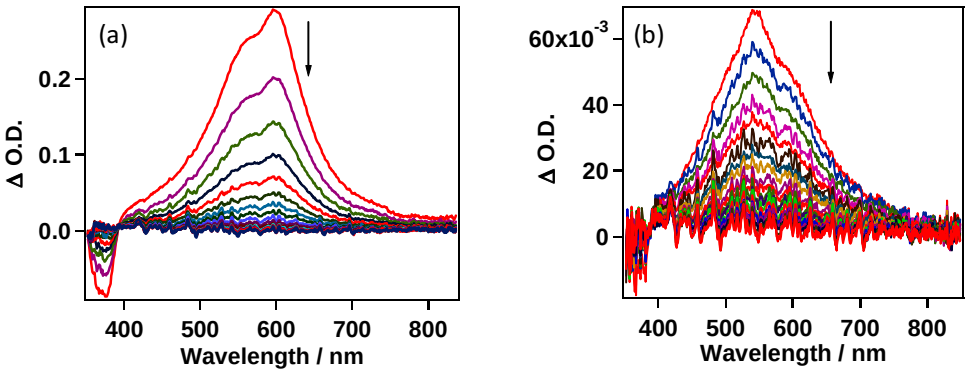

Fig. 28-29. Transient absorption difference spectra of **A** (OD ~ 0.7 at 355 nm and excited with the laser energy of ~7 mJ) in (a) methanol (initial delay = 70 ns, subsequent delay increment = 1 μs) and (b) water (initial delay = 70 ns, subsequent delay increment = 3 μs).

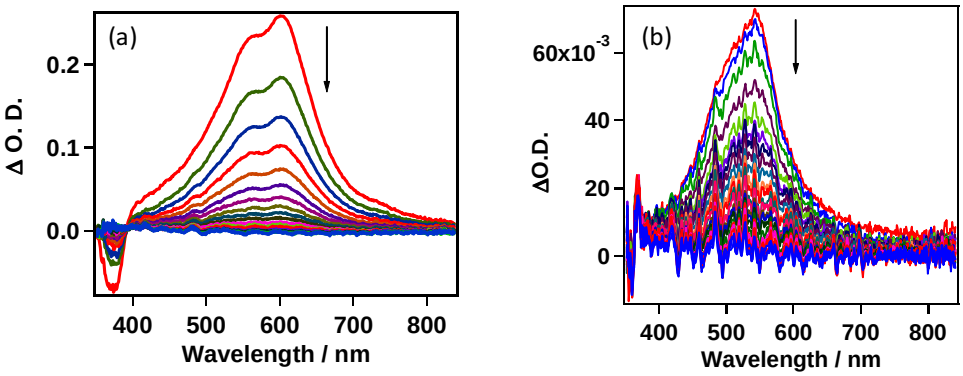

Fig. 30-31. Transient absorption difference spectra of **B** (OD ~ 0.7 at 355 nm and excited with the laser energy of ~7 mJ) in (a) methanol (initial delay = 70 ns, subsequent delay increment = 0.6 μs) and (b) water (initial delay = 50 ns, subsequent delay increment = 2 μs).

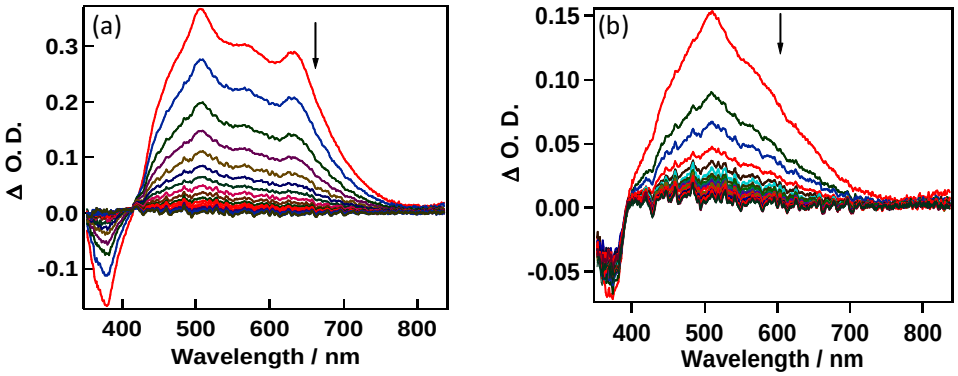

Fig. 32-33. Transient absorption difference spectra of **C** (OD ~ 0.7 at 355 nm and excited with the laser energy of ~7 mJ) in (a) methanol (initial delay = 70 ns, subsequent delay increment = 0.5 μs) and (b) water (initial delay = 50 ns, subsequent delay increment = 3.2 μs).

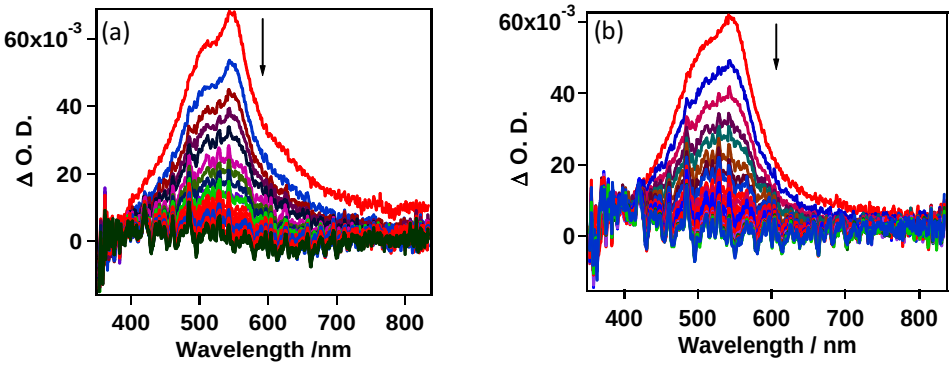

Fig. 34-35. Transient absorption difference spectra of **D** (OD ~ 0.7 at 355 nm and excited with the laser energy of ~7 mJ) in (a) methanol (initial delay = 80 ns, subsequent delay increment = 0.75 μs) and (b) water (initial delay = 65 ns, subsequent

delay increment = 1 μs).

In addition, we have measured the singlet oxygen ($^1O_2$) quantum yield of B in CH_3OD (Anand Parthasarathy, University of Florida). The result shows that B exhibits much higher $^1O_2$ quantum yield (0.30) (Fig. 3-36) than PPE (0.13). [66] In comparison to oligomers, PPEs have more aggregation and interchain fluorescence quenching in water, therefore, the singlet state of PPEs is, to some extent, quenched. Another way to calculate singlet oxygen quantum yield is also showing below (Fig. 3-37).

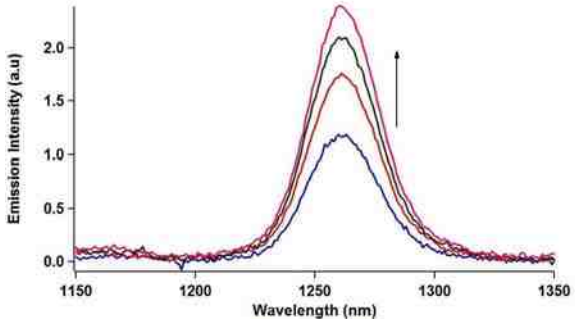

Fig. 3-36 Emission spectra of singlet oxygen. There is a characteristic peak at 1257 nm which is responsible for the singlet oxygen emission. The singlet oxygen was calculated under air atmosphere and results are an average of two values 0.33 and 0.29. (from Katsu Ogawa)

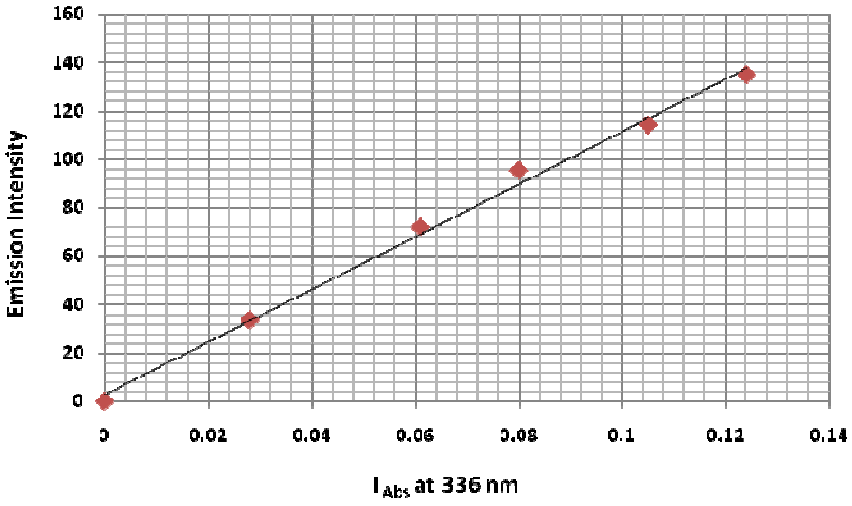

Fig. 3-37 Plot of singlet oxygen emission, Quantum yield (ϕ) = 0.3, λ_{ex} = 336 nm, 2'-acetonaphthone was the standard. (from Katsu Ogawa)

3.5 Self-assembly behavior of S-OPE-1s and EO-OPE-1s

3.5.1 Self-assembly behavior of S-OPE-1s

The anionic substrates, specifically, CMA, CMC, calf thymus DNA, and nanoparticles such as Laponite clay were used. We had expected that all those cationic S-OPE-1s would self-assembly onto these substrates through Coulombic attraction and π-π stack to form extended conjugated system (J-aggregation or planarization) or simply disorderly aggregates in the aqueous solution. However, the anionic S-OPE-1(COO^-) in neutral condition could not form aggregates because there should be no Coulombic attraction between the host and guest. S-OPE-1(COOEt) in the aqueous solution shows striking self-assembly behavior upon the addition of CMC solution. There were two red-shifted new bands formed in absorption spectra, and the fluorescence enhanced 16 folds with Stokes shift being ~ 40 nm. However, we have not seen significantly red-shifted spectral changes but very small with decreased intensity in the absorption of S-OPE-1(NH_2)/S-OPE-1($COCH_3$) upon addition of CMA/CMC/DNA solution though fluorescence enhanced significantly (Fig. 3-33~48).

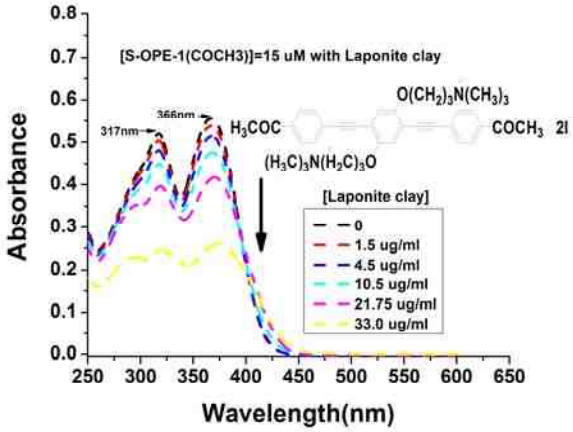

Fig. 3-33 Absorption spectra of S-OPE-1($COCH_3$) in H_2O upon addition of clay suspension solution.

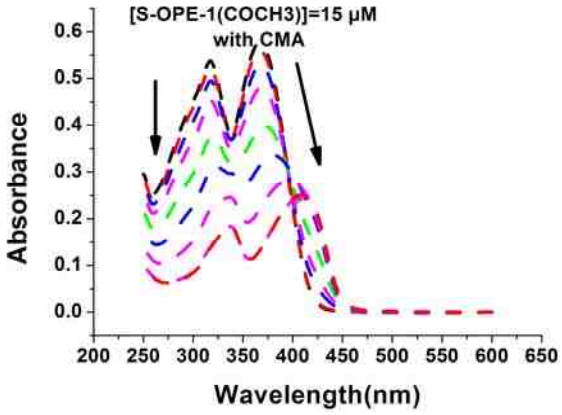

Fig. 3-34 Absorption spectra of S-OPE-1($COCH_3$) in H_2O upon addition of CMA

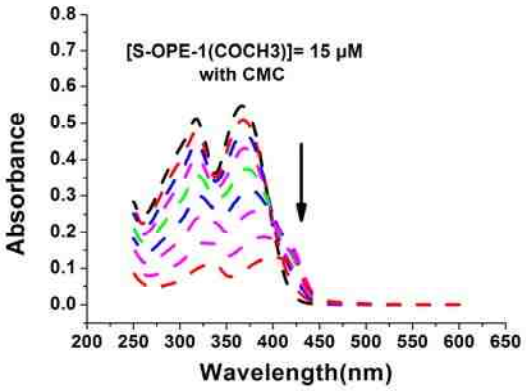

Fig. 3-35 Absorption spectra of S-OPE-1($COCH_3$) in H_2O upon addition of CMC solution.

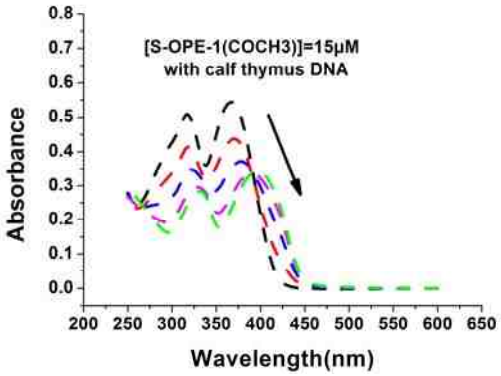

Fig. 3-36 Absorption spectra of S-OPE-1 ($COCH_3$) in H_2O upon addition of DNA solution.

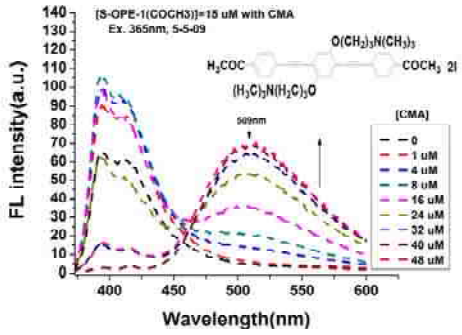

Fig. 3-37 Emission spectra of S-OPE-1($COCH_3$) in H_2O upon addition of CMA solution.

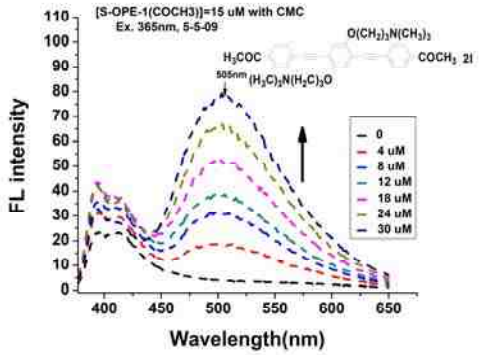

Fig. 3-38 Emission spectra of S-OPE-1($COCH_3$) in H_2O upon addition of CMC solution.

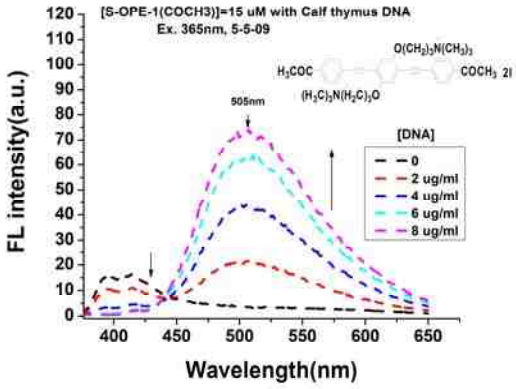

Fig. 3-39 Emission spectra of S-OPE-1($COCH_3$) in H_2O upon addition of DNA.

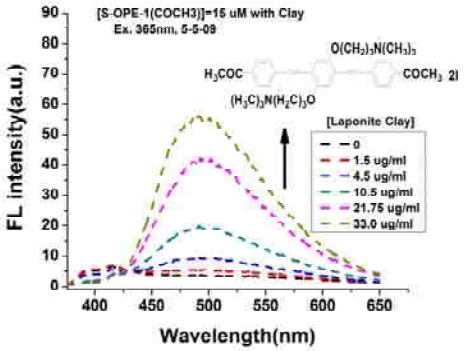

Fig. 3-40 Emission spectra of S-OPE-1($COCH_3$) in H_2O upon addition of clay suspension.

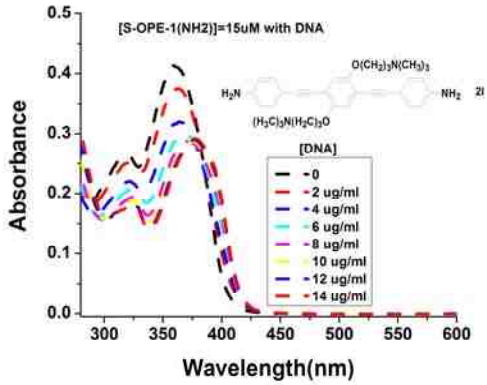

Fig. 3-41 Absorption spectra of S-OPE-1(NH_2) in H_2O upon addition of DNA solution.

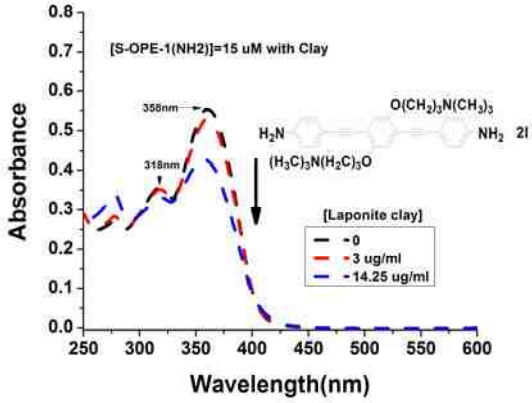

Fig. 3-42 Absorption spectra of S-OPE-1(NH_2) in H_2O upon addition of clay suspension.

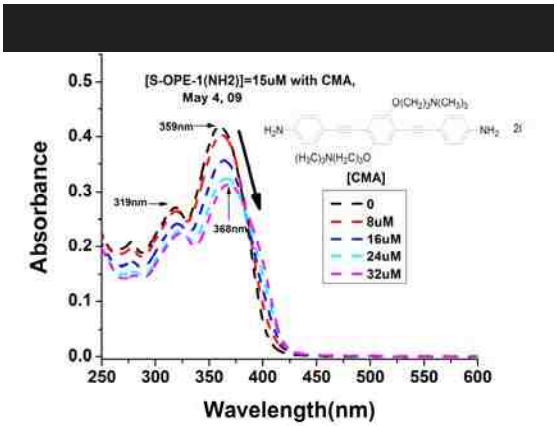

Fig. 3-43 Absorption spectra of S-OPE-1(NH_2) in H_2O upon addition of CMA solution.

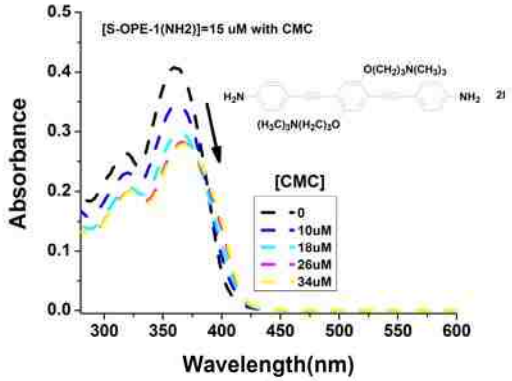

Fig. 3-44 Absorption spectra of S-OPE-1(NH_2) in H_2O upon addition of CMC solution.

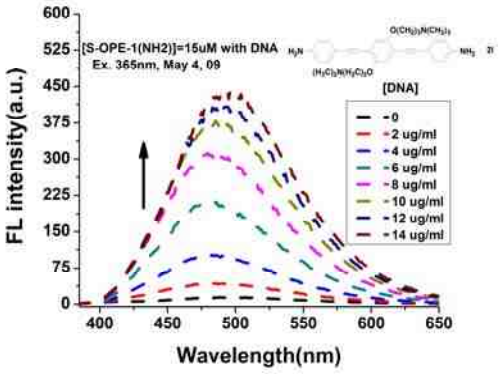

Fig. 3-45 Emission spectra of S-OPE-1(NH_2) in H_2O upon addition of DNA solution.

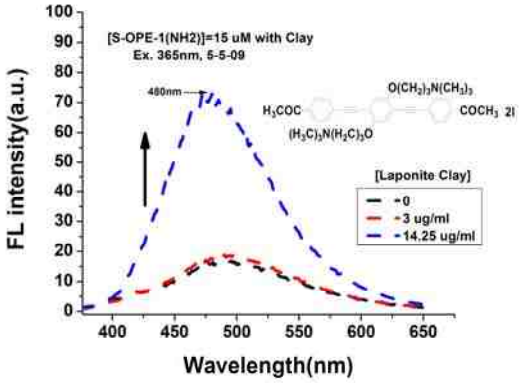

Fig. 3-46 Emission spectra of S-OPE-1(NH_2) in H_2O upon addition of clay suspension.

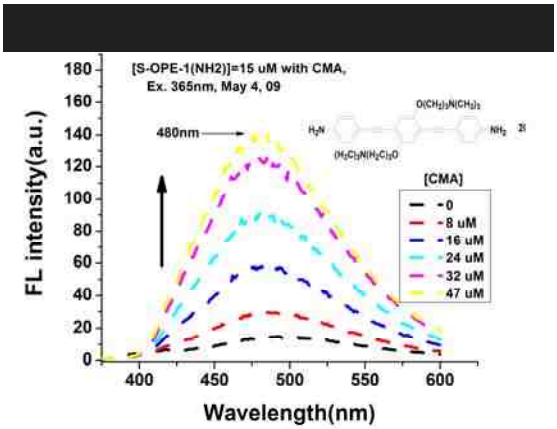

Fig. 3-47 Emission spectra of S-OPE-1(NH_2) in H_2O upon addition of CMA solution.

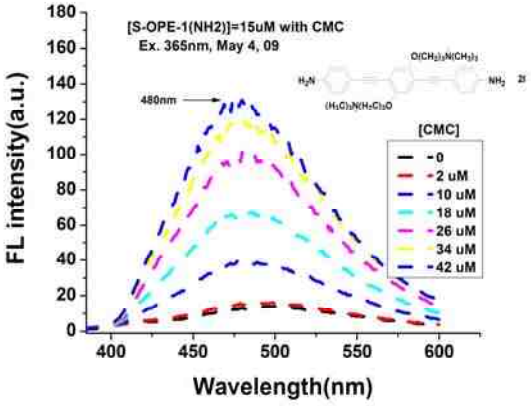

Fig. 3-48 Emission spectra of S-OPE-1(NH_2) in H_2O upon addition of CMC solution.

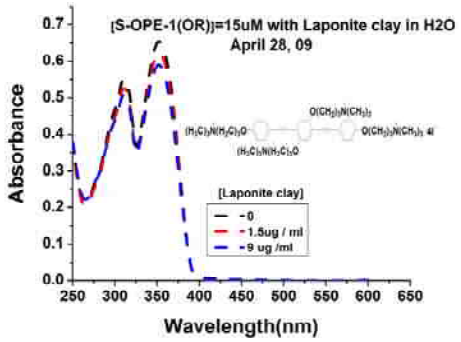

Fig. 3-49 Absorption spectra of S-OPE-1(OR) in H_2O upon addition of clay suspension.

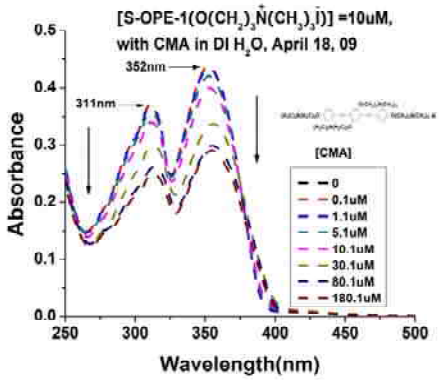

Fig. 3-50 Absorption spectra of S-OPE-1(OR) in H_2O upon addition of CMA solution.

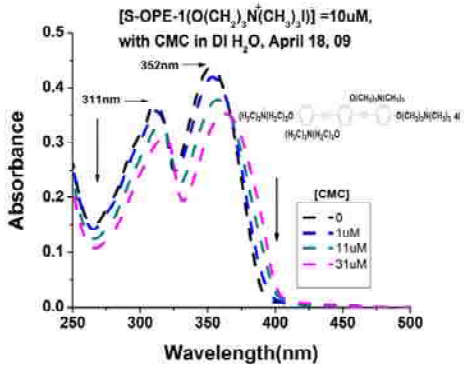

Fig. 3-51 Absorption spectra of S-OPE-1(OR) in H_2O upon addition of CMC.

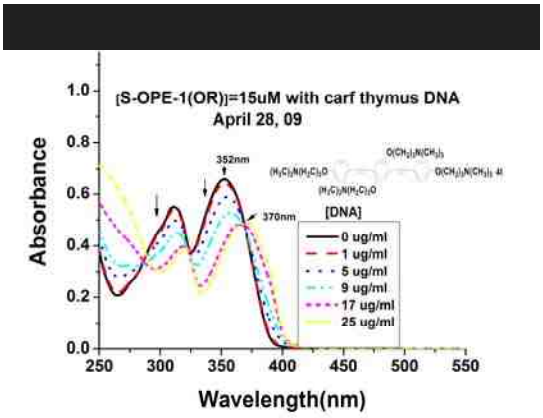

Fig. 3-52 Absorption spectra of S-OPE-1(OR) in H_2O upon addition of DNA solution.

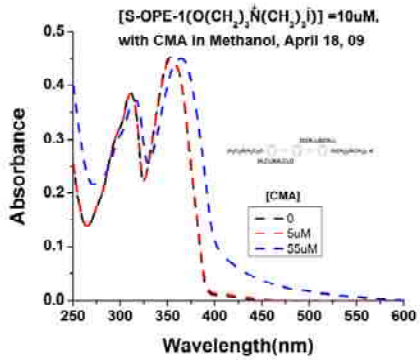

Fig. 3-53 Absorption spectra of S-OPE-1(OR) upon addition of CMA in CH_3OH.

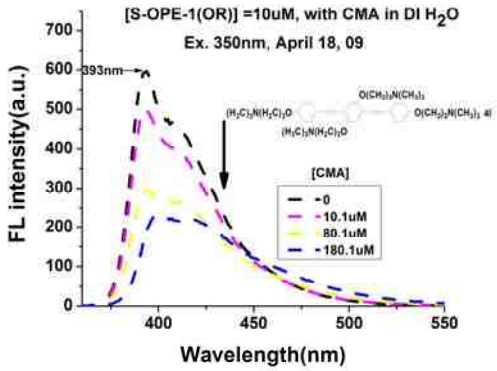

Fig. 3-54 Emission spectra of S-OPE-1 (OR) upon addition of CMA solution.

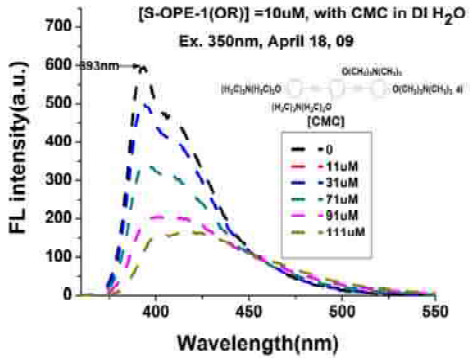

Fig. 3-55 Emission spectra of S-OPE-1(OR) in H_2O upon addition of CMC solution.

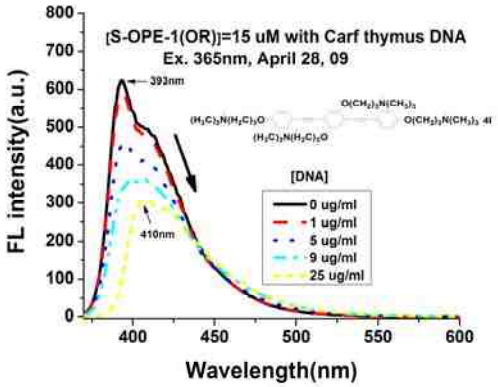

Fig. 3-56 Emission spectra of S-OPE-1(OR) in H_2O upon addition of DNA solution.

3.5.2 Self-assembly behavior of EO-OPE-1s

Unlike OPE-2, the preliminary results of EO-OPE-1(C3) showed that no significant red or blue-shifted bands were observed for absorption and fluorescence with scaffolds such as CMC, CMA, DNA, and synthetic clay (Fig. 3-57~64). More or less, fluorescence intensity has enhanced. More experiments should be done in the future since we found B was poor soluble in water, but we didn't consider this effect before, which probably caused the imprecise results here. It is understandable that EO-OPE-1(C3) fails to form J-aggregates since cationic charges locate on the ends, which probably limits the proximity of EO-OPE-1 molecules with each other because of Coulombic repulsion.

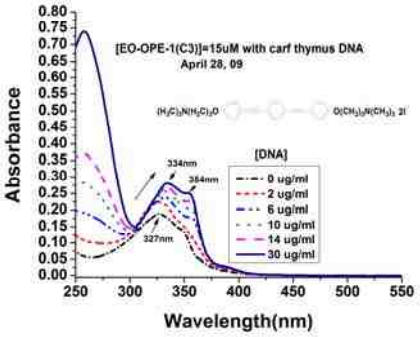

Fig. 3-57 Absorption spectra of B in H_2O upon addition of DNA aqueous solution.

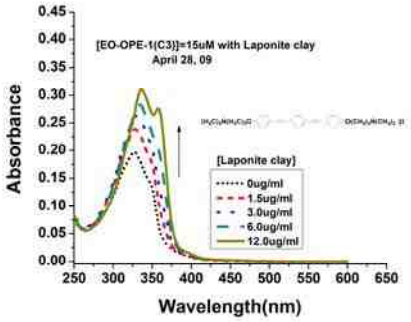

Fig. 3-58 Absorption spectra of B in H_2O upon addition of laponite clay suspension.

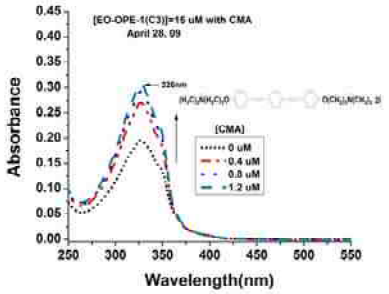

Fig. 3-59 Absorption spectra of B upon addition of CMA solution.

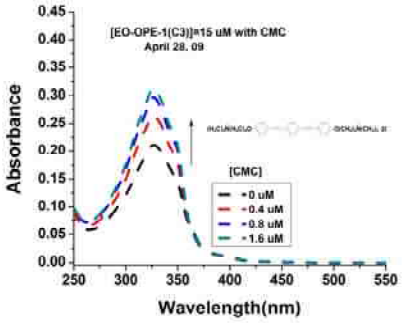

Fig. 3-60 Absorption spectra of B upon Addition of CMC solution.

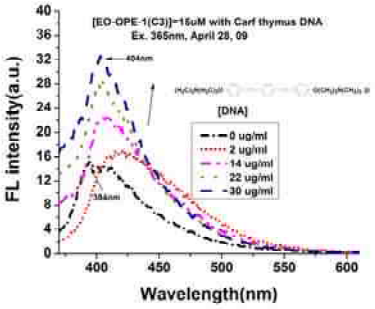

Fig. 3-61 Emission spectra of B in H_2O upon addition of DNA aqueous solution.

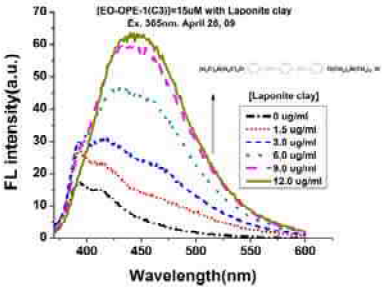

Fig. 3-62 Emission spectra of B in H_2O upon addition of laponite clay suspension.

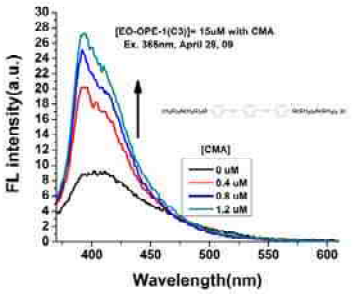

Fig. 3-63 Emission spectra of B in H_2O upon addition of CMA aqueous solution.

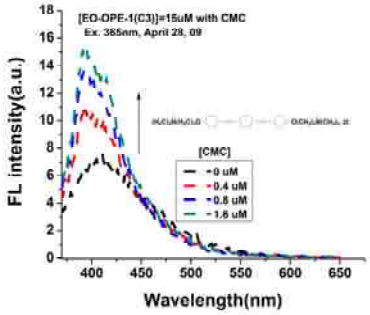

Fig. 3-64 Emission spectra of B in H_2O upon addition of CMC aqueous solution.

3.6 Conclusion

(1) Five S-OPE-1s and four EO-OPE-1s have been synthesized and characterized. The synthesis is straightforward and column chromatography/rescrystalization is used for the purification. The products are easily characterized by NMR and Mass Spectroscopy. However, low yields were obtained with EO-OPE-1(TH) precursors (compound 4 and 9). This may derive from the instability of compounds 4 and 9. So the new strategies should be developed to address this problem, such as *in situ* reaction. Another factor that could contribute to the low yields possibly comes from the good affinity of 4 and 9 to silica gel so that the majority of 4 and 9 attaches on the silica gel.

(2) Photophysical studies such as absorption, fluorescence and fluorescence lifetime, transient absorption, and singlet oxygen quantum yields for S-OPE-1s and EO-OPE-1s have been done. For S-OPE-1s, TA experiments and fluorescence quantum yield measurements are still on the way. We found that there are two absorption bands for all OPEs and S-OPE-1s, but just one for EO-OPE-1s. Further

studies by computer modeling discovered that there are two HOMOs existing in OPEs and S-OPE-1s molecules. EO-OPE-1(C3) has a very good singlet oxygen yield being 0.3, in contrast, PPE just yielded 0.13. These interesting results may probably contribute to light-induced biocidal activity of OPEs given that singlet oxygen plays an important role in the inactivation of bacteria.

(3) The investigation of self-assembly for OPEs, S-OPE-1s and EO-OPE-1s has been carried out. We found that OPE1, OPE2, and S-OPE-1(COOEt)/NH_2/$COCH_3$ in H_2O show self-assembly behavior upon the addition of CMC aqueous solution and either planarized monomers or J-aggregates occur in these systems. S-OPE-1(H), S-OPE-1(COO^-) and most EO-OPE-1s were not able to self-assembly upon CMC and CMA in aqueous solution. We have not observed any J-aggregation upon addition of HA solution or Laponite clay suspension for OPEs. Planarization should involve some shifts in absorption and small shift in emission considering the great enhancement in emission intensity. Coupled with π-π stack effect, spectral changes can be attributed to monomeric planarization and J-aggregation. More experiments should be done in the future.

Chapter 4 Biocidal activity of S-OPE-1s and EO-OPE-1s

4.1 Introduction

Bacterial infections in healthcare settings, such as in implanted devices, have become a global issue, and the resistance to many antibiotics used in treatment for pathogenic infections makes this problem even worse. It becomes essential to develop alternative strategies to treat infections, especially those infections caused by *S. aureus* that is responsible for most skin infections.[113,114] Among those strategies, light-induced inactivation of pathogens appears to be a promising candidate.[115] The photo-inactivation reaction has been well documented and the process is believed to involve 3 steps:[116] 1. A photosensitizer is excited from ground state S_0 (low energetic state and stable) to its excited singlet state S_1 (high energetic state and unstable); 2. S_1 decays to a lower energy but longer lived, triplet state S_3 after intersystem crossing (ISC), which in turn transfers its energy to molecular triplet oxygen to generate a reactive oxygen species (ROS, type I photo reaction) or to generate singlet oxygen ($^1O_2$, type II photo reaction); 3. ROS or $^1O_2$ may further oxidize a variety of biological substrates locally, such as lipids, proteins, nucleic acids and other unsaturated components, which can lead to many consequences, ultimately causing irreversible cellular damage and cell death. However, it is still not clear which ROS plays the major role, nevertheless much evidence has shown that singlet oxygen plays a pivotal role in the process.[117,118,119,120]

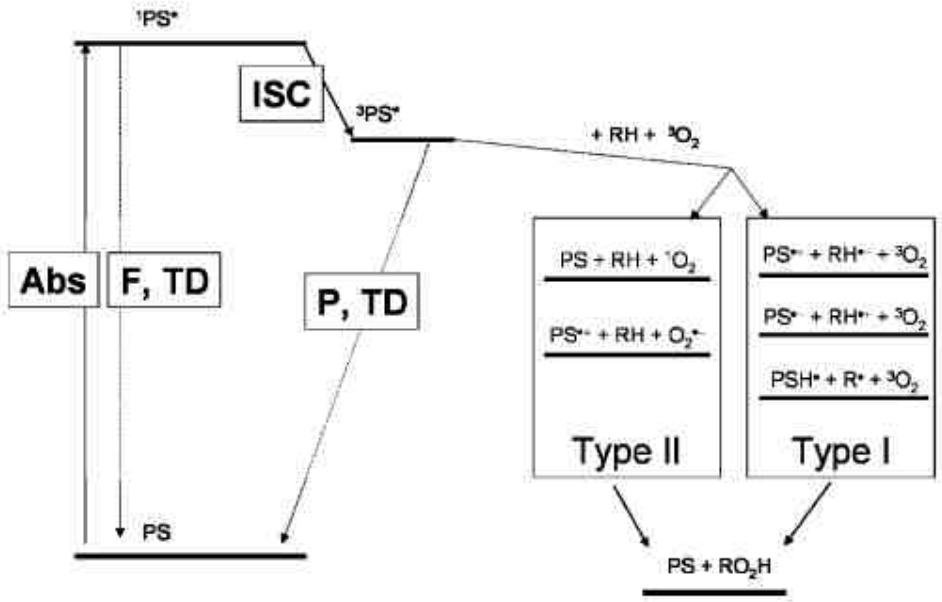

Fig. 4-1 Energy diagram showing the relevant photophysical pathways involved in the photosensitized oxidation of a biological substrate (RH): Upon absorption of light energy, a photosensitizer (PS) in its electronic ground state is promoted to a higher-energy excited singlet state (1PS*), which may deactivate by either fluorescence (F) or thermal decay (TD) back to the ground state or may undergo intersystem crossing (ISC) to the triplet state (3PS*). The thus-produced triplet excited sensitizer may subsequently either deactivate back to the ground state by phosphorescence (P) or thermal decay (TD) or react primarily with RH (type I mechanism) or oxygen (type II mechanism) to finally produce the oxidation product RO_2H.[121]

However, we know that light, especially in the visible region, is toxic only to very few bacteria such as *Propionobacterium acnes*, *Helicobacter pylori* and some oral pigmented bacteria. Even UV-365 nm cannot generally kill bacteria. Based on our previous studies and other studies about Photo Dynamic Inactivation (PDI),[122]

light-induced biocidal activity is oxygen-dependent. The process probably involves either the extracellular or intracellular excitation of photosensitizers.[121,137] In the case of intracellular excitation of photosensitizers, it is believed that cytotoxicity derives from the photo-stimulation of endogenous intracellular porphyrins, however, extracellular cytotoxicity requires addition of photosensitizers, such as the OPEs described in this dissertation. In most cases of PDT, addition of extracellular photosensitizer(s) is required. The development of photosensitizers providing high efficiency, broad-spectrum and controllable release antimicrobials plays a key role. Various classes of chemicals, such as porphyrins, C_{60} derivatives, phthalocyanines, and gold nanoparticles have been tested as biocides.[123] Among potential photosensitizers, poly(phenylene ethynylene) (PPE) derivatives have attracted intense research interest in recent years because of their interesting photophysical and photochemical properties. However the antimicrobial activity of this series of polymers has not yet been explored extensively. Our previous work has demonstrated that several PPEs with pendant quaternary ammonium groups are effective light-activated biocides, which inhibit the growth of Gram-positive spores and Gram-negative bacteria such as *E. coli*. Moreover, it has been shown that there is a strong correlation between activity and oxygen availability.[124,12,15]

To explore the correlation of chemical structure and biocidal activity, we have synthesized “end only” oligo(phenylene ethynylene)s (EO-OPE-1) with remarkable light inducible biocidal activity by functionalizing the ends with cationic groups. We present A, B, and C (Fig. 4-1) with two net positive charges, which are quaternary ammonium salts without pendant groups attached to the middle aromatic ring and anionic D (Fig. 4-1). These can kill Gram-negative bacteria such as *E. coli* and Gram-positive bacteria such as *S. epidermidis* and *S. aureus* under 365 nm radiation with the effect being C>A>B>D. Notably, C reaches 100% killing against *S. aureus* with concentration as low as 10 ng / mL in a half hour irradiation, which is much more efficient in comparison to other disinfectants. [125]

4.2 Material, instrumentation and general methods

4.2.1 Materials

A, B, C, D and all synthetic intermediates were synthesized through multi-step reactions. 2,5-diiodothiophene, ethynyl(trimethyl)silane, 2,2-dioxide,3-chloro-N, N-dimethyl-propan-1-amine, CuI, K_2CO_3, diisopropylamine, , potassium biocarbonate, palladium catalyst, 2-chloro-N,N-dimethyl-ethanamine, Oxathiolane, and 4-iodophenol, 1,4-diiodobenzene were purchased from Sigma-Aldrich (St. Louis, MO) and used as received. Solvents were HPLC grade purchased from Honeywell (Morristown, NJ) and no further purification was applied. The stains, Syto 9, Syto 24, and propidium iodide were obtained from Molecular Probes, Inc. (Eugene, OR).5.3 Synthesis of symmetric

OPE1s.

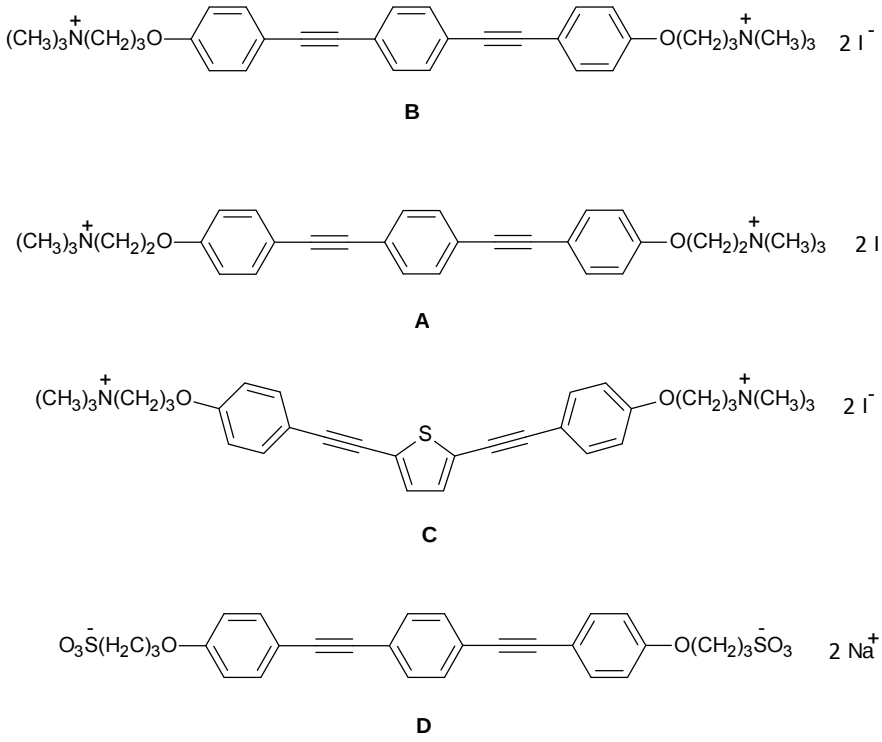

Fig. 4-1 The structures we have tested as biocides.

4.2.2 Biocidal studies and dead/live assay

All items which contacted bacteria were sterile before use. *E.coli*, *S.epidermidis*, and *S.aureus* were cultured in 50 mL of Difco^{TM} Nutrient broth (Becton, Dickinson and Company, Sparks, MD 21152 USA), Difco^{TM} Nutrient broth (Becton, Dickinson and Company, Sparks, MD 21152 USA), and BBL^{TM} Brain Heart Infusion (Becton, Dickinson and Company, Sparks, MD 21152 USA), respectively, for 18 h at 37°C under shaking. The bacteria were collected by centrifuging 50 mL of culture at 4,000 rpm in an Eppendorf centrifuge for 15 min at 4°C. The pellet was re-suspended with the assistance of vortex in 25 mL of 0.85% NaCl solution and repelleted. The wash cycle was repeated

twice. Bacterial concentrations were measured and normalized using a disposable hemocytometer (INCYTO Co., Ltd), counts being 2.5~3.0x10^7/mL. The diluted bacteria suspension was added to 1.5 mL of black and transparent microtubes with aliquots of 500 μL. Three groups of live controls were prepared with bacteria suspension in black microtubes, transparent microtubes, and quartz cuvettes at the same concentrations. These bacteria samples were titrated by EO-OPE-1s with various concentrations followed by remaining in the dark for dark samples/controls and exposing to UV 365 nm radiation in a photoreactor chamber (LZC-ORG, Luzchem Research Inc.) for light samples/controls with certain duration.

Dead/live assays were carried out using two sets of stains: SYTO 9/Propidium iodide for *E.coli* and SYTO 24/propidium iodide for *S.epidermidis* and *S.aureus*. SYTO 9 and SYTO 24 are cell membrane permeant nucleic acid stains with green (~498 nm for SYTO 9 and ~515 nm for SYTO 24) fluorescence and used to stain both live and dead cells; propidium iodide is a red-fluorescent nucleic acid stain that is membrane impermeable to viable cells but stains DNA or RNA of dead cells with compromised membranes and emits red (~617 nm) fluorescence, indicating cell death. Upon the completion of the above treatment, a 1 to 1 ratio mixture of the two dyes was prepared and added into the samples (2.4 μL mixed dyes for 500 μL suspension) and incubated for 15 minutes in the dark. Bacteria were then examined under a 40x oil objective on a Zeiss LSM 510 Meta confocal laser scanning microscope and an Accuri C6 flow cytometer (Accuri Cytometers,

Inc. Ann Arbor, MI USA) to identify and quantify those live and dead bacteria.

4.2.3 Setup of Confocal Laser Scanning Microscope

Rules for selecting channels and laser excitation wavelengths: (1) the laser can excite dyes but not S-OPE-1s or EO-OPE-1s; (2) no or very little cross-talking between the two dyes; (3) the laser intensity is appropriate so that images are bright enough and little photobleaching. So (a) Laser: 488 nm (32.7%) / 543 nm (80%) laser; (b) Channels: channel one (505-550 nm) / channel two (LP 560 nm); (c) Pinholes: 74 μm for channel one / 72μm for channel two were chosen.

4.2.4 Setup of Flow Cytometer

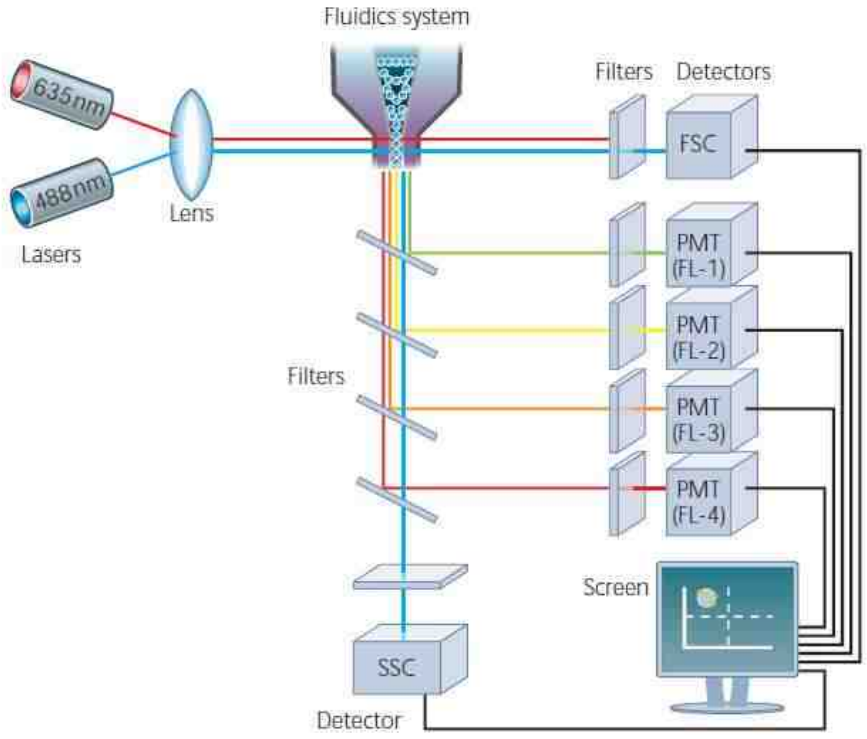

Fig. 4-1 Schematic overview of a typical flow cytometer[126].

Principles: (a) Each bacterium passes through one or more beams of lasers (488 nm and

640 nm); (b) Light scattering or fluorescence are collected through a series of filters (long pass, short pass and band pass or FL1-530 nm/ 30 nm, FL2-580 nm / 45 nm, FL3-670 nm, and FL4-675 nm / 25 nm, four fluorescence channels), which includes information of fluorescence, size, *etc*. (c) The visible information is shown up after PMT.

We are interested in recording two types of signals, one for Syto dye emission (498 nm for Syto 9 and 515 nm for Syto 24) and the other one for PI (617 nm). The green fluorescence (Syto dye emission) will be stronger when bacteria are alive, but red fluorescence (PI emission) will enhance dramatically when bacteria are dead. In our case, FL1-a (530 nm / 30 nm) and FL3-a (670 nm LP) were used to evaluate the viability of cells based on excitation and emission of dyes. 50,000 events with slow speed were recorded and the dead/live ratio was based on counts of FL-1/FL-3 area. Standard variant was ~25%. Standard cleaning cycle was applied to all biocidal experiments.

4.2.5 Absorption and fluorescence spectroscopy

The concentration of the stock solutions for the S-OPE-1s and EO-OPE-1s was 1 mM in 10 v/v % DMSO aqueous solution. 30 μL of the suspension of each EO-OPE-1 was diluted into 3 mL solution in a quartz cuvette to give a concentration of 10 μM. Absorption and fluorescence spectra were recorded on a plate reader (SpectroMax M-5 microplate reader, Molecular Devices) at 24^{o}C. Transient absorption spectra were recorded for EO-OPE-1 samples in both methanol and water using laser systems that are described elsewhere.[127,128] The optical density was adjusted to ~0.7 at the excitation wavelength (355 nm) with the laser energy being 6~7 mJ. Solutions were purged with

argon for 45 min before making transient absorption spectroscopy measurements.

4.3 Results and discussion

4.3.1 Absorption and fluorescence

Given that there are only two hydrophilic groups attached on both ends of EO-OPE-1s through a large hydrophobic aromatic segment, these compounds are poorly soluble in water, moderately soluble in CH_3OH, but quite soluble in DMF and DMSO. Further photophysical studies indicate that absorbance intensity measured immediately (1 min) for A and C under the concentration at 10 μM in H_2O is the same as that measured at 30 min later, in contrast, the intensity of B is enhanced around 2 times over 30 min and D is enhanced 1.5 times than that measured immediately (Fig. 3-8~22). These results indicate that B and D dissolve in water more slowly than the other EO-OPE-1s. Basically, this series of biocides has been demonstrated to be very efficient light harvesters with large molar extinction coefficients in water (Table 3-1 and Fig. 3-23~26), which are very similar to PPE. A, B, C, and D also have high fluorescent quantum yields (Φ_F) in water: 0.59, 0.52, 0.46, and 0.50, respectively.

4.3.2 Photophysics and singlet oxygen generation

In order to understand the mechanism by which oligo(phenylene ethynylene) derivatives A-D function as light-activated biocidal agents, a complete study of their photophysics was carried out in methanol and water. The photophysical data of A-D in methanol and water are consolidated in Table 4-1 and Table 4-2, respectively. A closer look at the results presented in Table 4-1 reveals several clear trends. First, all of the oligomers

absorb in the near-UV region; however, the absorption of C, which contains a thienylene unit, is slightly red-shifted. Fluorescence was observed for all of the oligomers in the near-UV region, and, in parallel with the absorption result, the emission from C is also red-shifted. Interestingly, the fluorescence quantum yield (Φ_F) is relatively high for the phenylene oligomers (A, B, and D), whereas it is significantly lower for C (Φ_F for C is ~6 times less than that of A and B). A similar trend is seen in the fluorescence decay data, where the lifetime (τ_F) of C is less than that of the other oligomers. Taken together, these data suggest that there is an accelerated singlet decay pathway operating in C. As suggested by the data discussed below, we believe that singlet decay is more rapid in C because the rate of ISC to the triplet state is enhanced.

Table 4-1. Photophysical data for compounds A - D in methanol solution

parameter	solvent	A	B	C	D
λ_{max} (absorption / nm)	MeOH	326	328	355	327
λ_{max} (fluorescence / nm)	MeOH	355	358	390	360
Φ_F [a]	MeOH	0.73 ± 0.03	0.69 ± 0.03	0.12 ± 0.01	0.53 ± 0.02
Φ_Δ [b]	CD_3OD	0.20± 0.02	0.17± 0.03	0.45± 0.03	0.09± 0.02
τ_F / ns	MeOH	0.4	0.45	0.23	0.52 (97%) 2 (3%)
TT_{Abs} (λ / nm)	MeOH	598	603	506	547
TT_{Abs} (ΔA, t=0)	MeOH	0.28	0.26	0.37	0.07
$\tau_{triplet}$ (μs)	MeOH	2.8	2.3	1.6	3.7

[a] Measured using quinine sulfate in 0.1 M sulfuric acid (Φ_F = 0.54) as actinometer.

[b] Measured in CD_3OD using 2′-acetonaphthone ($\Phi\Delta$ = 0.79) as actinometer.

Table 4-2. Photophysical data of substrates A-D in water

		A	B	C	D
λ_{max} (Absorption / nm)	Water	327	328	354	328
λ_{max} (Fluorescence / nm)	Water	388	390	410	397
Φ_F [a]	Water	0.44 ± 0.02	0.34± 0.02	0.11 ± 0.01	0.19 ± 0.03
TT_{Abs} (λ / nm) in Water		541	545	510	543
TT_{Abs} (ΔA, t=0) in Water		0.07	0.07	0.15	0.06
$\tau_{triplet}$ (μs) in Water		18.7	17.9	7.2	5.2

[a] Measured using Quinine sulfate in 0.1 M sulfuric acid (Φ_F = 0.54) as actinometer.

4.3.3 Biocidal study

4.3.3.1 EO-OPE-1s

The biocidal activities of the EO-OPE-1s containing cationic quaternary ammonium groups when exposed to 365 nm radiation in a photo reactor were evaluated against *E. coli*, *S. epidermidis*, and *S. aureus*. The results with ultraviolet irradiation are dramatic. After exposure of 30 min, significant kills of each bacteria occurred under very low concentration of EO-OPE-1s (Fig. 4-1~3) while much higher concentrations were needed for dark killing (Fig. 4-4~ 6). The most pronounced kills were seen for C both in the dark and light, which is different from a thiophene substituted PPE, where the thiophene modified PPE is good at dark killing but has very little light-activated killing.[129] In the thiophene substituted PPE system, the polymer is highly aggregated in aqueous solution which causes (1) less contact with bacteria and (2) fluorescence quenching, hence, the

light activated biocidal activity is attenuated. But small molecules such as C are less prone to aggregation, increasing the potential for cytoplasmic membrane penetration; hence, it is not surprising to see strong biocidal activity. We also noticed A is more efficient for killing bacteria in light than B, though they have very similar triplet yields (Table 4-1), which might be attributed to aggregation of B in aqueous solution. The anionic oligomer D exhibits lower biocidal activity towards *E.coli* and *S. aureus* (Fig. 4-1, 4-3), though it has a very similar triplet yield to cationic oligomers A and B. This phenomenon may be due to the Coulombic repulsion between anionic D and bacteria, which hinders D approaching and/or binding of bacteria, therefore, some of the $^1O_2$ has diffused into water and been quenched before it reaches bacteria.

To verify that microtubes do not affect biocidal activity or EO-OPE-1s, parallel control experiments with quartz cuvettes were carried out. It turned out that there was no considerable difference between the two systems. Time course experiments for each bacterium have been carried out, for control experiments, 365 nm irradiation does not have any effect onto *E.coli* or *S.epidermidis*, but there are significant kills for *S. aureus* over time, which is consistent with literature reports.[130]

To investigate the dose-dependent and time-dependent effects, various concentrations of each EO-OPE-1 were tested over 0 min, 30 min, and 60 min. The results show that higher concentration causes similar or more kills (Fig. 4-1~3). We previously reported that "inner filter" effects existed in polymer system at high concentrations,[131] but we didn't

observe this effect in the present study. It may derive from the low-dose response of these bacteria to EO-OPE-1s. Moreover, these biocides are much more active against Gram-positive bacteria than Gram-negative bacteria though their antibacterial activities against Gram-negative are excellent in light too. This phenomenon can be attributed to differences in the membrane structure. On the other hand, the time-dependent biocidal activity investigation suggests that the more kills will be obtained over time. This can be understood that over time more chemicals get into bacteria, and more $^1O_2$ is generated, which results in more killing.

Results from Flow Cytometry:

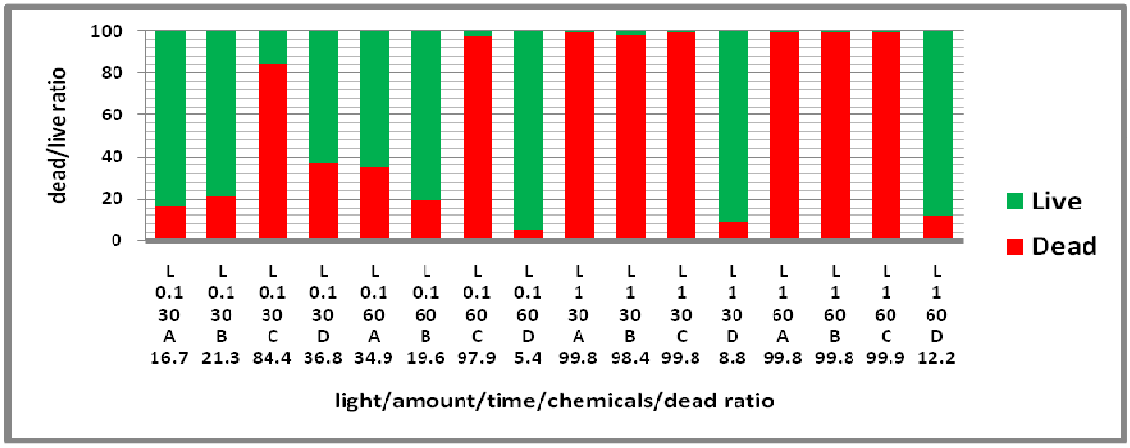

Fig. 4-1 The graph of A, B, C and D against *E.coli* with irradiation over 30 min and 60 min. The vertical axis represents the ratio of killed *E.coli.* For the X axis, 1st row- light, 2nd row- concentration(μg/mL), 3rd row-time (min), 4th row- chemicals, 5th row- dead ratio (%).

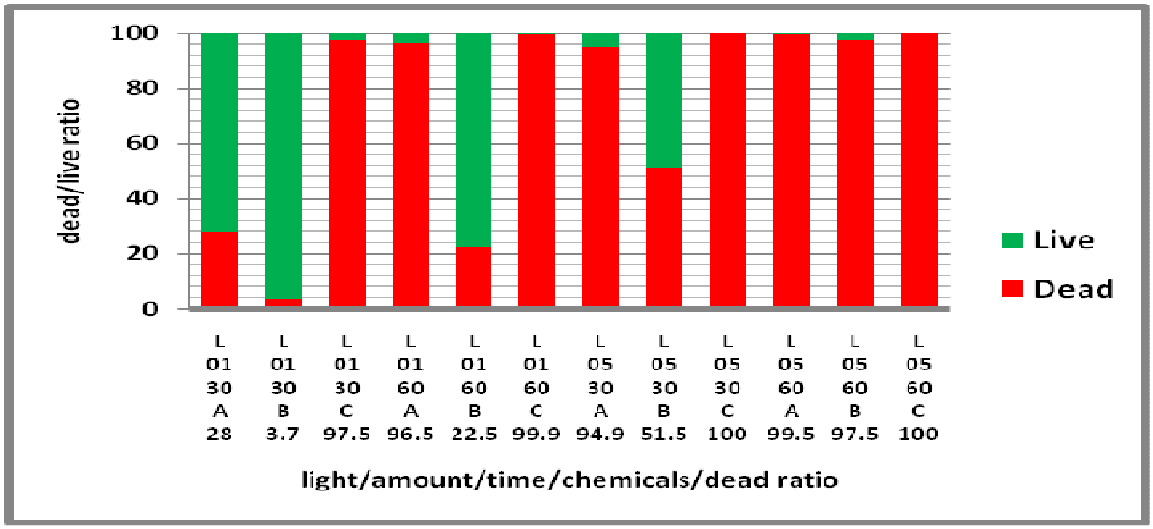

Fig. 4-2 The graph of A, B and C against *S.epidermis* with irradiation over 30 min and 60 min. The vertical axis represents the ratio of killed *S.epidermis.* For the X axis, 1st row- light, 2nd row- concentration(μg/mL), 3rd row-time (min), 4th row- chemicals, 5th row- dead ratio (%).

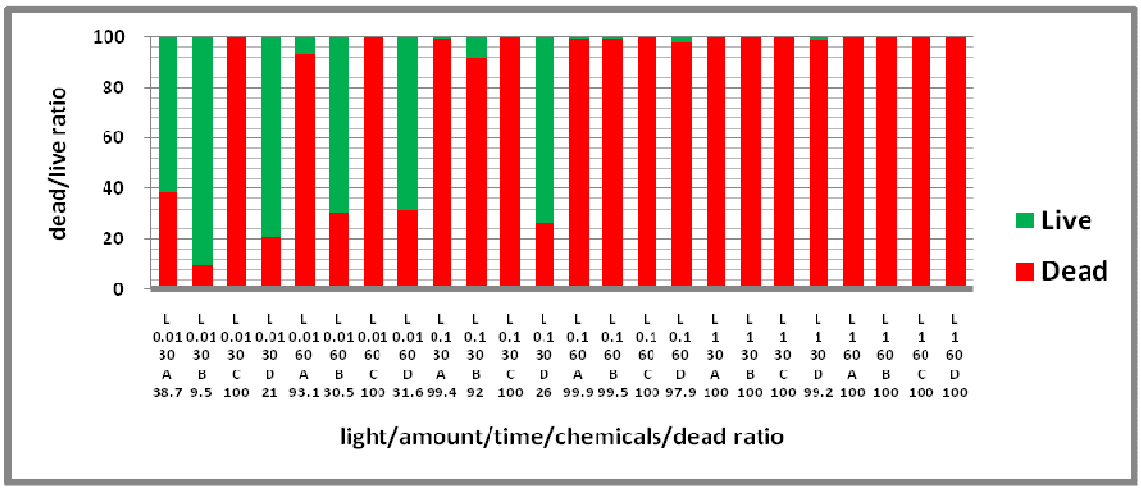

Fig. 4-3 The graph of A, B, C and D against *S.aureus* with irradiation over 30 min and 60 min. The vertical axis represents the ratio of killed *S.aureus.* For the X axis, 1st row- light, 2nd row- concentration(μg/mL), 3rd row-time (min), 4th row- chemicals, 5th row- dead ratio (%).

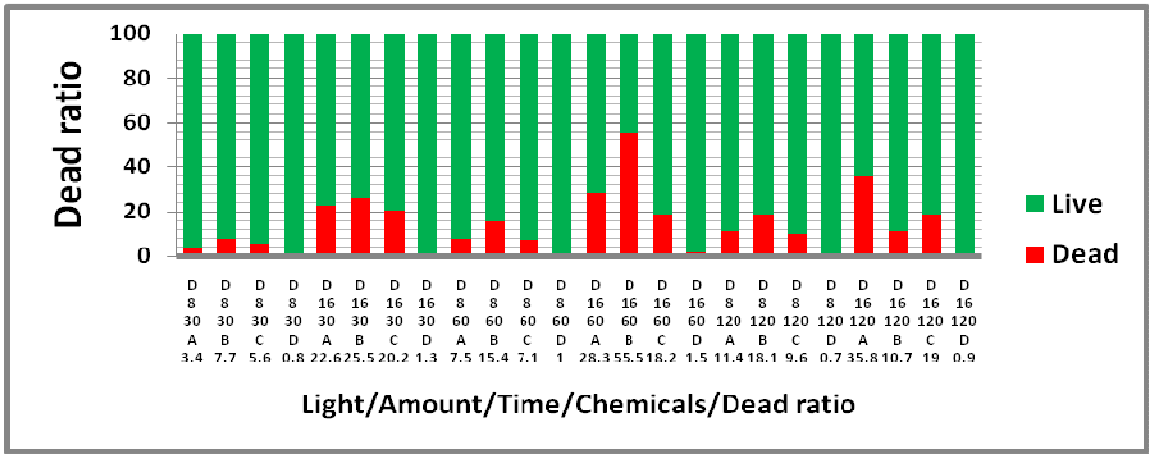

Fig. 4-4 The graph of A, B, C and D against *E.coli* in dark over 30 min and 60 min. The vertical axis represents the ratio of killed *E.coli.* For the X axis, 1st row- Dark, 2nd row- concentration(μg/mL), 3rd row-time (min), 4th row- chemicals, 5th row- dead ratio (%).

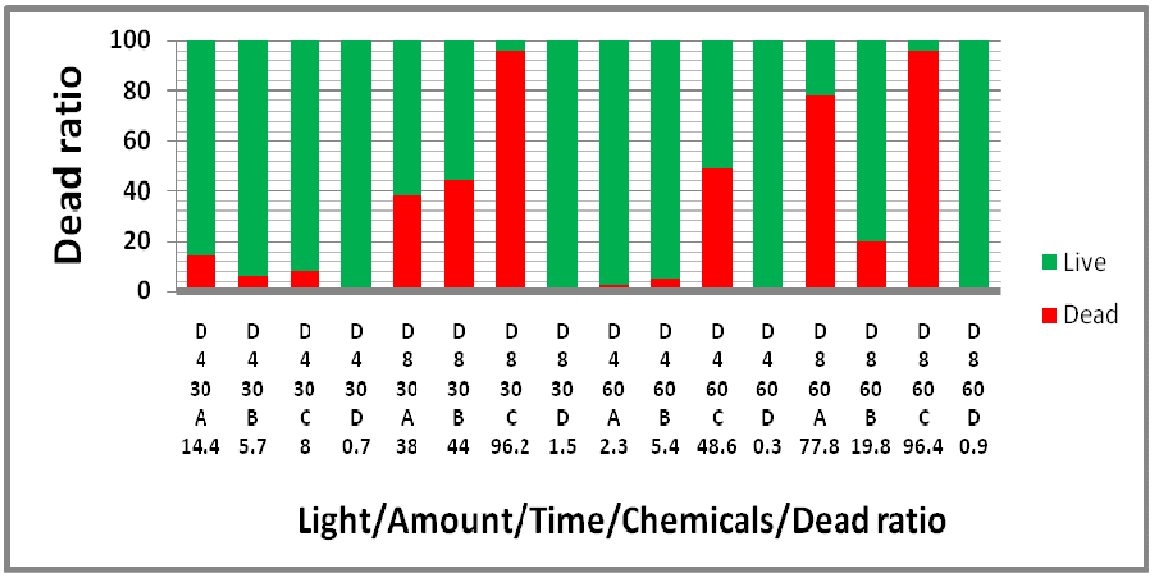

Fig. 4-5 The graph of A, B, C and D against *S.epidermis* in dark over 30 min and 60 min. The vertical axis represents the ratio of killed *S.epidermis.* For the X axis, 1st row- Dark, 2nd row- concentration(μg/mL), 3rd row-time (min), 4th row- chemicals, 5th row- dead ratio (%).

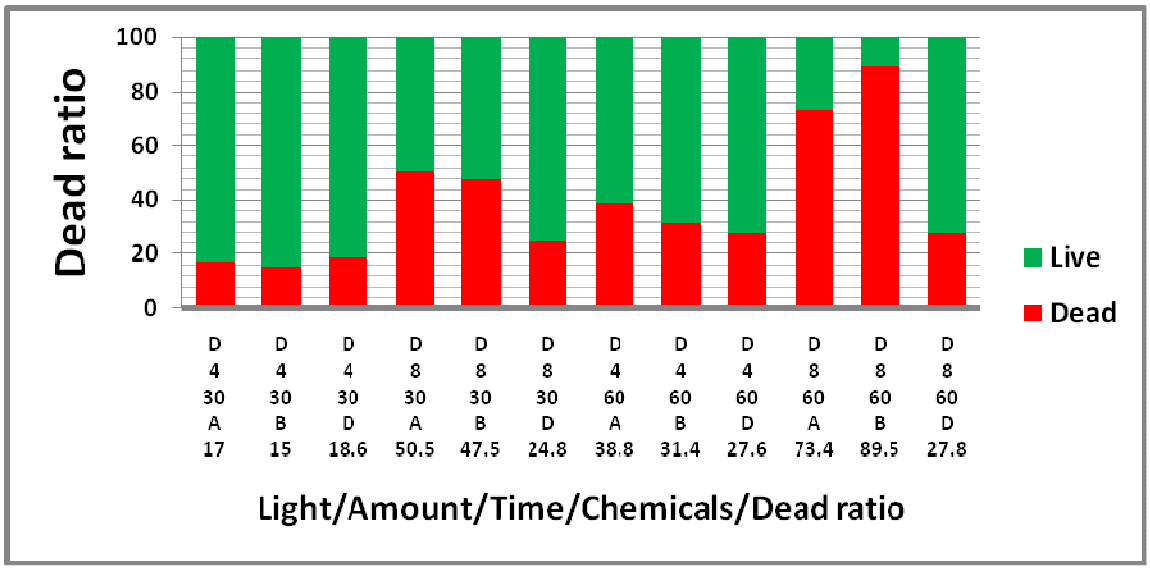

Fig. 4-6 The graph of A, B, and D against *S.aureus* in dark over 30 min and 60 min. The vertical axis represents the ratio of killed *S.aureus.* For the X axis, 1st row- Dark, 2nd row- concentration(μg/mL), 3rd row-time (min), 4th row- chemicals, 5th row- dead ratio (%).

Results from Laser Scanning Confocal Microscopy:

Confocal images of EO-OPE-1s against *E.coli* in the dark.

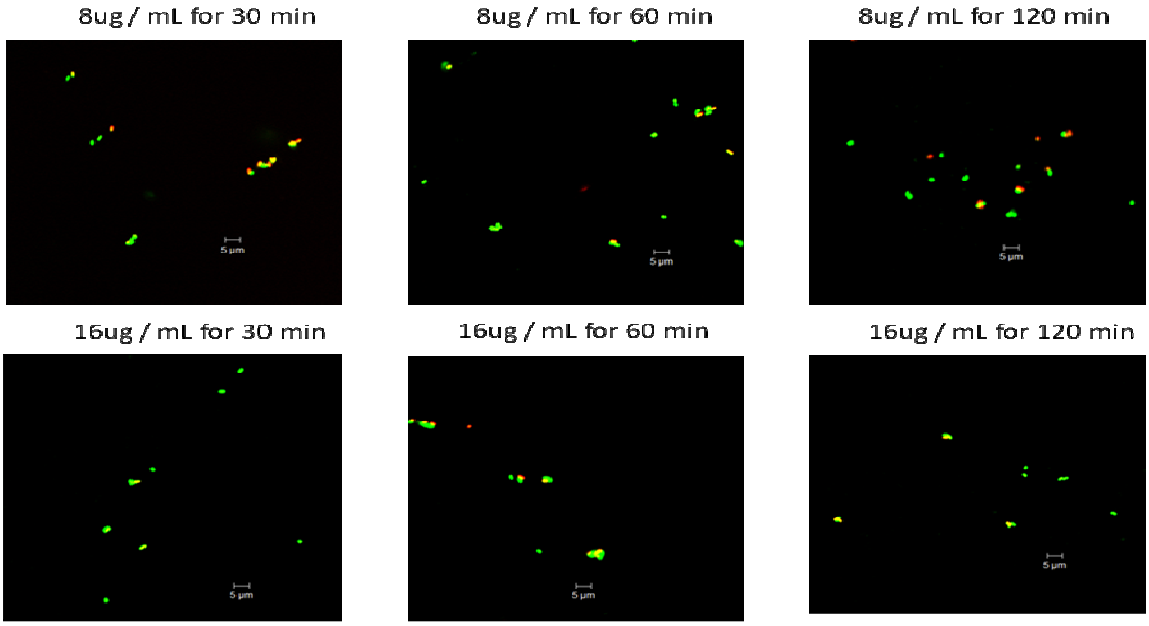

Fig. 4-6 A against *E.coli* in the dark over 30 min, 60 min and 120 min at room temperature. The concentration is 8 μg/mL and 16 μg/mL. Green-live, red-dead.

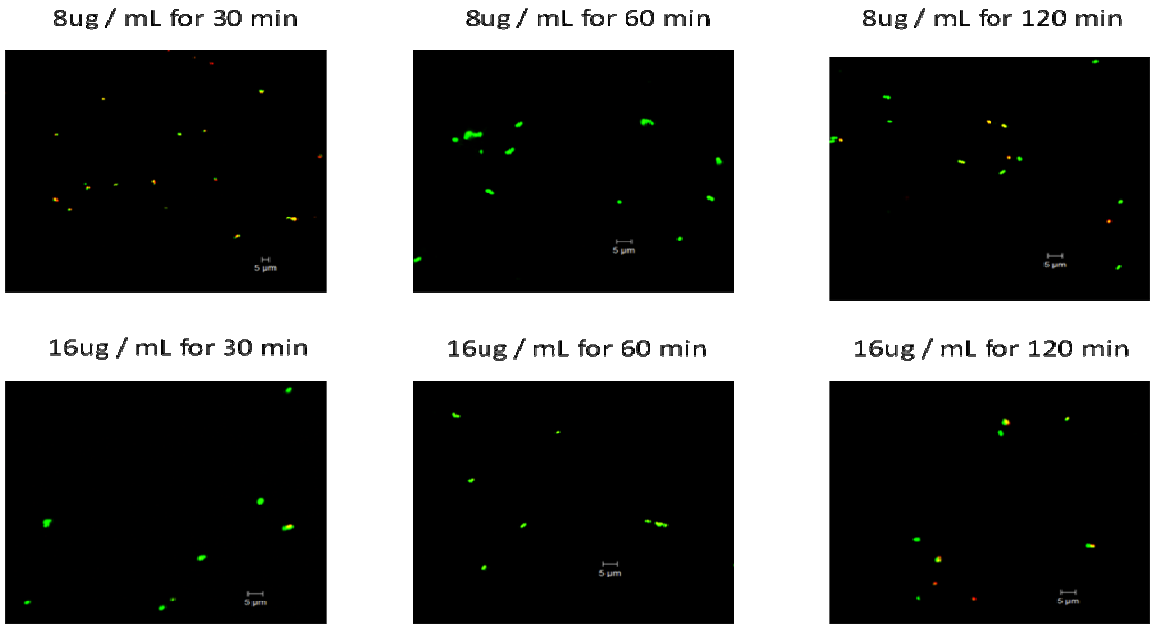

Fig. 4-7 B against *E.coli* in the dark over 30 min, 60 min and 120 min at room temperature. The concentration is 8 μg/mL and 16 μg/mL. Green-live, red-dead.

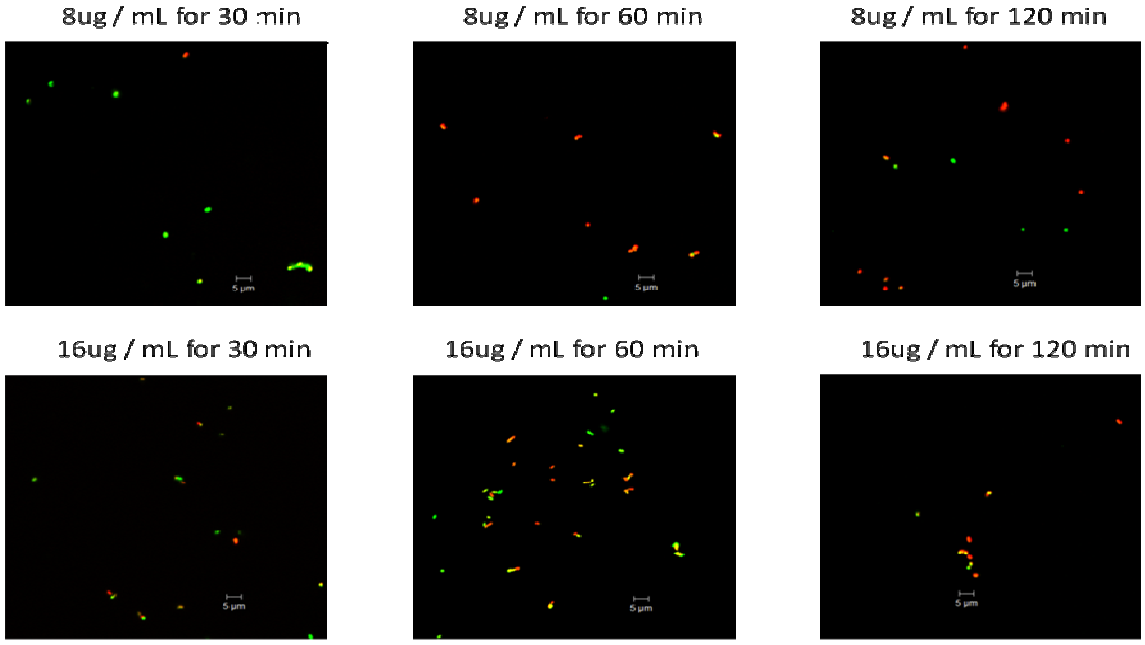

Fig. 4-8 C against *E.coli* in the dark over 30 min, 60 min and 120 min at room temperature. The concentration is 8 μg/mL and 16 μg/mL. Green-live, red-dead.

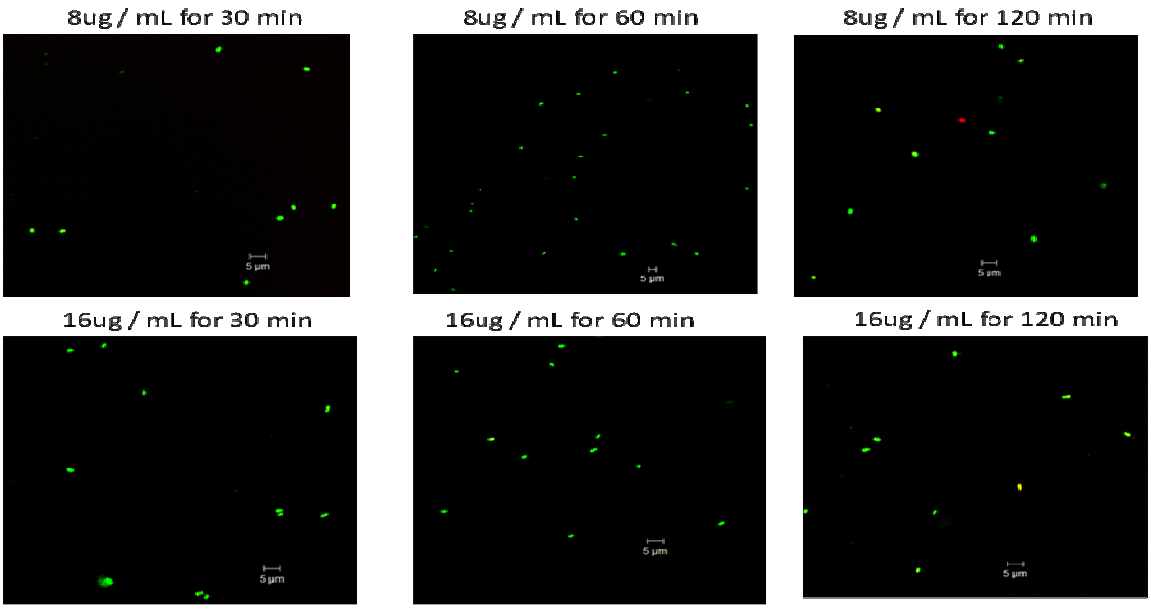

Fig. 4-9 D against *E.coli* in the dark over 30 min, 60 min and 120 min at room temperature. The concentration is 8 μg/mL and 16 μg/mL. Green-live, red-dead.

Confocal images for EO-OPE-1s against *S.epidermidis* in the dark over time.

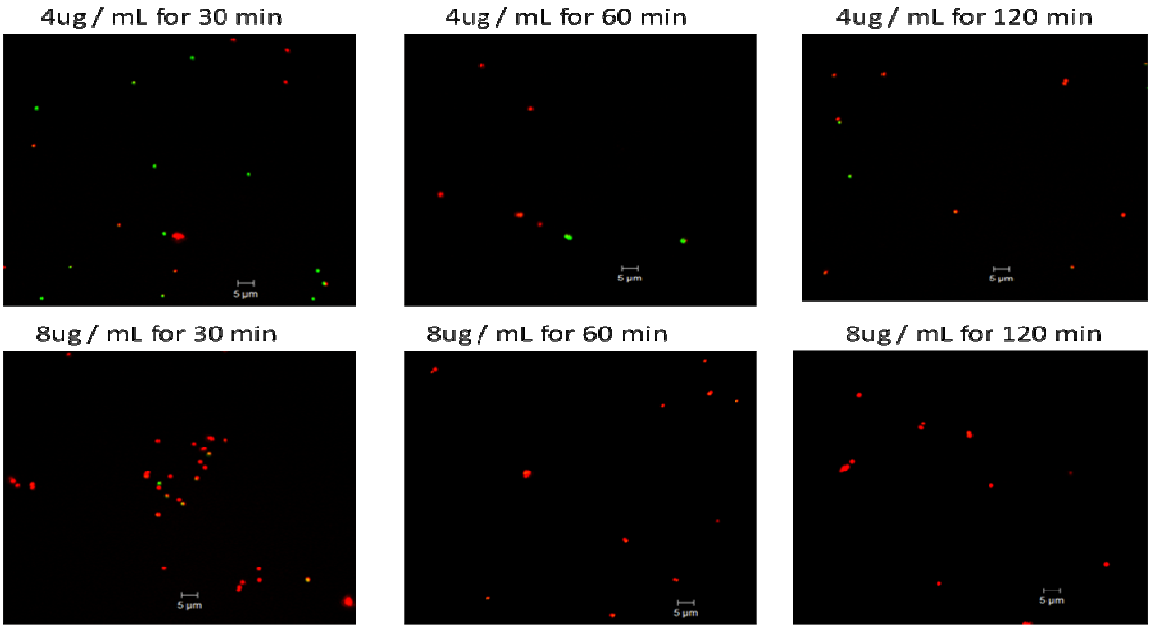

Fig. 4-10 A against *S.epidermidis* in the dark over 30 min, 60 min and 120 min at room temperature. The concentration is 4 μg/mL and 8 μg/mL. Green-live, red-dead.

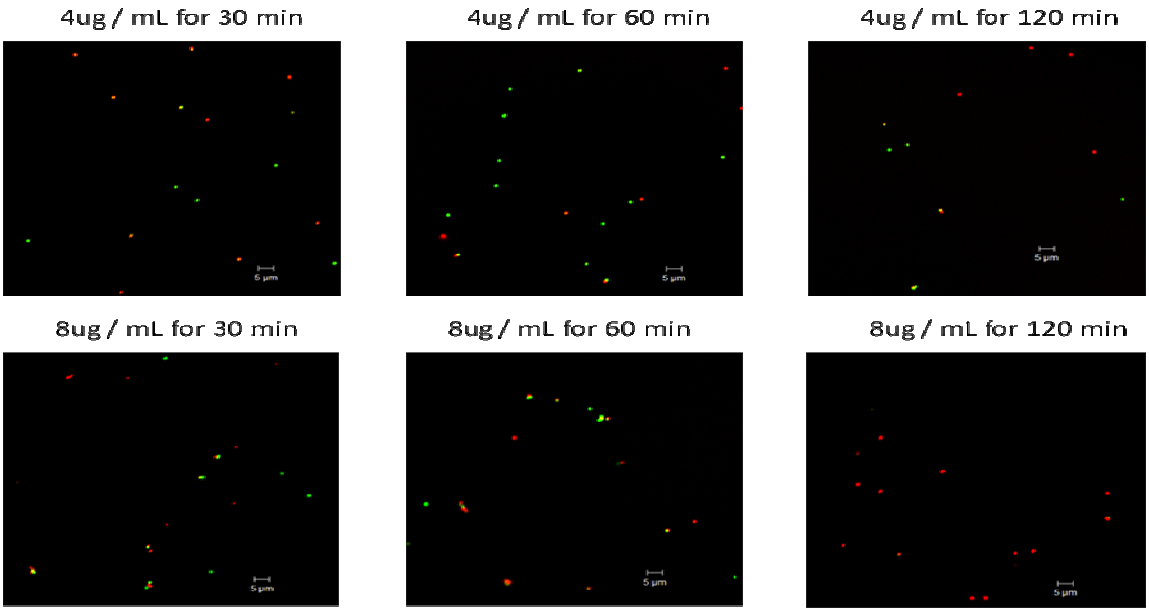

Fig. 4-11 B against *S.epidermidis* in the dark over 30 min, 60 min and 120 min at room temperature. The concentration is 4 μg/mL and 8 μg/mL. Green-live, red-dead.

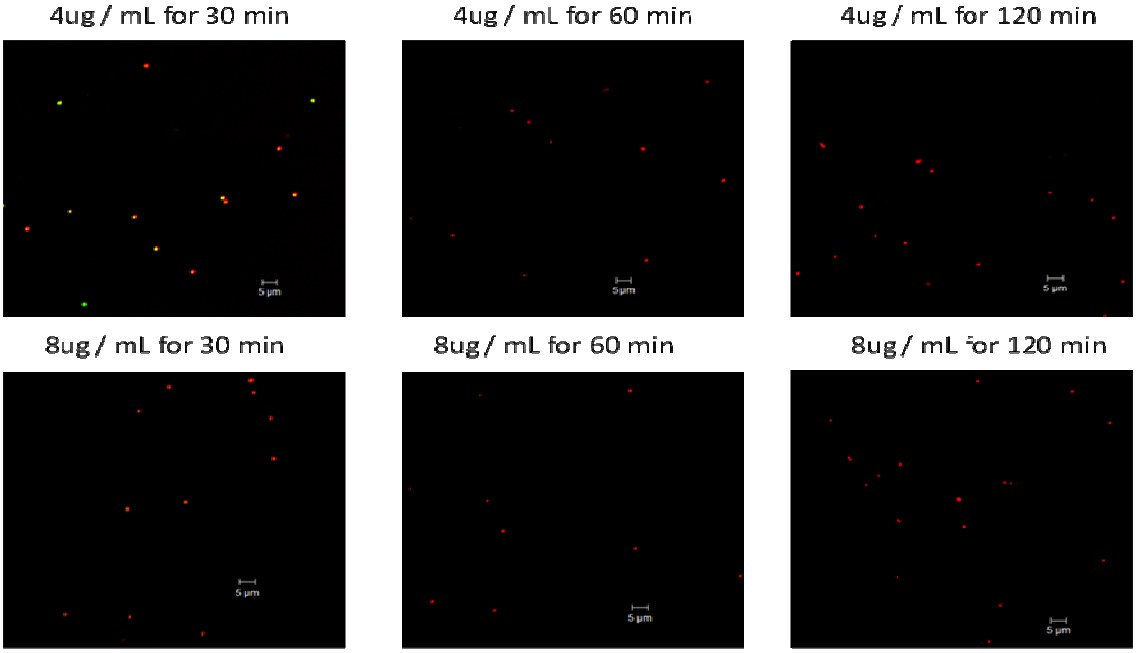

Fig. 4-12 C against *S.epidermidis* in the dark over 30 min, 60 min and 120 min at room temperature. The concentration is 4 μg/mL and 8 μg/mL. Green-live, red-dead.

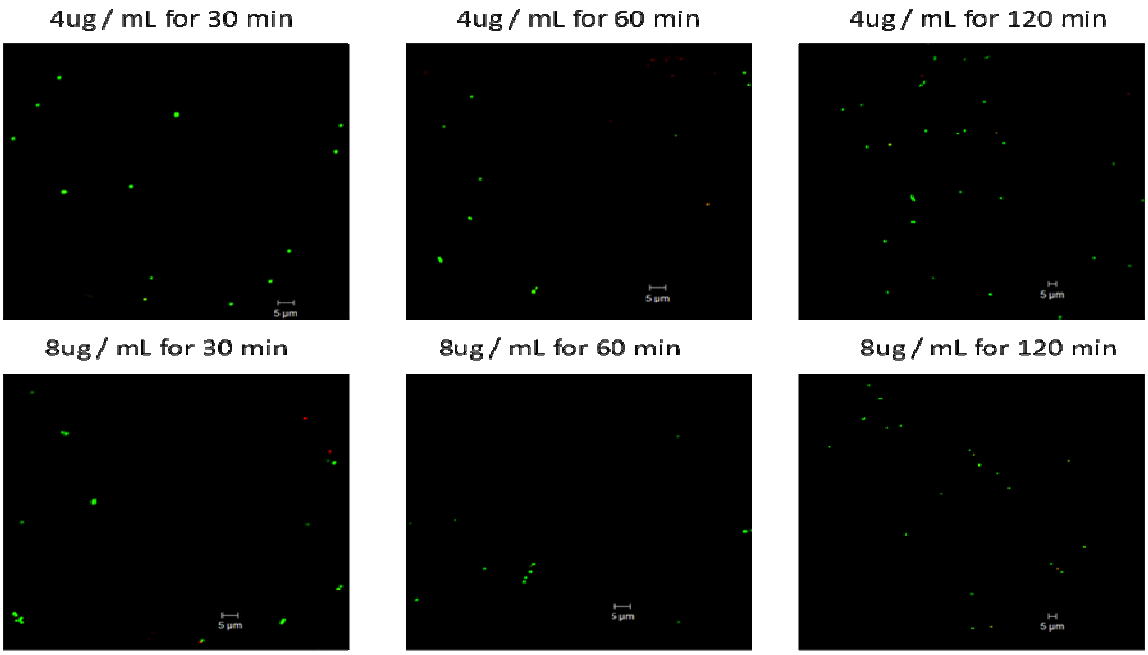

Fig. 4-13 D against *S.epidermidis* in the dark over 30 min, 60 min and 120 min at room temperature. The concentration is 4 µg/mL and 8 µg/mL. Green-live, red-dead.

Confocal images for EO-OPE-1s *against S.epidermidis* in the light.

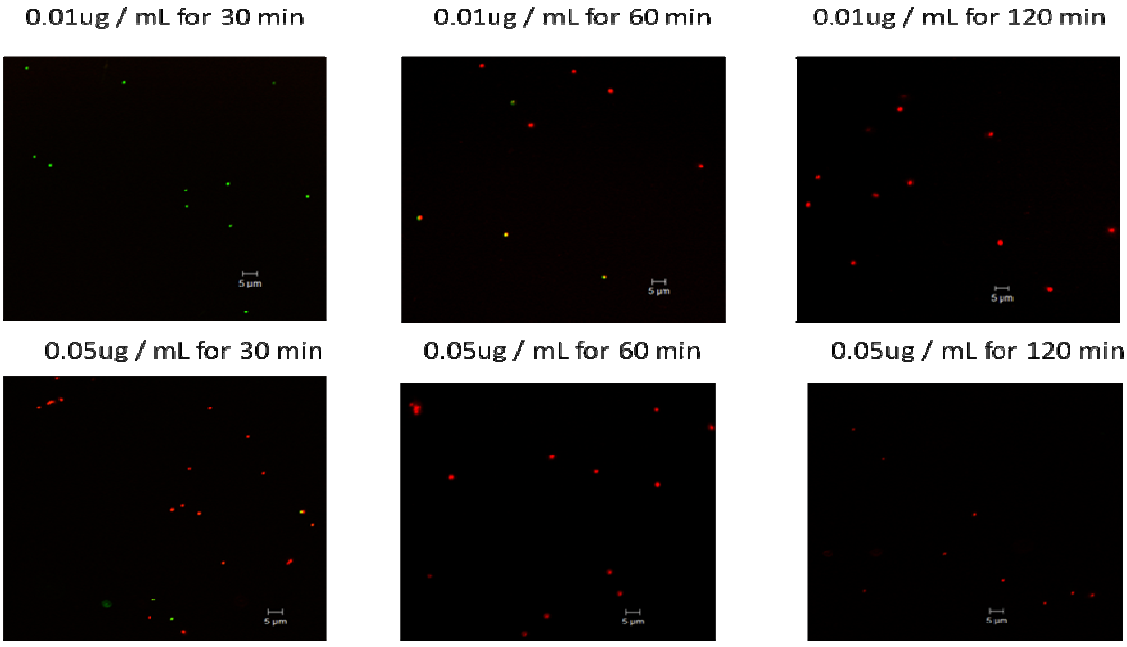

Fig. 4-14 A against *S.epidermidis* irradiated by UV-365 nm in a photoreactor chamber over 30 min, 60 min and 120 min at room temperature. The concentration is 0.01 µg/mL and 0.05 µg/mL. Green-live, red-dead.

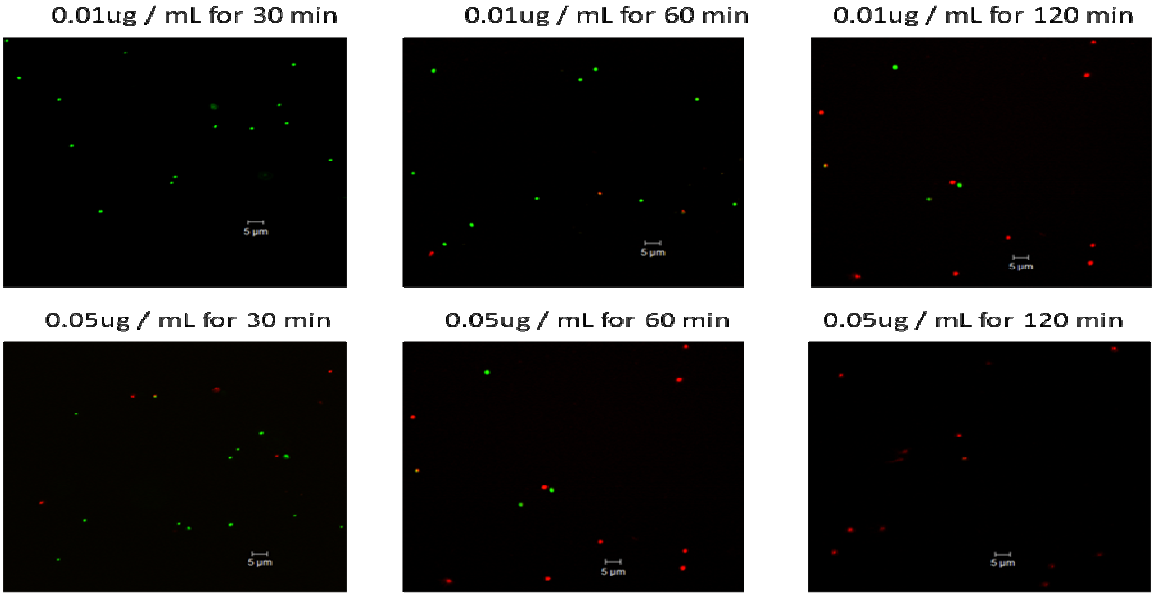

Fig. 4-15 B against *S.epidermidis* irradiated by UV-365 nm in a photoreactor chamber over 30 min, 60 min and 120 min at room temperature. The concentration is 0.01 µg/mL and 0.05 µg/mL. Green-live, red-dead.

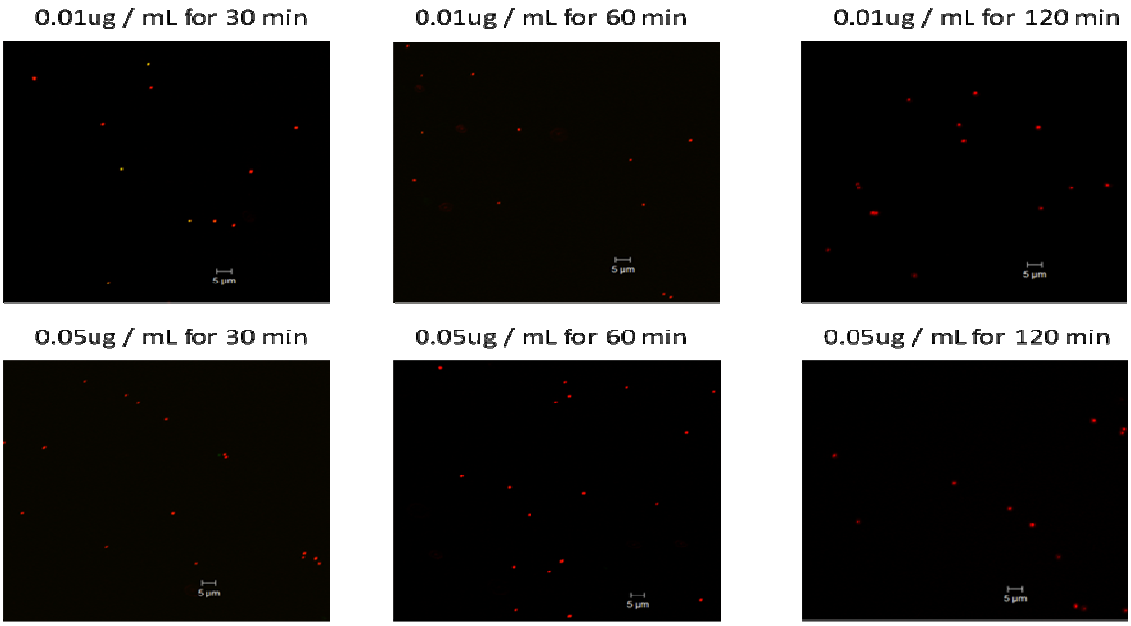

Fig. 4-16 C against *S.epidermidis* irradiated by UV-365 nm in a photoreactor chamber over 30 min, 60 min and 120 min at room temperature. The concentration is 0.01 µg/mL and 0.05 µg/mL. Green-live, red-dead.

Confocal images for EO-OPE-1s *against S.aureus* in the light.

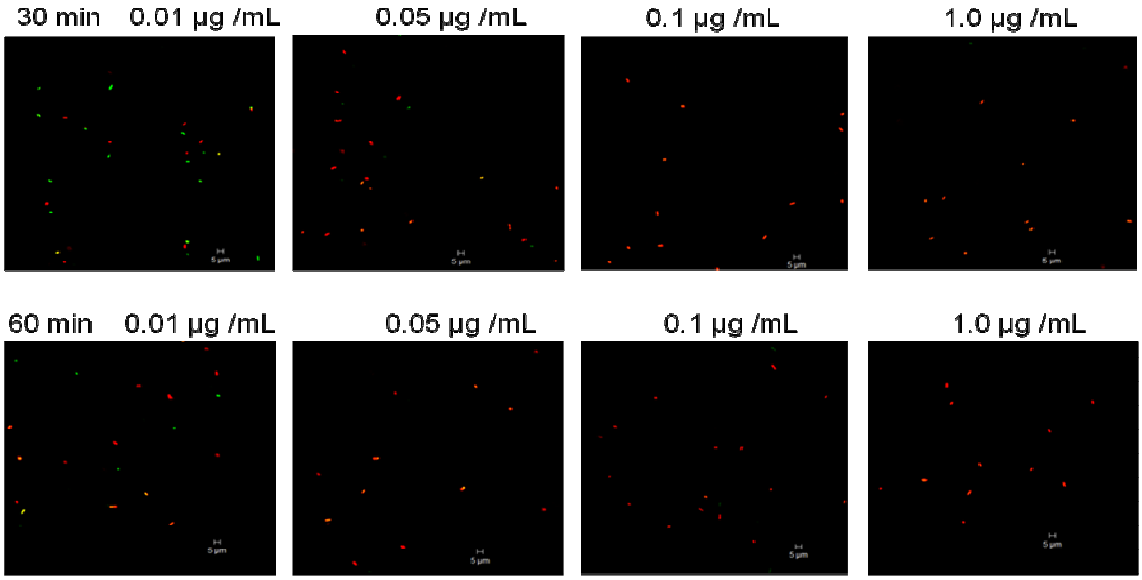

Fig. 4-17 A against *S.aureus* irradiated by UV-365 nm in a photoreactor chamber over 30 min and 60 min at room temperature. The concentration is 0.05 µg/mL, 0.1 µg/mL, and 1 µg/mL. Green-live, red-dead.

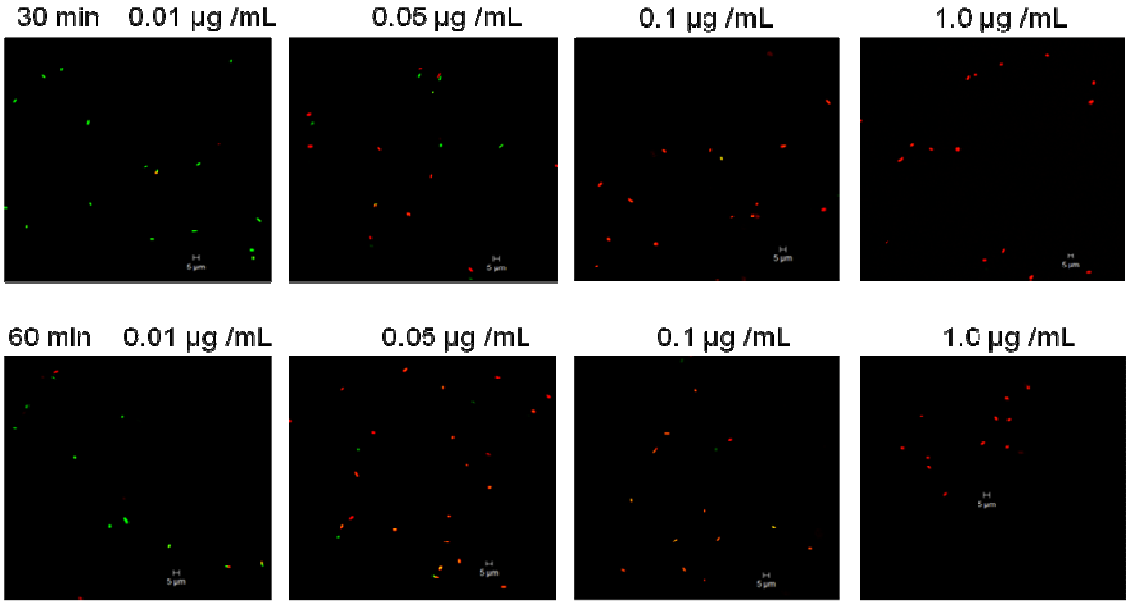

Fig. 4-18 B against *S.aureus* irradiated by UV-365 nm in a photoreactor chamber over 30 min and 60 min at room temperature. The concentration is 0.05 µg/mL, 0.1 µg/mL, and 1 µg/mL. Green-live, red-dead.

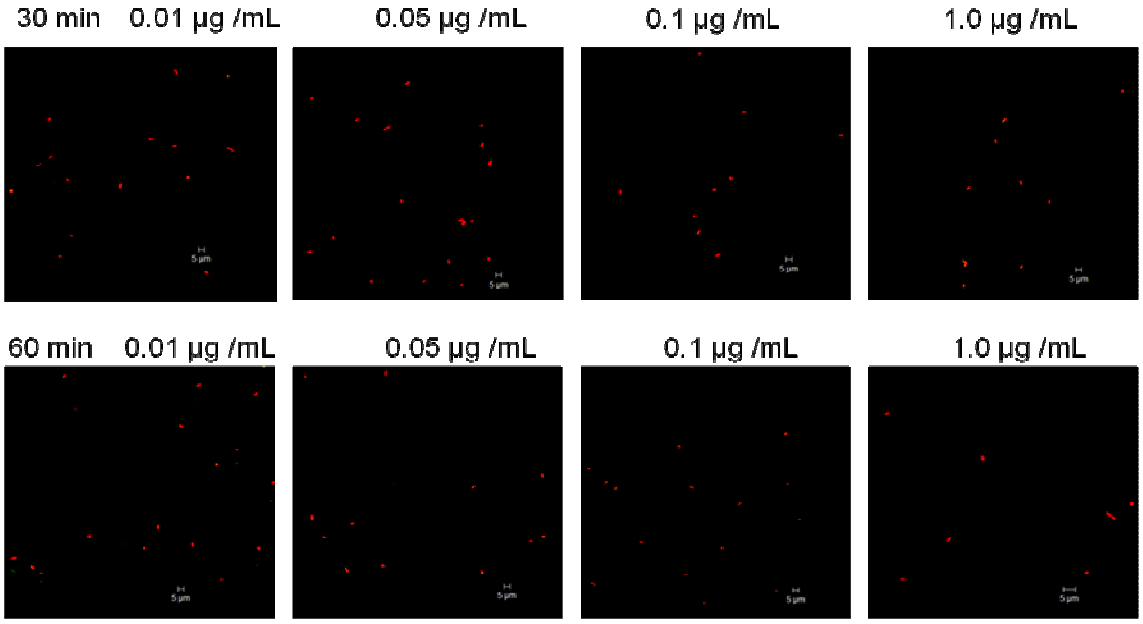

Fig. 4-19 C against *S.aureus* irradiated by UV-365 nm in a photoreactor chamber over 30 min and 60 min at room temperature. The concentration is 0.05 µg/mL, 0.1 µg/mL, and 1 µg/mL. Green-live, red-dead.

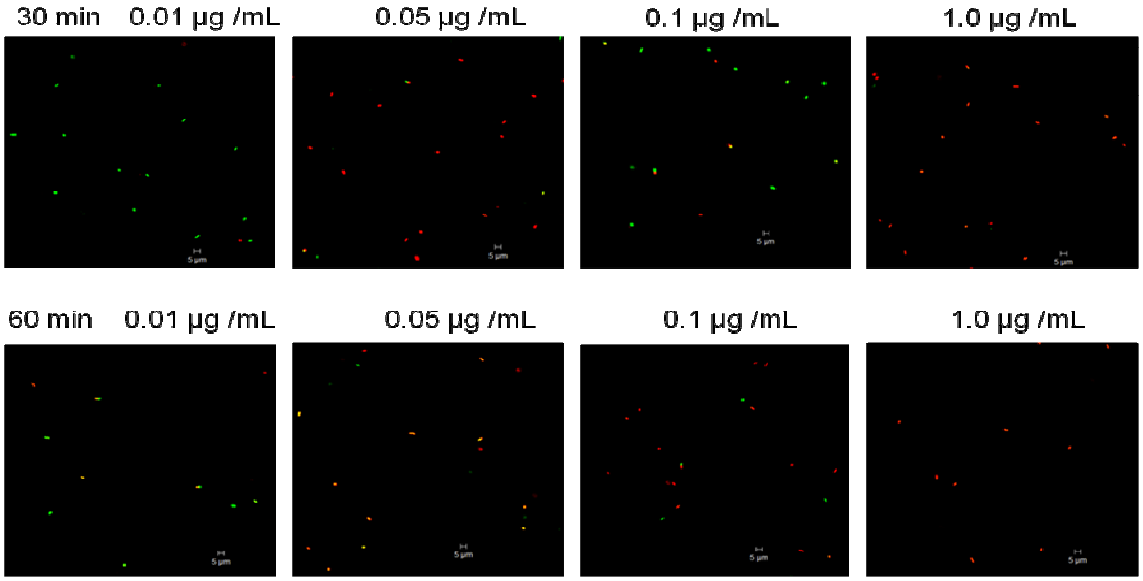

Fig. 4-20 D against *S.aureus* irradiated by UV-365 nm in a photoreactor chamber over 30 min and 60 min at room temperature. The concentration is 0.05 µg/mL, 0.1 µg/mL, and 1 µg/mL. Green-live, red-dead.

4.4.4.2 S-OPE-1s

We have tested S-OPE-1(OR), S-OPE-1($COCH_3$) against *E.coli* and *S.epidermidis*. Our

preliminary results have shown that S-OPE-1($COCH_3$) has similar light-induced biocidal activity to EO-OPE-1s.

Confocal Images against *E.coli.*

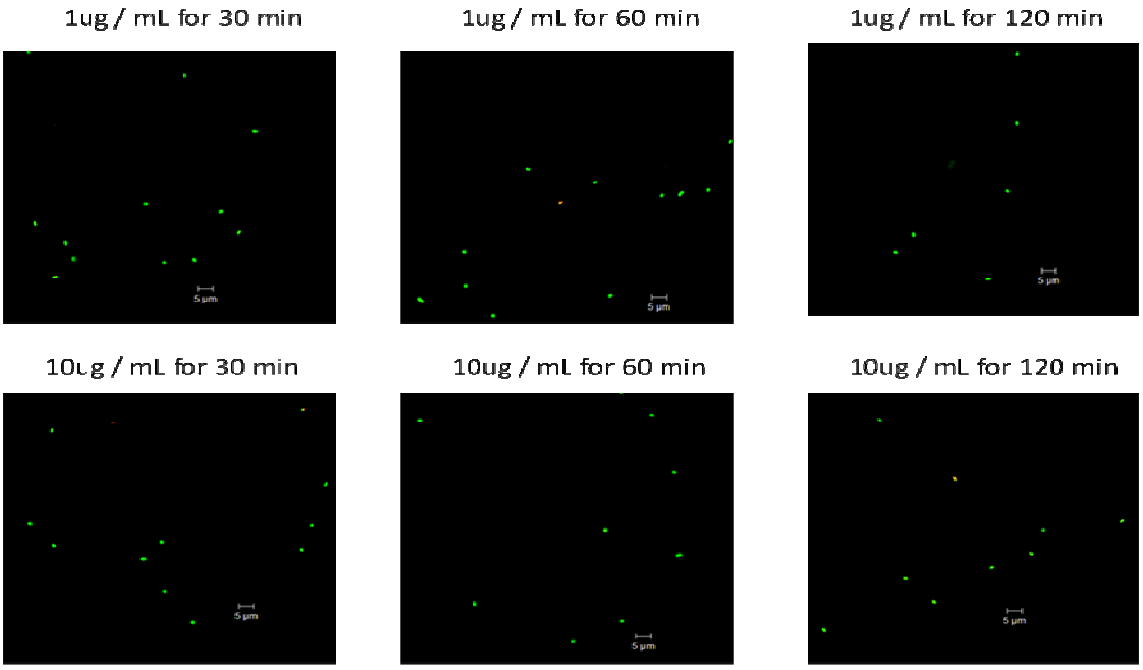

Fig. 4-21 S-OPE-1(OR) against *E.coli.* over 30 min, 60 min and 120 min in the dark with concentration of 1 μg/mL and 10 μg/mL at room temperature. Green-live, red-dead.

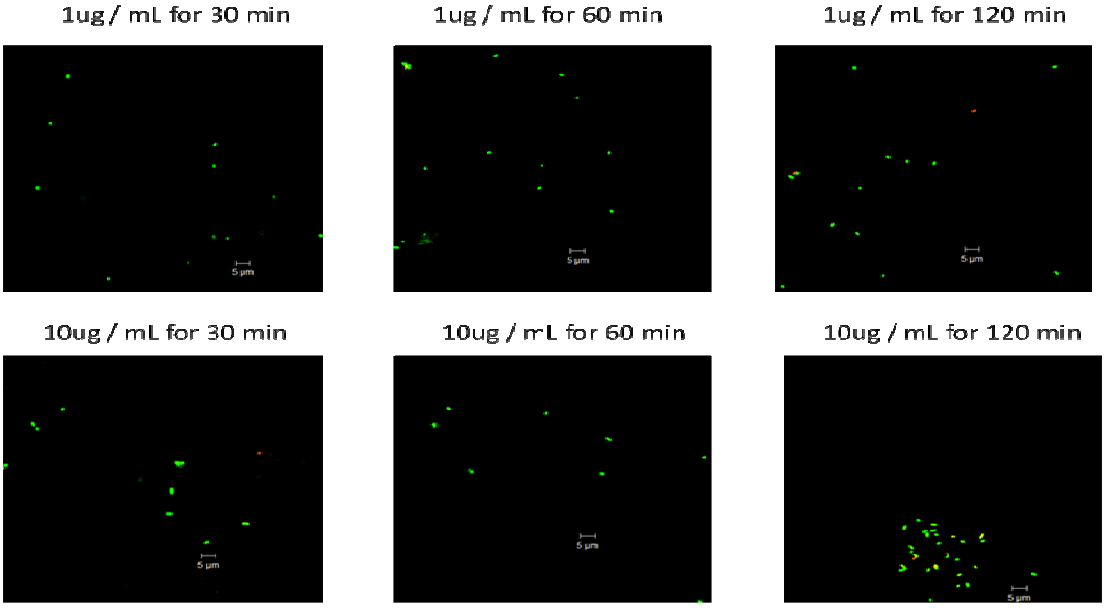

Fig. 4-22 S-OPE-1($COCH_3$) against *E.coli* over 30 min, 60 min and 120 min in the dark

with concentration of 1 µg/mL and 10 µg/mL at room temperature. Green-live, red-dead.

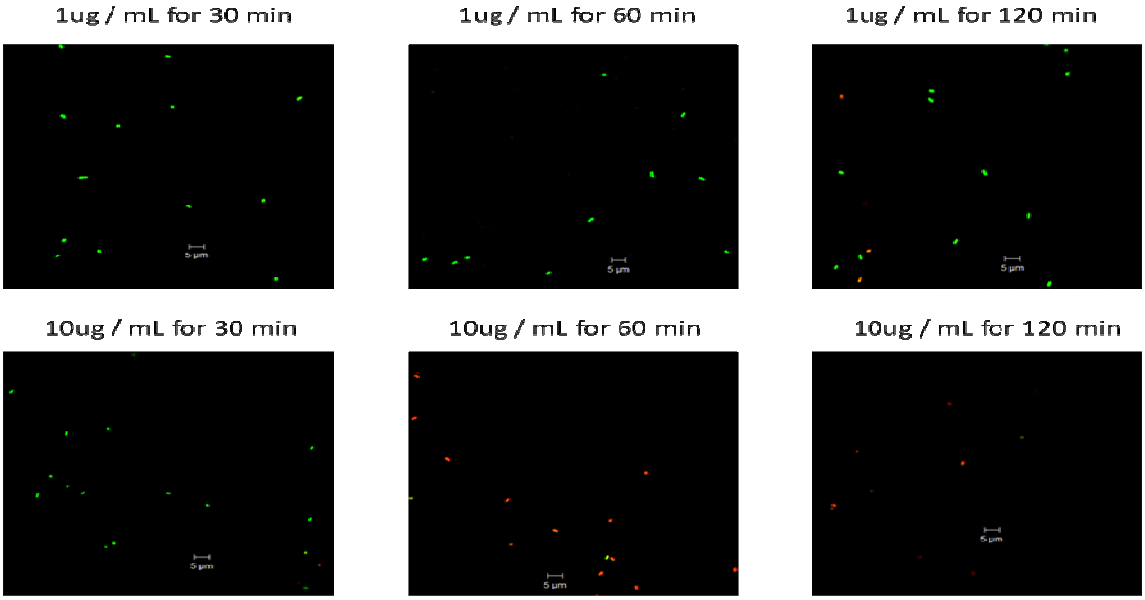

Fig. 4-23 UV-365 nm radiation for S-OPE-1(OR) against *E.coli.*over 30 min, 60 min and 120 min in the dark with concentration of 1 µg/mL and 10 µg/mL at room temperature. Green-live, red-dead.

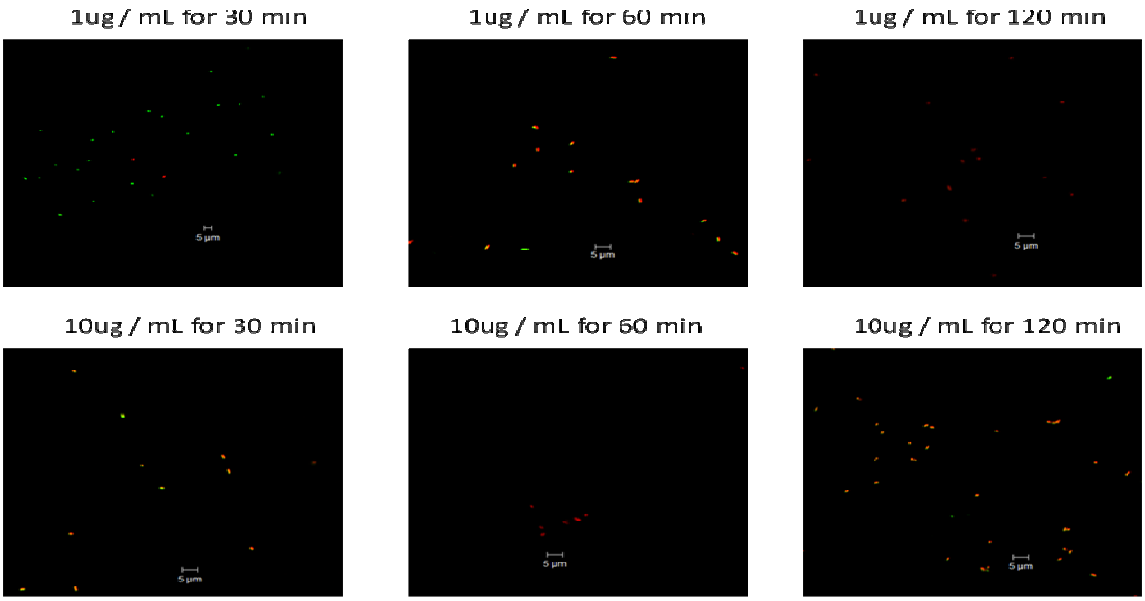

Fig. 4-24 UV-365 nm radiation for S-OPE-1($COCH_3$) against *E.coli.*over 30 min, 60 min and 120 min in the dark with concentration of 1 µg/mL and 10 µg/mL at room temperature. Green-live, red-dead.

4.4 Conclusion

The oligomers we present here show dramatic light-induced biocidal activity. To the best

of our knowledge, this is the first study that demonstrates light-induced biocidal activity of OPEs. We have correlated the light-induced biocidal activities and triplet yields of EO-OPE-1s, and a higher triplet yield suggests a better light-induced biocidal activity. Anionic molecule D, exhibits relatively poor light-induced biocidal activity due to Coulombic repulsion that probably results in little or no attachment of D to the surface or insertion into the membrane. We also found that hydrophobic nature of EO-OPE-1s series plays an important role in the biocidal activity, which is consistent with the reported results with nucleic acid stains.[132] Taken together with our previous work about the interactions of EO-OPE-1s with DOPC/cholesterol vesicles, which has demonstrated that EO-OPE-1s are readily to insert vesicles and induce leakage of components in vesicles,[133] we believe the biocidal process involves (1) EO-OPE-1s penetrates the bacterial membrane (2) EO-OPE-1s photosensitizes the generation of singlet oxygen and other reactive oxygen species and (3) singlet oxygen and/or reactive oxygen species triggers the cytotoxicity (Fig. 4-25~26).

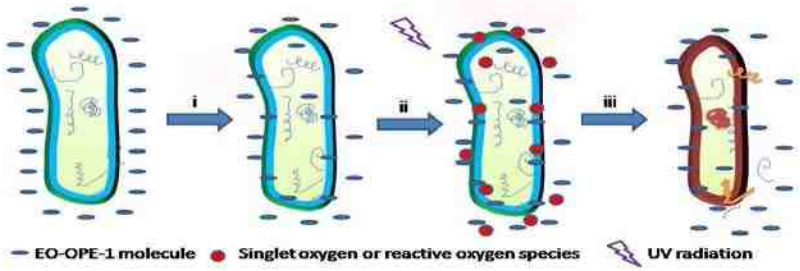

Fig. 4-25 ⅰ. EO-OPE-1s penetrates the bacterial membrane, ⅱ. EO-OPE-1s photosensitizes the generation of singlet oxygen and other reactive oxygen species, ⅲ. Singlet oxygen and/or reactive oxygen species triggers the cytotoxicity.

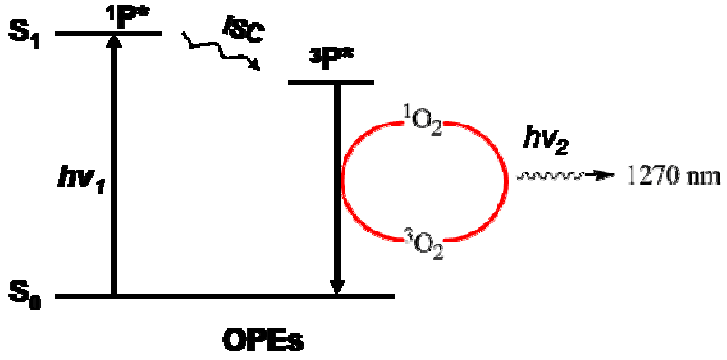

Fig. 4-26 The generation of singlet oxygen by sensitizing OPEs. The process involves ⅰ. OPEs is excited to singlet excited states (S_0 to S_1), ⅱ. excited states decay to excited triplet states through intersystem crossing (ISC, 1P* to 3P*) and ⅲ. Excited triplet states decay to ground state and release energy (3P* to S_0), which directly excites triplet oxygen to singlet oxygen.

Chapter 5 Summary and future work

Overall, this dissertation is centered on (1) biosensor development and (2) light-induced biocidal activity studies of EO-OPE-1s and S-OPE-1s. EO-OPE-1s and S-OPE-1s are first reported and protected by patents.

5.1 Progress

Biosensor: Two novel cyanines were synthesized: 2a and Cy2. We provided a universal strategy for the synthesis of unsymmetric cyanines with a high overall yield. We have found these cyanines are very weak or non-fluorescent, but strong fluorescence will be induced upon self-assembling onto some biomolecules such as CMA and CMC. Further studies by circular dichroism have indicated that helices are induced during self-assembling onto CMA but not for CMC. The remarkable fluorescent enhancement has encouraged us to develop an optical biosensor based on self-assembly. We have demonstrated that this concept is reasonable and practical by developing a protease biosensor DEVD-Cyanine with high sensitivity.

OPEs: (a) Five S-OPE-1s and four EO-OPE-1s have been synthesized and characterized. Basically, the synthesis is straightforward and easily characterized through NMR and Mass Spectroscopy, however, low yields were obtained for the conversion into EO-OPE-1 precursors, which probably can be attributed to the high affinity of these precursors to silica gel when we were doing column chromatography; (b) The photophysical studies including absorption, fluorescence and lifetime, transient

absorption, and singlet oxygen quantum yields have been carried out for S-OPE-1s and EO-OPE-1s. The measurements of TA and fluorescence quantum yields for S-OPE-1s are still on the way; We found EO-OPE-1(TH) showed a very high triplet state yield compared to other EO-OPE-1s, and the high triplet state probably indicates a high singlet oxygen quantum yield; (c) Investigation of self-assembly has been done for S-OPE-1s and some EO-OPE-1s. We found S-OPE-1(COOEt)/NH_2/$COCH_3$ are able to self-assembly onto CMA and CMC, in contrast, self-assembly behavior was not observed for S-OPE-1(H), S-OPE-1(COO^-) and EO-OPE-1(C3). All of S-OPE-1s and EO-OPE-1(C3) don't have self-assembly behavior upon Laponite clay; (d) the biocidal experiments have been carried out and the major techniques involved in the use of Flow Cytometry and Laser Scanning Confocal Microscopy for the investigation of the viability of bacteria. Very similar counts were obtained through both techniques. EO-OPE-1s show very good light-induced biocidal activity while exposed to UV-365 nm radiation. EO-OPE-1(TH) is the best one both in the dark and irradiation so far, which is different from PPETH (poor light-induced biocidal activity but good in dark). We have attributed these properties to high triplet yields of EO-OPE-1s and the unique linear structures of EO-OPE-1s. From time- and concentration-dependence experiments, we found higher concentration and extension of time were good for light-induced biocidal activity. Biocidal activities of S-OPE-1s are very similar to that of EO-OPE-1s, which probably suggests triplet yields are playing a major role not the linear structures of EO-OPE-1s. We believe the biocidal process involves (1) EO-OPE-1s penetrate the bacterial

membrane (2) EO-OPE-1s photosensitize the generation of singlet oxygen and other reactive oxygen species (Scheme 4-1) and (3) singlet oxygen and/or reactive oxygen species triggers the cytotoxicity (Fig. 1-9).

5.2 Issues needed to be addressed

Theoretically, DEVD-Cyanine offers a new method for high throughput screening, but this biosensor compromised by its low signal background ratio.

Our TA experiments indicate that EO-OPE-1s are very fast photobleached. These results are consistent with photophysical experiments conducted by Eric Hill in our group. So in the process of photo-induced biocidal experiments, it is still debatable if we can attribute the inactivation of bacteria completely to singlet oxygen since the photobleached products could be cytotoxicity and/or photosensitizers. So the mechanism could be clearer if the cytotoxicity of photobleached products can be excluded.

The synthesis of EO-OPE-1s and S-OPE-1s are straightforward, but yields for some steps are relatively low. New synthetic strategies and/or purification methods should be developed to address this issue.

Singlet oxygen quantum yields for EO-OPE-1(C2), EO-OPE-1(TH), EO-OPE-1(SO3) and S-OPE-1s haven’t been done. But reasonable assumption has been made that triplet yields of OPEs are proportional to singlet oxygen quantum yields. We hope the coming results about singlet oxygen quantum yields are consistent with triplet yields. On the other hand, other ROS could also play an important role in the inactivation of bacteria, but it is hard to trap ROS chemically or physically, which makes the determination of

specific role complicated.

All of these biocides are UV activated antimicrobial agents, which possibly limits their use in humans. On the other hand, EO-OPE-1(TH) seems more attractive since it has excellent dark killing too.

5.3 Future work

(a) Mechanism studies with PPE derivatives are being carried out in our group. The preliminary results show that PPE-DABCO is easier to penetrate DOPC/ cholesterol vesicles and induce a leakage of the inner components from the vesicles. This nature of PPE-DABCO may indicate a good biocidal activity in the dark. So it could be possible to give an even better biocidal activity by functionizing the ends of EO-OPE-1 with DABCO group (Fig. 5-1, E and F). The synthesis of E and F is slightly different from C and B, respectively.

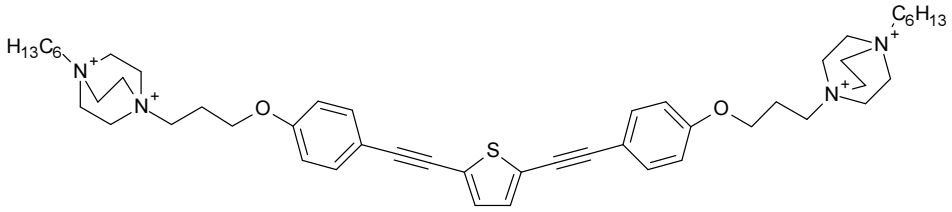

E

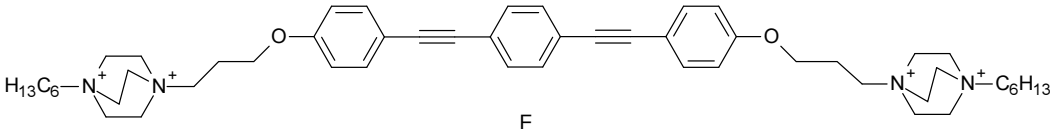

F

Fig. 5-1 Structures of E and F with DABCO on both ends. E has the same backbone as EO-OPE-1(TH), and F has the same backbone as EO-OPE-1(C3).

(b) Clarification of the mechanism for light-induced biocidal activity of OPE-1s: i. Measurements of singlet oxygen quantum yields for compound A, C, D and S-OPE-1s should be done in the future and we will correlate the $^1O_2$ yield with triplet state yield. ii. Photophysical and photochemical studies about singlet oxygen generation and photobleaching of S-OPE-1s and EO-OPE-1s. iii. Studies of membrane perturbation using model membrane(s).

(c) More bacteria and bacterial spores will be tested.

References

1. (a) Feldman B.J.; Osterloh J.D.; Hata B.H; D'Alessandro A. *Anal. Chem.* **1994**, *66*, 1983-1987, (b) Jagner D.; Renman L..; Wang Y.D.; *Electroanalysis* **1994**, *6*, 285-291.

2. Binder H.; Weber P.C.; Siess W. *Anal. Biochem*. **1985**, *148*, 220-227.

3. Potter B.V.L.; Lampe D. *Angew. Chem., Int. Ed. Engl.* **1995**, *34*, 1933-1972.

4. Turner A.P.F. *Science,* **2000**, *290*, 1315-1317.

5. Thevenot D.R.; Toth K.; Durst R.A.; Wilson G.S. *Biosens. Bioelectron*, **2001**, *16*, 121-131.

6. Sassolas A.; Leca-Bouvier B.D.; Blum L.J. *Chem. Rev.*, **2008**, *108*, 109-139.

7. Yuan Q.; Wang Z.K.; Nian S.; Yin Y.P.; Chen G.; Xia Y.X. *Appl. Biochem. Biotechnol.* **2009**, *152*, 224-234.

8. a). Ferapontova E.E.; Gothelf K.V. *Electroanalysis*, **2009**, *21*, 1261-1266. b). Ferapontova E.E.; Olsen E.M.; Gothelf K.V. *J. Am. Chem. Soc.*, **2008**, *130*, 4256-4258. c). Churchman L.S.; Oeten Z.; Rock R.S.; Spudich J.A. *Biophys. J.* **2005**, *88*, 664A-664A. d). Tedeschi L.; Citti L.; Domenici C. *Biosens. Bioelectron*, **2005**, *20*, 2376-2385. e). Baeumner A.J.; Cohen R.N.; Miksic V. Min J.H. *Biosens. Bioelectron* **2003**, *18*, 405-413. f). Kleinjung F.; Klussmann S.; Erdmann V.A; Scheller F.W.; Fürste J.P.; Bier F.F. *Anal. Chem.*, **1998**, *70*, 328-331.

9. Jelinek R.; Kolusheva S. *Chem. Rev*., **2004**, *104*, 5987-6015.

10. a). Chen H.; Hu Q.Y.; Yue Z.; Jiang J.H.; Shen G.L.; Yu R.Q. *Anal. Chim. Acta.* **2010**, *657*, 204-209. b). Shih W.C.; Yang M.C.; Lin M.S. *Biosens. Bioelectron* **2009**, *24*, 1679-1684. c). Liu N.; Gao Z.X.; Zhou H.Y.; Yue M.X. *Biosens. Bioelectron* **2007**, *22*, 2371-2376.

11. a). Zanoni M.V.B.; Rogers E.I.; Hardacre C.; Compton R.G.. *Anal. Chim. Acta* **2010**, *659*, 122-128. b). Daniel R.; Almog R.; Shacham D.R. *IEEE Sens. J*. **2010**, *10*, 274-280. c). Close D.M.; Ripp S.; Sayler G.S. *Sensors*, **2009**, *9*, 9147-9174. d). Ben-Yoav H.; Biran A.; Pedahzur R.; Belkin S.; Buchinger S.; Reifferscheid G.; Shacham-Diamand Y. *Electrochim. Acta*, **2009**, *54*, 6113-6118. e). Park T.J.; Zheng S.; Kang Y.J.; Lee S.Y. *FEMS Microbiol. Lett.* **2009**, *293*, 141-147.

12. Clark L.C. *Trans Am. Soc. Artif. Intern. Organs*, **1956**, 2, 41-57.

13. a). Downs M.E.A.; Kobayashi S.; Karube I. *Anal. Lett.* **1987**, *20*, 1897-1927. b). Millan K.M.; Saraullo A.; Mikkelsen S.R. *Anal. Chem.* **1994**, *66*, 2943-2948. c). Ferguson J.A.; Boles T.C.; Adams C.P.; Walt D.R. *Nat. Biotechnol*. **1996**, *14*, 1681-1684. d). Wang J.; Cai X.H.; Rivas G.; Shiraishi H.; Farias P.A.M; Dontha N. *Anal. Chem.* **1996**, *68*, 2629-2634. f). Wang J.; Cai X.H.; Rivas G.; Shiraishi H.; Farias P.A.M; Dontha N. *Anal. Chem.* **1996**, *68*, 2251-2254. g). *Electroanalysis*, **1997**, *9*, 1132-1137. h). Moser I.; Schalkhammer T.; Pittner F.; Urban G. *Biosens. Bioelectron.* **1997**, *12*, 729-737. i). *Oxidants and Antioxidants*, PT B book series, Methods in enzymology, **1999**, *300*, 314-321. j). Brett A.M.O.; Macedo T.R.A.; Raimundo D.; Marques M.H.; Serrano S.H.P. *Biosens. Bioelectron.* **1998**, *13*, 861-867. k). Siontorou C.G.; Nikolelis D.P.; Tarus B.; Dumbrava J.; Krull U.J. *Electroanalysis*, **1998**, *10*, 691-694. l). *Abstr. Pap. Am. Chem. Soc.* **1998**, *216*, U936-U936. m). Marrazza G.; Chiti G.; Mascini M.; Anichini M. *Clin. Chem.* **2000**, *46*, 31-37. n). Cloarec J.P.; Martin J.R.; Polychronakos C.; Lawrence I.; Lawrence M.F.; Souteyrand E. *Sens. Actuators B: Chem.* **1999**, *58*, 394-398. o). Liu X.J.; Tan W.H. *Anal. Chem.***1999**, *71*, 5054-5059. p). Erdem A.; Kerman K.; Meric B.; Akarca U.; Ozsoz M. *Electroanalysis*, **1999**, *11*, 586-588. q). Berney H.; West J.; Haefele E.;

Alderman J.; Lane W.; Collins J.K. *Sens. Actuators B: Chem.* **2000**, *68*, 100-108. r). Li J.; Lu Y. *J. Am. Chem. Soc.* **2000**, *122*, 10466-10467. s). Ozsoz M.; Erdem A.; Kara P.; Kerman K.; Ozkan D. *Electroanalysis*, **2003**, *15*, 613-619. t). Cai H.; X. Cao X.; Jiang Y.; He P. *Anal. Bioanal. Chem.* **2003**, *375*, 287-293. u). Kanga K.; Masaaki K.; Eiichi T. *Meas. Sci. Technol.* **2004**, *15*, R1-R-11. v). Cheng G. F.; Zhao J.; Tu Y.H.; He P.G.; Fang Y.Z. *Anal. Chim. Acta* **2005**, *533*, 11-16. w). Hu K.C.; Lan D.X.; Li X.M.; Zhang S.S. *Anal. Chem.* **2008**, *80*, 9124-9130. x). Kim D.K.; Kerman K.; Saito M.; Sathuluri R.R.; Endo T.; Yamamura S.H.; Kwon Y.S.; Tamiya E. *Anal. Chem.* **2007**, *79*, 1855-1864.

14. a). Elena E. Ferapontova E.E.; Olsen E.M.; Gothelf K.V. *J. Am. Chem. Soc*., **2008**, *130*, 4256-4258. b). Baeumner A.J.; Cohen R.N.; Miksic V.; Min J.H. *Biosens. Bioelectron*, **2003**, *18*, 405-413. c). Kleinjung F.; Klussmann S.; Erdmann V.A.; Scheller F.W.; Fürste J. P.; Bier F. F. *Anal. Chem.* **1998**, *70*, 328-331.

15. a). Lee S.J.; Youn B.S.; Park J.W.; Niazi J.H.; Kim Y.S.; Gu M.B. *Anal. Chem.* **2008**, *80*, 2867-2873. b). Prowa T.W.; Bhutto I.; Grebe R.; Uno K.; Merges C.; Mcleod D.S.; Lutty G.A. *Vision Res.* **2008**, *48*, 478-485.

16. Pohanka M.; Skladal P.; Kroea M.; *Def. Sci. J.* **2007**, *57*, 185-193.

17. Luckarift H.R.; Greenwald R.; Bergin M.H.; Spain J.C.; Johnson G.R. *Biosens. Bioelectron*. **2007**, *23*, 400-406.

18. a). Pohanka M.; Jun D.; Kuca K. *Drug Chem. Toxicol.* **2007**, *30*, 253-261, b). Valimaa A.L.; Kivisto A.T.; Leskinen P.I.; Karp M.T. *J. Microbiol. Methods*, **2010**, *80*, 44-48.

19. Wu Z.S.; Jiang J.H.; Fu L.; Shen G.L.; Yu R.Q. *Anal. Biochem.* **2006**, *353*, 22-29.

20. Yeh H.C.; Ho Y.P.; Wang, T.H. *Nanomedicine*, **2005**, *1*, 115-121.

21. Nomura Y.; Fuchigami H.; Kii H.; Feng Z.G.; Nakamura T.; Kinjo M.; *Anal. Biochem.*

2006, *351*, 196-201.

22. Stojanovic M. N.; Stofanovic D. *J. Am. Chem. Soc.* **2003**, *125*, 3214.

23. Castaneda M.T.; Merkoci A.; Pumera M.; Alegret S. *Biosens.Bioelectron.* **2007**, *22*, 1961-1967.

24. Zhai J.H.; Cui H.; Yang R.F. *Biotechnol. Adv.* **1997**, *15*, 43-58.

25. Fischer E. *Ber. Dt. Chem. Ges.* **1894**, *27*, 2985–2993.

26. Koshland D.E. *Proc. Natl. Acad. Sci.* **1958**, *44*, 98–104.

27. Jelinek R.; Kolusheva S. *Chem. Rev.* **2004**, *104*, 5987-6016.

28. Martin M. F. C. *Microchimica Acta,* **2004**, *148*, 107-132.

29. (a) Jelley E.E. *Nature* **1936**, *138*, 1009-1010. (b) Scheibe G. *Angew. Chem. Int. Ed. Engl.* **1936**, *49***,** 563-563.

30. West W.; Carroll B.H.; Whitcomb D. *J. Photogr. Sci.* **1953**, *1*, 173.

31. Katoh T.; Inagaki Y.; Okazaki R. *Bull. Chem. Soc. Jpn.* **1997**, *70*, 2279-2286.

32. Dr. Komandoor Achyuthan's presentation.

33. Kim O. K.; Je J.; Jernigan G.; Buckley L.; Whitten D. G. *J. Am. Chem. Soc.* **2006**, *128*, 510-516.

34. Whitten D.G.; Achyuthan K.E.; Lopez G.P.; Kim O.K. *Pure Appl. Chem.* **2006**, *78*, 2313-2323.

35. Achyuthan K.E.; Lu L.D.; Lopez G.P.; Whitten D.G. *Photochem. Photobiol. Sci.* **2006**, *5*, 931-937.

36. Deboer S.; Wiersma D.A. *Chem. Phys. Lett.* **1990**, *165*, 45-53.

37. Tani T.; Suzumoto T.; Kemnitz K.; Yoshihara K. *J.Phys. Chem.* **1992**, *96*, 2778-2783.

38. Achyuthan K.E.; Bergstedt T.S.; Chen L.; Jones R.M.; Kumaraswamy S.; Kushon

S.A.; Ley K.D.; Lu L.; McBranch D.; Mukundan H.; Rininsland F.; Shi X.; Xia W.; Whitten D.G. *J. Mater. Chem.* **2005**, *15*, 2648-2656.

39. Ober C.K.; Wegner G. *Adv. Mater.* **1997**, *9*, 17–31.

40. Chen L.H.; McBranch D.W.; Wang H.L.; Helgeson R.; Wudl.; Whitten D.G. *Proc. Natl. Acad. Sci. U.S.A.* **1999**, *96*, 12287–12292.

41. Peyratout C.S.; Dähne L. *Angew. Chem., Int. Ed.* **2004**, *43*, 3762–3783.

42. Tan C.Y.; Schanze K.S. *J. Am. Chem. Soc.* **2004**, *126*, 14964–14971.

43 . *Handbook of Conducting Polymers. Conjugated Polymers: Processing and Applications*, 3rd ed.; Skotheim, T. A., Reynolds, J. R., Eds.; CRC Press: Boca Raton, FL, **2007**.

44.Zhou Q.; Swager T.M. *J. Am. Chem. Soc.* **1995**, *117*, 7017-7018.

45. Zeineldin R.; Piyasena M.E.; Sklar L.A.; Whitten D.G.; Lopez G.P. *Langmuir,* **2008**, *24*, 4125-4131.

46. Jones R.M.; Lu L.D.; Helgeson R.; Bergstedt R.S.; McBranch D.W.; Whitten D.G. *J. Am. Chem. Soc.* **2001**, *123*, 6726–6727.

47. Jones R.M.; Bergstedt T.S.; Buscher C.T.; McBranch D.; Whitten D.G. *Langmuir*, **2001**, *17*, 2568–2571.

48. Kushon S.A.; Ley K.D.; Bradford K.; Jones R.M.; McBranch D.; Whitten D.G. *Langmuir,* **2002**, *18*, 7245–7249.

49. Kushon S.A.; Bradford K.; Marin V.; Suhrada C.; Armitage B.A.; McBranch B.; Whitten D.G. *Langmuir,* **2003**, *19*, 6456–6464.

50. Lu L.D.; Jones R.M.; McBranch D.; Whitten D.G. *Langmuir,* **2002**, *18*, 7706–7713.

51.Lu L.D.; Helgeson R.; Jones R.M.; McBranch D.; Whitten D.G. *J. Am. Chem. Soc.*

2002, *124*, 483–488.

52. Jiang H.; Zhao X.Y.; Schanze K.S. *Langmuir,* **2006**, *22*, 5541–5543.

53. Jiang H.; Zhao X.Y.; Schanze K.S. *Langmuir*, **2007**, *23*, 9481–9486.

54. Liu Y.; Ogawa K.; Schanze K.S. *Anal. Chem.* **2008**, *80*, 150–158.

55. Liu Y.; Schanze K.S. *Anal. Chem*. **2009**, *81*, 231–239.

56. Zhao X.Y.; Jiang H.; Schanze K.S. *Macromolecules,* **2008**, *41*, 3422–3428.

57. Liu Y.; Schanze K.S. *Anal. Chem,* **2008**, *80*, 8605–8612.

58. Tan C.Y.; Atas E.; Müller J.G.; Pinto M.R.; Kleiman V.D.; Schanze K.S. *J. Am. Chem. Soc*. **2004**, *126*, 13685–13694.

59. Corbitt T.S.; Sommer J.R.; Chemburu S.; Ogawa K.; Ista L.K.; Lopez G.P.; Whitten D.G.; Schanze K.S. *ACS Appl. Mater. Interfaces,* **2009**, *1*, 48-52.

60. Chemburu S.; Corbitt T.S.; Ista L.K.; Ji E.; Fulghum J.; Lopez G.P.; Ogawa K.; Schanze K.S.; Whitten D.G. *Langmuir,* **2008**, *24*, 11053–11062.

61.Jones L.; Schumm J.S; Tour J.M. *J. Org. Chem.* **1997**, *62*, 1388-1410.

62. Huang S.L.; Tour J.M. *J. Am. Chem .Soc*, **1999**, *121*, 4908-4909.

63. *Abstr. Pap. Am. Chem. Soc.* **2002**, *223*, 320-ORGN Part 2 APR 7.

64. Hwang J.J.; Tour J.M. *Tetrahedron*, **2002**, *58*, 10387-10405.

65. Huang S.; Tour J. M. *Tetrahedron Lett.* **1999,** *40*, 3347-3350.

66. Zhao J.L.; Bo Z.S. *Synth. Commun.* **2005**, *35*, 1391-1402.

67.Yang X. W.; Yuan L. H.; Yamato K.; Brown A. L.; Feng W.; Furukawa M.; Zeng X. C.; Gong, B.*J. Am. Chem. Soc*. **2004**, *126*, 3148-3162.

68. Yang X.W.; Brown A.B.; Furukawa M.F.; Li S.J.; Gardinier W.E.; Bukowski E.J.; Bright F.V.; Zheng C.; Zeng X.C.; Gong B. *Chem. Commun.* **2003**, *1*, 56-57.

69. Yamato K.; Gong B. *Supramol. Chem.* **2009**, *21*, 196-201.

70. Dholakia G.R.; Fan W.; Koehne J.; Han J.; Meyyappan M. *J Nanosci Nanotechnol.* **2003**, *3*, 231-234.

71. Prest P.J.; Prince R.B.; Moore J.S. *J. Am. Chem. Soc.* **1999**, *121*, 5933-5939.

72. Mio M. J.; Prince R. B.; Moore J. S.; Kuebel C.; Martin D.C. *J. Am. Chem. Soc.* **2000**, *122*, 6134-6135.

73. García F.; Aparicio F.; Fernández G.; Sánchez L. *Org. Lett.* **2009**, *11*, 2748-2751.

74. Tang Y.L.; Zhou Z.J.; Ogawa K.; Lopez G.P.; Schanze K.S.; Whitten D.G. *Langmuir*, **2009**, *25*, 21-25

75. Gram H.C. *Fortschritte der Medizin*, **1884**, *2*, 185–189.

76. Tew G.N.; Scott R.W.; Klein M.L.; DeGrado W.F. *Acc. Chem. Res.* **2010**, *43*, 30-39.

77. See reviews a) Hamblin M.R.; Hasan T. *Photochem. Photobiol. Sci.* **2004**, *3*, 436-450, b) Jori G.; Fabris C.; Soncin M.; Ferro S.; Coppellotti O.; Dei D.; Fantetti L.; Chiti G.; Roneucci G. *Lasers Surg. Med.* **2006**, *38*, 468-481, c) Maisch T. Mini *Rev. Med. Chem.* **2009**, *9*, 974-983, d) Garland M.; Cassidy C.M.; Woolfson D.; Donnelly R.F. *Future Med. Chem.* **2009**, *1*, 667-691.

78. Nicholson D.W.; Thornberry N.A. *Trends Biochem. Sci.* **1997**, *22*, 299–306.

79 . Fernandesalnemri T.; Litwack G.; Alnemri E.S. *J. Biol. Chem.* **1994**, *269*, 30761-30764.

80. Tewari M.; Quan L.T.; Orourke K.; Desnoyers S.; Zeng Z.; Beidler D.R.; Poirier G.G.; Salvesen G.S.; Dixit V.M. *Cell*, **1995**, *81*, 801-809.

81. Bedner E.; Li X.; Gorczyca W.; Melamed M.R.; Darzynkiewicz Z. *Cytometry*, **1999**, *35*, 181-195.

82. Gurtu V.; Kain S.R.; Zhang G.H. *Anal. Biochem.* **1997**, *251*, 98–102.

83. Wang Z.Q.; Liao J.F.; Diwu Z.J. *Bioorg. Med. Chem. Lett.* **2005**, *15*, 2335-2338.

84. Zhou Z.J.; Tang Y.L. Whitten D.G.; Achyuthan K.E. *ACS Appl. Mater. Interfaces*, **2009**, *1*, 162-170

85. Achyuthan K.E.; Mcclain.L.; Zhou Z.J.; Whitten D.G.; Branch D.W. *Anal Sci.* **2009**, *25*, 469-474.

86. Edited by Kobayashi T. "*J-Aggregates*", **1996**, World Scientific Publishing Company: Singapore.

87. Oh-Kil Kim O.K.; Je J.; Jernigan G.; Buckley L.; Whitten D.G. *J. Am. Chem. Soc.* **2006**, *128*, 510–516.

88. Edited by Kobayashi T. *J-Aggregates*, World Scientific Publishing Company: Singapore, **1996**, 228.

89.Edited by Bernards D.A.; Owens R.M.; Malliaras G.G. *Organic Semiconductors in Sensor Applications, Springer Series in Materials Science*, **2008**, *107*, Springer, Berlin/Heidelberg.

90. Achyuthan K.E.; Lu L.D.; Lopez G.P.; Whitten D.G. *Photochem. Photobiol. Sci.* **2006**, *5*, 931–937.

91. Salvesen G.S.; Riedl S.J. *Adv. Exp. Med. Biol.* **2008**, *615*, 13–23.

92. Earnshaw W.C.; Martins L.M.; Kaufmann S.H. *Annu. Rev. Biochem.* **1999**, *68*, 383–424.

93. Talanian R.V.; Quinlan. C.; Trautz S.; Hackett M.C.; Mankovich J.A.; Banach D.; Ghayur T.; Brady K.D.; Wong W.W. *J. Biol. Chem.* **1997**, *272*, 9677–9682.

94. Rininsland F.; Wensheng Xia W.S.; Wittenburg S.; Shi X.B.; Stankewicz C.;

Achyuthan K.; McBranch D.; Whitten D.G. *Proc. Natl. Acad. Sci.* **2004**, *101*, 7511–7515.

95. Meek T.D.; Dreyer G.B. *Ann. N.Y. Acad. Sci.* **1990**, *616*, 41–53.

96. Eriks J.C.; Goot H.V.D.; Geert Jan Sterk G.J.; Timmerman H. *J. Med. Chem.*, **1992**, *35*, 3239.

97. Achyuthan K.E.; Whitten D.G. *Comb. Chem. HTS*, **2007**, *10*, 399–412.

98. Achyuthan K.E. *Luminescence*, **2001**, *16*, 257–262.

99. Earnshaw W.C.; Martins L.M.; Kaufmann S.H. *Annu. Rev. Biochem.* **1999**, *68*, 383–424.

100. (a) Lien S.; Pastor R.; Sutherlin D.; Lowman H.B. *Protein J.* **2004**, *23*, 413–425, (b) Henning R. Stennicke H.R.; Renatus M.; Meldal M.; Salvesen G.S. *Biochem. J.* **2000**, *350*, 563–568, (c) Nicholson D.W.; Ah A.; Thornberry D. *Nature*, **1995**, *376*, 37–43, (d) Fu G.X.; Alexander A. Chumanevich A.A.; Agniswamy J.; Fang B.; Harrison R.W.; Weber I.T. *Apoptosis* **2008**, *13*, 1291–1302, (e) Lozanov V.; Ivaylo P. Ivanov I.P.; Bistra Benkova B.; Mitev V. *Amino Acids* **2008**, *36*, 581-586.

101. Cen H.; Mao F.; Aronchik I.; Fuentes R.J.; Firestone G.L. *FASEBJ.* **2008**, *22*, 2243–2252.

102. Wang M.M; Gloria L. Silva G.L.; Armitage B.A. *J. Am. Chem. Soc.* **2000**, *122*, 9977–9986.

103. Delaey E.; van Laar F.; De Vos D.; Kamuhabwa A.; Jacobs P.; de Witte P. *J. Photochem. Photobiol. B* **2000**, *55*, 27–36.

104. Sima P.D.; Kanofsky J.R. *Photochem. Photobiol.* **2000**, *71*, 413–421.

105. Tang Y.L.; Zhou Z.J.; Ogawa K.; Lopez G.P.; Schanze K.S.; Whitten D.G. *J Photochem. Photobiol. A Chem.* **2009**, *207*, 4-6.

106. James P.V.; Sudeep P.K.; Suresh C.H.; George T.K. *J. Phys. Chem. A* **2006**, *110*, 4329-4337.

107. Wang Y. S.; Schanze K. S. *Chem. Phys.* **1993**, *176*, 305-319.

108. Farley R. T., Ph. D. Dissertation, University of Florida, **2007**.

109. Lin C.Y.; Lo C.F.; Luo L.Y.; Lu H.P.; Hung C.S.; Diau E.W.G. *J. Phys. Chem. C*, **2009**, *113*, 755–764.

110. Chemburu S.; Corbitt T.S.; Ista L.K.; Ji E.; Fulghum J.; Lopez G.P.; Ogawa K.; Schanze K.S.; Whitten D.G. *J. Phys. Chem. B*, **2008**, *112*, 14492–14499.

111. Wang Y. S.; Schanze K. S. *Chem. Phys.* **1993**, *176*, 305-319.

112. Farley R. T., Ph. D. Dissertation, University of Florida, **2007**.

113. Nickerson E.K.; West, T. E.; Day, N.P.; Peacock, S.J. *Lancet Infect. Dis.* **2009**, *9*, 130-135.

114. Gorwitz R.; Fridkin S.K. Workowski K.A. *Ann. Intern. Med.* **2008**, *148*, 310-312.

115. Hamblin M.R.; Hasan T. *Photochem. Photobiol. Sci.* **2004**, *3*, 436-450.

116. Kuimova M.K.; Yahioglu G.; Ogilby P.R. *J. Am. Chem. Soc.* **2009**, *131*, 332-340.

117. EPE B. *Chem. Biol. Interact.* **1991**, *80*, 239-260.

118. Bachowski G.J. ; Pintar T.J.; Girotti A.W. *Photochem. Photobiol.*, **1991**, *53*, 481-491.

119. Triantaphylides C.; Krischke M.; Hoeberichts F.A.; Ksas B.; Gresser G.; Havaux M.; Van Breusegem F.; Mueller M.J. *Plant Physiol.* **2008**, *148*, 960-968.

120. Brezova V.; Valko M.; Breza M.; Morris H.; Telser J.; Dvoranova D.; Kaiserova K.; Varecka L.; Mazur M.; Leibfritz D. *J. Phys. Chem. B*, **2003**, *107*, 2415-2425.

121. Flors C.; Nonell S. *Acc. Chem. Res.* **2006**, *39*, 293-300.

122. Maclean M.; MacGregor S.J.; Anderson J.G.; Woolsey G.A. *J. Photochem. Photobiol.*

B, Biol. **2008**, *92*, 180-184.

123. See reviews a) Hamblin M.R.; Hasan T. *Photochem. Photobiol. Sci.* **2004**, *3*, 436-450, b) Jori G.; Fabris C.; Soncin M.; Ferro S.; Coppellotti O.; Dei D.; Fantetti L.; Chiti G.; Roneucci G. *Lasers Surg. Med.* **2006**, *38*, 468-481, c) Maisch T. *Mini Rev. Med. Chem.* **2009**, *9*, 974-983, d) Garland M.; Cassidy C.M.; Woolfson D.; Donnelly R.F. *Future Med. Chem.* **2009**, *1*, 667-691.

124. Corbitt T.S.; Sommer J.R.; Chemburu S.; Ogawa K.; Ista L.K.; Lopez G.P.; Whitten D.G.; Schanze K.S. *ACS Appl. Mater. Interfaces,* **2009**, *1*(1), 48-52.

125. (a) Walsh S.E.; Maillard J.-Y.; Russell A.D.; Catrenich C.E.; Charbonneau D.L.; Bartolo R.G. *J. Appl.Microbiol.* **2003**, *94,* 240–247, (b) Lienkamp K.;Madkour A.E.; Kumar K.-N.; Nüsslein K.;Gregory N. Tew, *Chem. Eur. J.* **2009**, *15*, 11715-11722.

126. Misha R. Introduction to flow cytometry, AbD serotec.

127. Wang Y. S.; Schanze K. S. *Chem. Phys.* **1993**, *176*, 305-319.

128. Farley R. T., *Ph. D. Dissertation, University of Florida,* **2007**.

129. Corbitt T. S.; Ding L. P.; Ji E.; Ista L.K.; Ogawa K.; Gabriel P. L.; Schanze. K. S.; Whitten D. G.. *Photochem. Photobiol. Sci.,* **2009**, *8*, 998-1005.

130. Lipovsky A.; Nitzan Y.; Friedmann H.; Lubart R. *Photochem. Photobiol.* **2009**, *85*, 255–260.

131. Achyuthan K. E.; Lu L.D.; Lopez G.P.; Whitten D.G. *Photochem. Photobiol. Sci.* **2006**, *5*, 931–937.

132. (a) Yue S. T.; Johnson I.D.; Huang Z.J.; Haugland R.P. *U.S. Patent 5321130*, **1994**, **(**b) Chang A.C.; Gillespie J.B.; Tabacco M.B. *Anal. Chem.* **2001**, *73*, 467-470.

133. Wang Y.; Tang Y.L.; Zhou Z.J.; Ji E.; Lopez G. P.; Chi E. Y.; Schanze S. K.; Whitten

D.G. *Langmuir*, **2010**, 26, 12509-12514.

134. Miteva T.; Palmer L.; Kloppenburg L.; Neher, D.; Bunz U. H. F. *Macromolecules* **2000**, *33*, 652 – 654.

Publications

Zhijun Zhou, Yanli Tang, David G. Whitten, and Komandoor E. Achyuthan. *ACS Appl. Mater. Interfaces*, **2009**, *1*, 162-170.

Komandoor E. Achyuthan, Jaime M. Mcclain, **Zhijun Zhou**, David G. Whitten, Darren W. Branch, *Anal. Sci.*, **2009**, *25*, 469-474.

Yanli Tang, **Zhijun Zhou**, Katsu Ogawa, Gabriel P. Lopez, Kirk S. Schanze, David G. Whitten, *J. Photochem. Photobiol. A: Chem.*, **2009**, *207*, 4-6.

Ying Wang, Yanli Tang, **Zhijun Zhou**, Eunkyung Ji, Gabriel P. Lopez, Eva Y. Chi, Kirk S. Schanze, David G. Whitten, Langmuir, **2010**, *26*, 12509-12514.

Zhijun Zhou, Thomas S. Corbitt, Anand Parthasarathy, Yanli Tang, Linnea K. Ista, Kirk S. Schanze, David G. Whitten, *J. Phys. Chem. Lett.*, **2010**, *1*, 3207-3212.

Yanli Tang, **Zhijun Zhou**, Katsu Ogawa, Gabriel P. Lopez, Kirk S. Schanze, David G. Whitten, *Langmuir*, **2009**, *25*, 21-25.